SEDIMENTOLOGY the journal of the International Association of Sedimentologists

Sedimentology (2023) doi: 10.1111/sed.13097

Sedimentology and stratigraphic architecture of Barremian synrift barrier island–estuarine depositional systems from blended field and drone-derived data

ANA R. SORIA* , CARLOS L. LIESA* , ROCÍO NAVARRETE† and JUAN PEDRO RODRÍGUEZ-LÓPEZ‡'§

**GEOTRANSFER Research Group, Departamento de Ciencias de la Tierra-Instituto de Ciencias Ambientales (IUCA), Facultad de Ciencias, Universidad de Zaragoza, C/Pedro Cerbuna 12, 50009, Zaragoza, Spain (E-mail: anasoria@unizar.es)*

†I.E.S. Pilar Lorengar, C/Miguel de Asso 5, 50014, Zaragoza, Spain

‡Department of Geology, Faculty of Science and Technology, University of the Basque Country (UPV/EHU), Ap. 644, E-48080, Bilbao, Spain

§Department of Geography, Permafrost Laboratory, University of Sussex, Falmer, Brighton, BN1 9SJ, UK

Associate Editor – Theresa Schwartz

ABSTRACT

The Lower Cretaceous (Barremian) Camarillas Formation in the Galve Sub-basin of eastern Spain is an exceptionally muddy, synrift, aggradational then retrogradational paralic succession. Deposition within these arid, equatorial paralic systems was strongly controlled by crustal rifting of the Iberia plate linked to the geodynamic evolution of the Atlantic Ocean, the Bay of Biscay and the Tethys Ocean. Although synsedimentary extensional tectonics controlled thickness and facies distributions, the parasequence stacking patterns point to a superimposed high-order allogenic control on the paralic succession. Field data and drone imagery are combined to document changes in sedimentology and three-dimensional stratigraphic architecture of these deposits to interpret changes in depositional environments as this basin filled. Three evolutionary stages are identified: (i) tide-dominated estuary; (ii) mixed-energy estuary, with a well-developed wave-dominated barrier island system; and (iii) barrier island–tidal inlet suite. An exceptional record of back-barrier-island depositional interactions is preserved in this high-subsidence, extensional-basin setting, including deposition of washover fans, flood-tidal deltas and ebb-tidal deltas. Drone-derived imagery facilitates three-dimensional architectural characterization of these complex paralic deposits, including multi-episodic tidal inlets, and correlation of basin scale stratigraphic markers. Spatio-temporal interactions between climate change, sea-level variations and rift-related subsidence generated complex estuarine and barrier island geobodies. The general transgressive trend recorded in the Camarillas Formation correlates well with global eustatic sea-level rise during the Barremian.

Keywords Back barrier lagoon, barrier island, Early Cretaceous, estuary, rift basin, tidal stratigraphy.

INTRODUCTION

The Lower Cretaceous Camarillas Formation was deposited synchronous with crustal thinning of the Iberia microplate (Liesa *et al.*, 2019) and contains an exceptional record of aggrading to retrograding coastal depositional systems in the Iberian Basin. This record provides information on Early Cretaceous palaeoclimate variations that can be compared with the oceanic record of the Cretaceous Tethys Sea to assess the degree of coupling between depositional environment changes and global Barremian palaeoclimate reversals. Barrier island systems and coeval depositional systems are not commonly preserved because of extensive reworking of sediment during transgression (Mulhern *et al.*, 2019, 2021). The depositional dynamics of these sedimentary systems led to the preservation of complex geobodies formed by both depositional and erosional processes, and large-scale heterogeneities (e.g. Plink-Björklund, 2005, 2008; Steel *et al.*, 2012; Chentnik *et al.*, 2015; Benallack *et al.*, 2016; Johnson *et al.*, 2017; Mulhern & Johnson, 2017). Inlet migration eroding the expanding ebb-tidal delta is an example of destructive–constructive dynamics that lead to clastic geobodies with complicated geometries and compartmentalization (Green *et al.*, 2019).

Outcrop successions of the Camarillas Formation are hundreds of metres thick and can be steeply dipping along exposed anticlines (Liesa *et al.*, 2023). Unmanned aerial vehicle (drone) imagery provides a new tool for documenting the architectural variability of facies associations (FA) within these dipping strata. Combining drone imagery together with detailed field observations allows for more accurate 3D analysis for the interpretation of depositional systems, and characterization of subsurface reservoir analogues (e.g. Danish Central Graben, Sixsmith *et al.*, 2008; Johannessen *et al.*, 2010). Similar facies associations formed during different stages of rift evolution provide a unique opportunity to compare the variability of preserved geobodies formed in similar depositional environments within aggradational and retrogradational settings.

This paper focuses on defining the continuum of preserved geobodies in transgressive settings, the analysis of complex synrift paralic systems, the analysis of allogenic controls and the palaeoclimatic implications. This research establishes a foundation for the architectural analysis of complex estuarine and barrier island–lagoon systems using a drone-field blended approach in order to achieve the following objectives: (i) perform sedimentological characterization of lithofacies and facies associations; (ii) analyse the stratigraphic architecture at the basin-scale based on field recognition of key stratigraphic surfaces together with drone-derived images for correlation purposes; (iii) make palaeogeographical interpretations; (iv) provide a model for sedimentary evolution and its controlling factors; and (v) discuss the importance of this Barremian siliciclastic succession in terms of synrift configuration, Early Cretaceous palaeoclimate and Tethys palaeogeography.

GEOLOGICAL SETTING

The study area is located in the Galve Sub-basin of the Maestrazgo Basin (eastern Iberian Chain, eastern Iberia) (Fig. 1A). This part of Iberia experienced latest Jurassic–Early Cretaceous rifting that led to the breakup of Jurassic platforms and triggered the formation of several extensional basins and sub-basins (Capote *et al.*, 2002; Liesa *et al.*, 2019) (Fig. 1B). Differential tectonic subsidence was encompassed by a broad uplift related to rifting-triggered doming in eastern Iberia. The most rapid domal uplift during the Berriasian–Hauterivian (Antolín-Tomas *et al.*, 2007; Liesa *et al.*, 2019) was coeval with long-term global sea-level rise during the Early Cretaceous (Haq, 2014).

The Galve Sub-basin was one of several sub-basins that developed in the western Maestrazgo Basin during this rifting stage (Fig. 1B). Extensional tectonics controlled its geometry, the location of depocentres and internal facies distributions (Figs 1B and 2B). Cretaceous ENE–WSW striking listric normal faults system (for example, Aliaga, Remenderuelas, Camarillas, El Batán and Jorcas faults) laterally constrained by near-vertical, reactivated NNW–SSE striking normal faults with a high dip-slip component (Miravete, Cañada Vellida, Alpeñés and Ababuj faults) were the main structures controlling the accumulation of the Lower Cretaceous units (Soria, 1997; Liesa *et al.*, 2000, 2004, 2006, 2019, 2023; Navarrete *et al.*, 2013a). In this sub-basin, latest Jurassic synrift sedimentation was dominated by shallow marine to coastal carbonates (Cedrillas and Aguilar del Alfambra formations; Aurell *et al.*, 2016, 2019; Liesa *et al.*, 2019), in contrast to the subsequent terrestrial and lacustrine sedimentation that occurred during the earliest Cretaceous (Galve and El Castellar formations; Soria, 1997; Meléndez *et al.*, 2009; Aurell *et al.*, 2016). Early Cretaceous sedimentation began with deposition

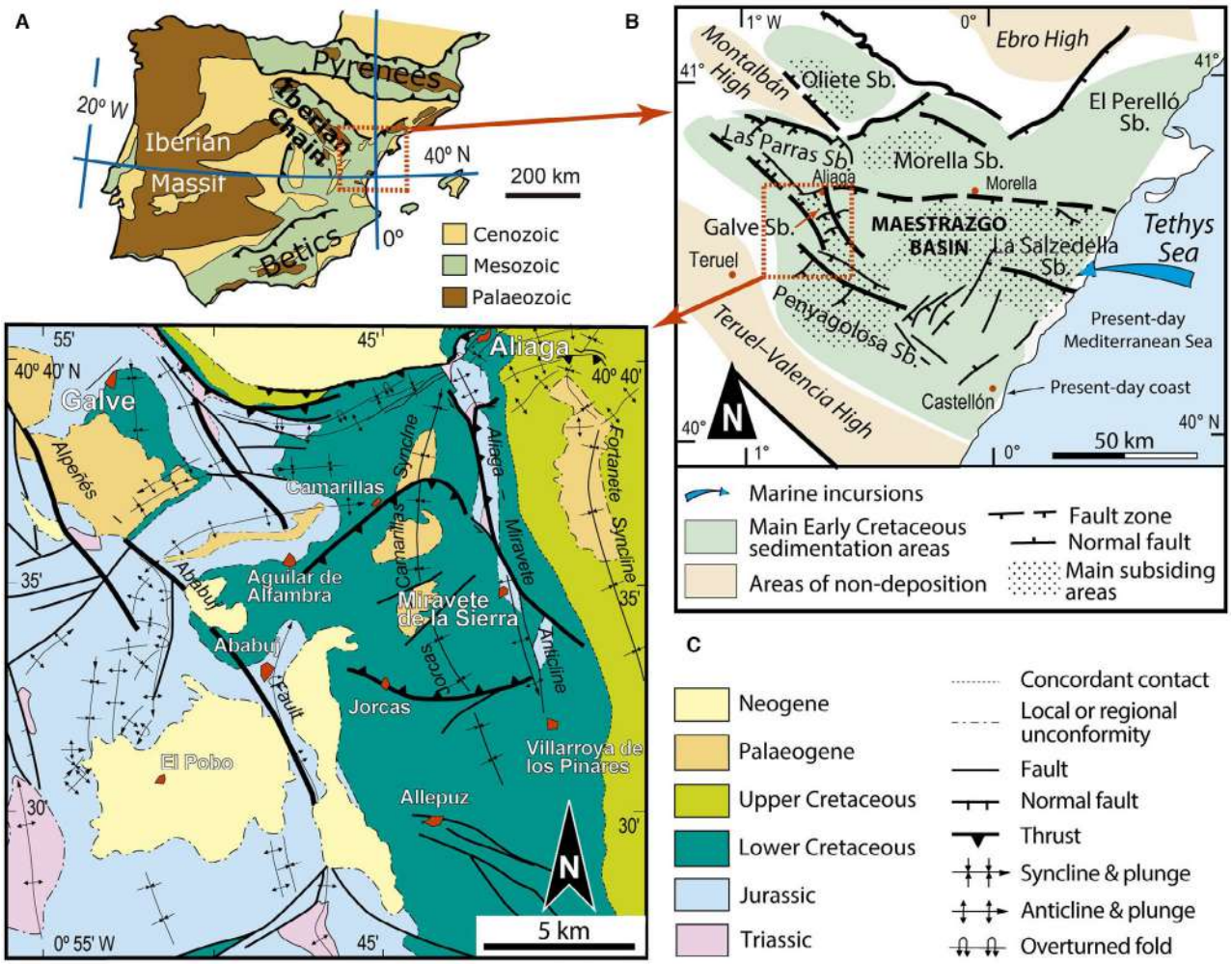

Fig. 1. Geological setting of the study area. (A) Present-day geological map of the Iberian microplate (after Navarrete *et al.*, 2014). (B) Palaeogeographical reconstruction during the Early Cretaceous for eastern Iberia (see location in A) showing the sub-basins and structural highs of the Maestrazgo Basin, as well as the main synextensional faults (modified from Liesa *et al.*, 2019). (C) Geological map of the latest Jurassic–Early Cretaceous Galve Sub-basin and surrounding areas (see B for location) (after Navarrete *et al.*, 2014).

of the silicislastic Camarillas Formation and mixed siliciclastic–carbonate Artoles and Morella formations (Soria, 1997; Navarrete *et al.*, 2013a; Navarrete, 2015); these deposits transitioned upward to carbonate-dominated shallow marine environments (Chert, Forcall, Villarroya de los Pinares and Benasal formations; Bover-Arnal, 2010; Peropadre, 2012). The Early Cretaceous synrift stage ended with an increase in normal fault activity and coeval deposition of coastal mudstones and sandstones with coal (Escucha Formation; Salas *et al.*, 2001), deposits that are recognized in contemporaneous sedimentary basins across central-eastern Iberia (Rodríguez-López, 2008).

The Camarillas Formation is Lower Barremian to early Upper Barremian in age based on biostratigraphy of charophytes (Canerot *et al.*, 1982; Salas, 1987; Martín-Closas, 1989; Soria, 1997), ostracods (Schudack & Schudack, 2009) and palynomorphs (Villanueva-Amadoz, 2009; Villanueva-Amadoz *et al.*, 2015), as well as cyclostratigraphy (Navarrete, 2015). The formation varies in thickness from 300 to 1000 m in the Galve Sub-basin associated with the locations of synsedimentary normal faults, and is mainly made up of metre-thick intercalated intervals of red mudstones and white sandstones (Soria, 1997; Navarrete *et al.*, 2013a,b; Navarrete, 2015).

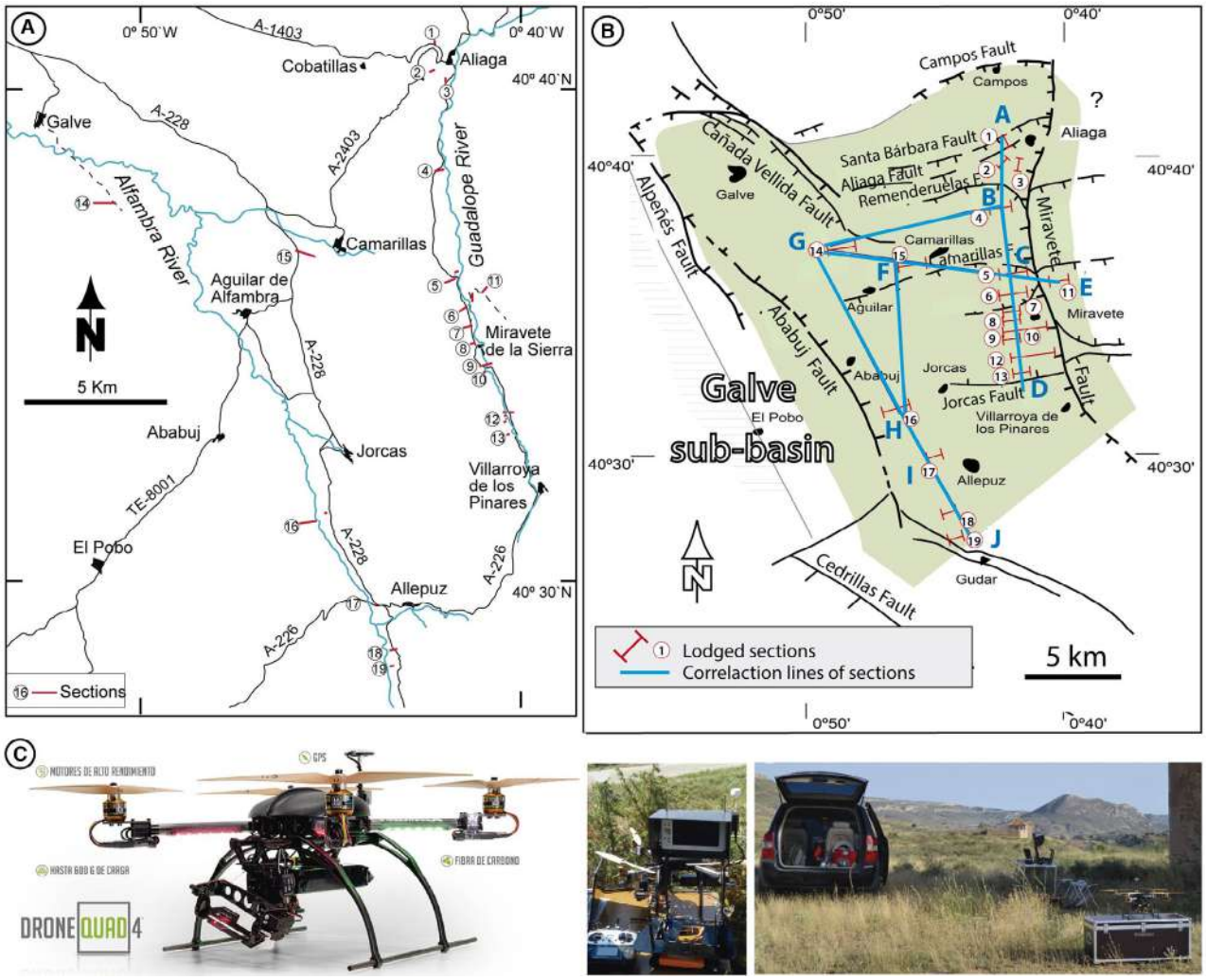

Fig. 2. (A) Road maps showing the location of the studied sections of the Camarillas Formation in the Teruel Province, Spain. (B) Spatial distribution of the studied sections with respect to the main Cretaceous extensional faults. (C) Drone technology and deployment in the field for the aerial photography surveys.

Although the Camarillas Formation was originally interpreted as fluvial in origin, showing only minor tidal influences within its upper part (e.g. Díaz Molina & Yébenes, 1987; Salas, 1987; Soria, 1997), recent work shows that fluvial facies are restricted to the lower part of the succession (Navarrete *et al.*, 2013b, 2014, 2016; Navarrete, 2015). This unit is the focus of this paper, and shows a general retrogradational trend that corresponds to a globally recognized increase in eustatic sea level during the Barremian (Haq, 2014; Navarrete, 2015). A similar retrogradational trend is recognized in Barremian coastal successions in Svalbard (Gjelberg & Steel, 2012).

MATERIALS AND METHODS

Structural and stratigraphic mapping was completed using orthoimagery from SIGPAC (*Ministerio de Agricultura*), SITAR (*Sistema de Información Territorial de Aragón*) and PNOA (*Plan Nacional de Ortografía Aérea*). Orthoimagery helped to locate the best and most continuous outcrops for measuring and describing stratigraphic sections and sedimentological and architectural analysis. A combined stratigraphic thickness of more than 5.6 km was measured across 19 stratigraphic sections and sedimentological logs (Fig. 2A and B). Photographic panels for architectural analysis were taken in the field

for the spatial tracking and analysis of lateral variations in facies. Palaeocurrent measurements were made with a compass in the field and were corrected to account for the structural dip (see section 2 in Appendix S1). More than 700 rock samples were collected for sedimentological, petrographic, geochemical, mineralogical and palaeontological analysis. Siliciclastic rock classification was based on Pettijohn *et al.* (1973), and carbonate rock classification was based on Dunham (1962) and Embry & Klovan (1971), with carbonate microfacies following Flügel (2010).

Field investigation of the stratigraphic architecture, lithofacies and sedimentology of successions followed the approach of Plink-Björklund (2005, 2008) and Steel *et al.* (2012). High-resolution aerial images of the deposits were taken using a Canon IXUS 800 IS digital camera (Canon, Tokyo, Japan) suspended from a drone (Fig. 2C). The battery-driven drone (DroneQuad4 model, DroneTools, Sevilla, Spain) had a carbon fibre quad chassis of *ca* 3 kg, four Axi motorsand four wood Xoar propellers. The altitude and direction of the drone, which ultimately determine the photograph scale, were controlled from the ground transmitter station. The drone in flight GPS mode maintains its position aided from a GPS location and previous compass calibration with the incorporated magnetometer. The camera's carbon fibre mount includes movement along two axes (pan and tilt), allowing an almost complete rotation of the camera. The camera views are transmitted as video signal to a ground station with screen of LED 7″ of high luminosity and parasol. A downlink video system in 5.8 GHz with circular polarization antennas ensures the quality of the image, which facilitates the selection of the best views. The ground station allows image selection and focus. Better images for describing and analysing the sedimentary bodies were taken in a direction perpendicular to the outcrop and dipping down the bedding plane.

SEDIMENTOLOGY: RESULTS AND INTERPRETATIONS

Nineteen stratigraphic sections of the Camarillas Formation, with a total measured thickness of 5.6 km, were logged in the Galve Sub-basin (Fig. 2A and B). These sections are located along two NNW–SSE trending cross-sections (Aliaga-Villarroya de los Pinares to the east and Camarillas-Gúdar to the west) following limbs of the Camarillas syncline (Fig. 1C).

The Camarillas Formation, contains metre-thick intervals of red mudstones and white sandstones (Fig. 3) that were differentiated into 30 facies associations. Seismic scale (metre to tens of metres-thick and kilometre-length) sandy intervals (geobodies) show great facies variability both horizontally (spatially) and vertically (temporally). Such variability is expected in transitional (coastal) environments, where relative fluctuations in sea level led to changes in the location of the coastline and abrupt lateral variations in depositional environment (see Cattaneo & Steel, 2003; Plink-Björklund, 2005, 2008; Allen & Johnson, 2010, 2011; Gallin *et al.*, 2010; Steel *et al.*, 2012; Johnson *et al.*, 2017). Detailed descriptions and interpretations for the 30 facies associations are included in Appendix S1. The facies associations (FA) characteristics are compiled in Tables 1–3. These tables include, for each FA, the description of the lithology and geometry of the sedimentary bodies, the sedimentary structures and the palaeocurrents, as well as the fossil content and bioturbation of sediments.

Changes in the proportion of facies associations up-section allowed the Camarillas Formation to be divided into three intervals, each defining different depositional stages; Stage 1 records a tide dominated estuary, Stage 2 records a mixed-energy estuary, and Stage 3 records sedimentation in a barrier island-back barrier system.

Stage 1

Nine facies associations (FA1.1 to FA1.9) were distinguished in the tide-dominated estuary deposits of Stage 1 (Table 1, Fig. 4 and Appendix S1). Fluvial channel sandstone deposits (FA1.1) show palaeoflow towards the ESE (azimuth range of 090–155) (Appendix S1: Fig. S1A to C). Lateral accretion surfaces were observed only locally, suggesting a low sinuosity fluvial channel pattern and frequent lateral reworking of fluvial sand bars during internal channel migration (Sharma *et al.*, 2002; Roberts, 2007). Tide-influenced fluvial channel sandstone deposits (FA1.2) show a mean ESE palaeocurrent direction, with bipolarity towards the NNW (from cross-bedding). The occurrence of mud drapes and flaser bedding (Appendix S1: Fig. S1D to G) suggest variations in water flow velocity and periods of stagnant water in the main channel, consistent with tidal influence on the channel thalweg and margins (Shanley *et al.*, 1992; Willis *et al.*, 1999). The presence of rhythmic mud drapes, neap–spring bundles and bi-directional palaeocurrent patterns also suggest

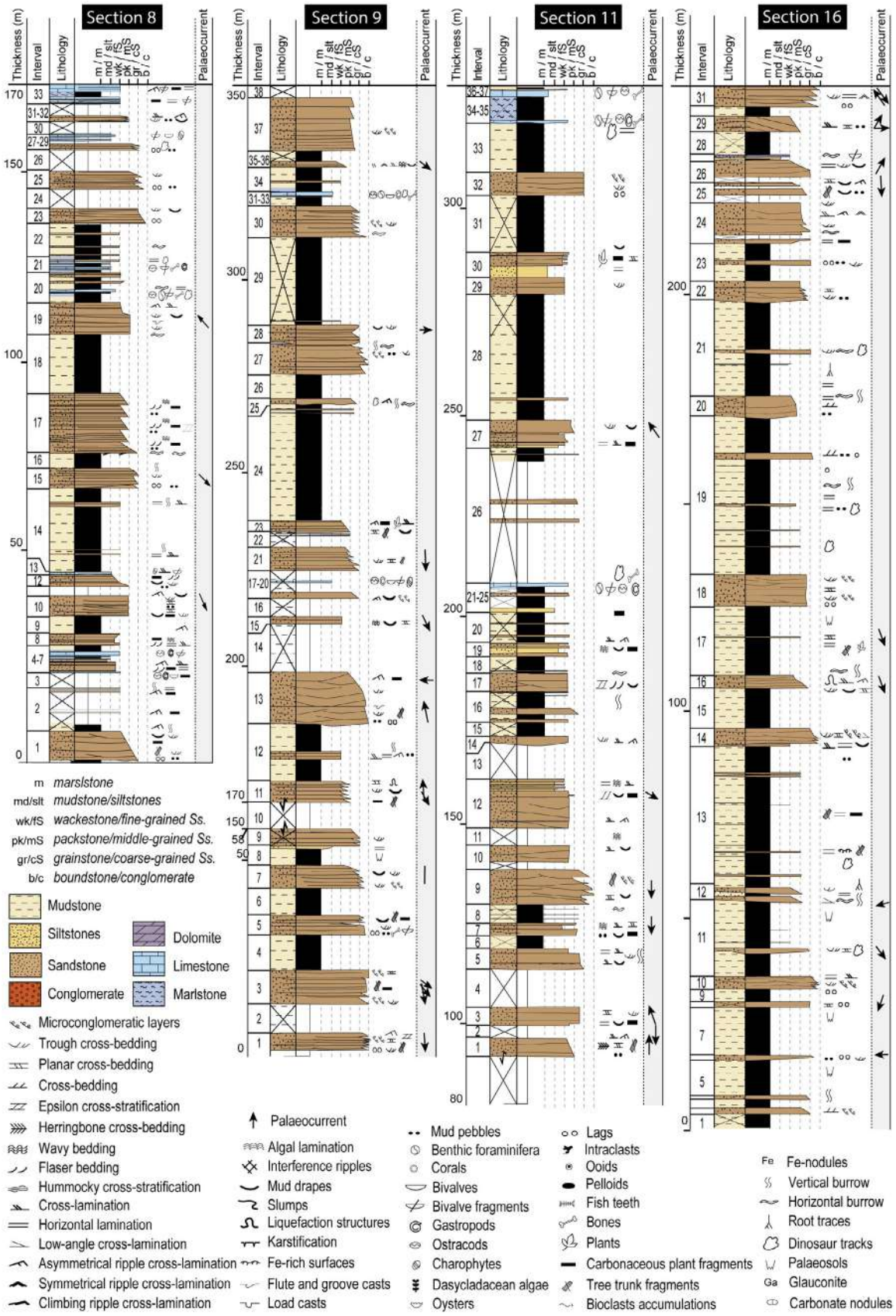

Fig. 3. Representative sedimentary logs of studied stratigraphic sections.

Table 1. Facies associations of the tide-dominated estuary (Stage 1) of the Camarillas Formation in the Galve Sub-basin. See detailed explanation and interpretation in Appendix S1.

Facies Association (FA)	Lithology and geometry	Sedimentary structures	Interpreted palaeoflow	Fossils and bioturbation
Fluvial environment				
FA1.1 Fluvial channel	Coarse, to very-coarse-grained ochre sandstones, pebbly (up to 1 cm) coarse-grained sandstones (Fig. S1A–C). Lags of quartzite and mud clasts (Fig. S1B). Fining-upward, tabular and lenticular strata (0.75–9 m thick), irregular and erosive concave bases and flat bed tops (Fig. S1A). Internal erosion surfaces dip to the SE.	Trough and planar cross-bedded sandstones (25 cm to 1 m thick; Fig. S1C). Locally, sole marks at the erosive bases. Internally parallel lamination, and iron oxides to the top.	ESE to SE	Tree trunk and bone fragments. Unidentified horizontal and vertical burrows.
FA1.2 Tidally influenced fluvial channel	Very coarse to fine-grained white and ochre sandstones. Up to 10 m thick fining-upward successions. Tabular and lenticular metre to decimetre-thick strata. Internal erosional surfaces (Fig. S1D).	Trough and planar cross-bedded sets (up to 70 cm and 20 cm thick, respectively). Reactivation surfaces, pebble lags on foresets (Fig. S1E). Asymmetrical ripples and locally wave ripples, cross-lamination, flaser bedding and basal groove casts. Tidal bundles on foresets, and mud drapes (Fig. S1F, G).	ESE and NNW	Tree trunk fragments and disseminated organic matter (mixed with the sand). Unidentified horizontal and vertical burrows.
FA1.3 Floodplain	Metre-thick structureless red mudstones with interbedded centimetre-thick tabular strata of fine-grained sandstones (Fig. S1D).	Green mottling.	Not applicable (NA).	Root traces.
Tide-dominated estuary				
FA1.4 Muddy supratidal flat with marshes	Metre-thick tabular intervals of variegated mudstone with organic rich layers (Fig. 4A and Fig. S2A, B).	Parallel lamination, Fe-concretions, gypsum.	NA	Carbonaceous plant fragments and palynomorphs.
FA1.5 Muddy intertidal flat with crevasse splays	Metre-thick maroon to dark-red, violet and grey mudstones in tabular intervals (Fig. 4A and Fig. S2A, B). Interbedded centimetre to decimetre-thick tabular to lenticular grey to red, fine-grained sandstone strata.	Mudstones: structureless and laminated. Sandstones: trough and low-angle cross-bedding, parallel lamination and drapes.	SW and NE	Tree trunk fragments, organic matter, carbonaceous plant fragments. Horizontal and vertical burrows, dinosaur tracks.

Table 1. (continued)

Facies Association (FA)	Lithology and geometry	Sedimentary structures	Interpreted palaeoflow	Fossils and bioturbation
FA1.6 Intertidal and subtidal flats	Tabular beds up to 1 m of interbedded sandstones and siltstones (Fig. 4B, 4D and Figs S2C–F and S3A–D). Fine to medium-grained sandstones organized in centimetre to metre-thick tabular and lenticular strata (5–10 cm thick) with irregular bases and tops for bioturbation. Ochre and grey siltstones in tubular to lenticular strata up to 1.5 m thick.	Sandstones: flaser, wavy and lenticular bedding, asymmetrical ripples, cross-lamination, mud drapes, fluid-escape structures. Siltstones: parallel and cross-lamination, double mud drapes of organic matter, fluid-escape structures.	NA	Tree trunk fragments, carbonaceous plant fragments. Horizontal burrows and dinosaur tracks on bed bases and vertical burrows to the bed top.
FA1.7 Carbonate ponds	Interbedded grey marlstones and limestones. Laminated mudstones form decimetre to centimetre-thick tabular intervals. Limestones in decimetre to metre-thick lenticular intervals (up to 1.5 m thick) with mudstone and bioclastic packstone (with quartz grains) textures (Fig. S3D).	Marlstones with parallel lamination and water-escape structures. Limestones with asymmetrical ripples to the top of beds.	NA	Ostracods, charophytes, bivalve fragments, oysters, gastropods, organic matter. Locally, tree trunk fragments and bones. Fish teeth.
FA1.8 Tidal channel (tidal creek)	Metre-thick (up to 3.5 m thick) intervals of medium to fine-grained sandstones, with very coarse to coarse-grained sandstones at the bed bases. Sandstone bodies with concave bases and flat–sharp to slightly convex tops (Fig. 4B,C, E, F and Figs S2C and S3A). Internal lenticular layers (20–50 cm thick) bounded by sharply inclined surfaces, some erosive (Fig. S3B, C).	Quartzite and mud clasts lags, trough, planar and sigmoidal cross-bedding. Mud drapes (Fig. S2D), flaser and wavy bedding, symmetrical and asymmetrical ripples, cross-lamination (Fig. S3C), tidal bundles and inclined heterolithic stratification (IHS).	Bipolarity ESE and N.	Tree trunk and carbonaceous plant fragments, and organic matter.
FA1.9 Subtidal sandbars	Very coarse-grained yellowish-white sandstones with pebbly (up to 2 cm) coarse-grained sandstones, and medium to fine-grained sandstones (Fig. 4D and Fig. S2E and S4). Up to 8 m thick fining upward intervals that pinch out to the NW, with internal inclined (prograding) tabular to lenticular strata (10 cm to 1.7 m thick) bounded by erosional surfaces with basal quartzite basal lags dipping to the NE.	Trough (up to 30 cm thick) and planar (20–50 cm thick) cross-bedded sets (Fig. S4A–C) with grain-size variations in the foreset lamination (Fig. S4B). Sigmoidal stratification (Fig. S4D), symmetrical and asymmetrical ripple cross-lamination with cross and parallel-lamination among cross-bedded sets (Fig. S4E). Locally, mud drapes, flaser bedding, and Fe-rich surfaces.	Trough cross-bedding: E and SE, subordinate NE; ripple cross-lamination NNW, and E-W bipolarity.	Tree trunk fragments, rudists (Fig. S2F), bivalves, oysters, bones, fish teeth and carbonaceous plant fragments.

Table 2. Facies associations of the mixed-energy, wave-dominated tide-influenced estuary (Stage 2) of the Camarillas Formation in the Galve Sub-basin. See detailed explanation and interpretation in Appendix S1.

Facies Association (FA)	Lithology and geometry	Sedimentary structures	Interpreted palaeoflow	Fossils and bioturbation
Estuary – Inner zone				
FA2.1 Inner tidal bar	Poorly sorted coarse to medium-grained ochre and white sandstones with scattered quartzite pebbles. Quartzite and mud pebble lags and fining upward successions. Lenticular bodies up to 15 m thick and 150 m long (Fig. 5A, 5C and Figs S5 and S6). Sharp and flat bed bases with quartzite and mud pebbles. Convex bed tops. Internal large-scale frontal accretion surfaces, with basal lags, defining discrete 15 cm to 2 m thick lenticular inclined beds with wavy bases and tops (Figs S5E and S6).	Single beds with up to 1.20 m thick trough cross-bedded sets (Fig. S5C), and up to 50 cm thick planar cross-bedded sets with grain-size variations on the foreset lamination (Fig. S5D). Sigmoidal cross-bedding, flaser bedding, symmetrical and asymmetrical ripple cross-lamination, climbing ripple cross-lamination, parallel lamination, double mud drapes (Fig. S5B), and organic matter drapes both in the foresets and bottomsets.	Progradation SSE, secondarily NE (Fig. S6). Palaeoflow NE to NW, with bipolarity S and WNW.	Carbonaceous plant fragments, bioturbation (*Rhizocorallium*; Fig. S5A) in bed bases. Indeterminate vertical and horizontal burrows. Root traces.
FA2.2 Bayhead delta	Coarse to medium and fine-grained greyish-white and yellowish-white sandstones with scattered quartzite and mud pebbles arranged in coarsening-upward successions (Fig. 5A and Fig. S7A). Lenticular and tabular sedimentary bodies (2–3 m thick) with irregular flat bases and flat to convex tops. Internal discrete lenticular beds up to 1 m thick bounded by reactivation surfaces.	Single beds with trough cross-bedded sets (up to 70 cm thick; Fig. S7B, C), planar cross-bedded sets (up to 15–20 cm thick), and sigmoidal cross-bedding. Asymmetrical ripple cross-lamination, locally symmetrical and cross-lamination. Flaser bedding, double mud drapes, and grain-size variations in the foreset lamination. Fluid-escape structures.	Dominant ESE and SE (from cross-bedded sets). Subordinate N and WNW (from sigmoidal cross-bedding).	Vertical and horizontal burrows. Tree trunk fragments and organic matter.
FA2.3 Supratidal and intertidal mudflat with crevasse splays and ponds	Red, green and grey mudstones and interbedded grey marlstones, fine-grained sandstones, and limestones (Fig. 5A–C and Figs S6 and S8A). Mudstones in metre to decametre-thick tabular intervals, with mottling and interbedded carbonate horizons. Grey marlstones in metre-thick tabular intervals. Sandstones in centimetre to metre-thick tabular intervals. Limestones (mudstone to bioclastic packstone) in decimetre to metre-thick lenticular layers (up to 300 m long; Fig. S8B–D).	Mudstones: structureless with subordinate parallel lamination, Fe and carbonate nodules. Marlstones: parallel lamination. Sandstones: cross and parallel lamination and load structures. Limestones: asymmetrical ripple cross-lamination, and cross and parallel lamination. Fluid-escape structures.	NA	Mudstones and marlstones: bivalves (*unionids*; Fig. S8B). Sandstones: root traces. Limestones: bivalves, ostracods, charophytes, gastropods and organic matter (Fig. S8C, D).
FA2.4 Inner heterolithic intertidal flat	Tabular intervals up to 3 m thick of medium to fine-grained heterolithic ochre and white sandstones and black and grey mudstones (Fig. 5A, 5D and Figs S8E–G and S9A), and interbedded tabular and lenticular (up to 1.5 m thick) ochre and grey siltstones. FA organized in centimetre to decimetre-thick beds with slightly irregular bases and tops, and fining-upward successions (Fig. S8F).	Sandstones: lenticular, flaser and wavy bedding (Fig. S8G), and planar cross-bedding. Symmetrical and asymmetrical ripple cross-lamination, double mud drapes, and soft sediment deformation structures. Mudstones: parallel lamination. Siltstones have parallel lamination.	S and SE from planar cross-bedding. N and S from asymmetrical ripple cross-lamination.	Carbonaceous plant fragments, organic matter. Horizontal and vertical burrows, and dinosaur tracks.

Table 2. (continued)

Facies Association (FA)	Lithology and geometry	Sedimentary structures	Interpreted palaeoflow	Fossils and bioturbation
FA2.5 Tidal channel (inner estuary)	Very coarse to coarse, medium and fine-grained, white and ochre (locally red) sandstones in fining-upward successions (Fig. 5A, 5B, 5D, 5E and Figs S8E and S9). Up to 5.2 m thick sedimentary bodies, with concave base and flat to convex tops (Fig. S9A, B). Internal 10 cm to 1.20 m thick lenticular layers bounded by erosive reactivation surfaces and lateral accretion surfaces (Fig. S9C, D).	Trough and planar cross-bedded sets up to 30 cm thick, flaser and wavy bedding, and mud drapes (Fig. S9E). Sigmoidal and herringbone cross-bedding, symmetrical and asymmetrical ripple cross-lamination. Interference ripple crests, planar and cross-lamination, tidal bundles and fluid escape structures.	Strong bipolarity, SE and WNW to NW.	Organic matter and tree trunk and carbonaceous plant fragments. Locally, oysters, bones, and fish teeth.
Central estuary				
FA2.6 Muddy central bay	Decametre-thick intervals of black-greenish, dark maroon mudstones, and interbedded centimetre-thick tabular, coarse to fine-grained maroon and grey-greenish sandstones (Fig. 6A, 6C and Figs S8E, S10 and S14A).	Mudstones: structureless, locally parallel lamination, and baryte and phosphate nodules. Sandstones: structureless.	NA	NA
Mouth of estuary – outer zone				
FA2.7 Outer estuary tidal channel	Coarse, medium and fine-grained, white, grey and ochre sandstones with red colouration towards the bed top (Fig. 6A and Fig. S10). Up to 6 m thick bodies with concave bases and flat tops, and fining-upward bedsets. Internal centimetre to metre-thick lenticular beds bounded by N and S-dipping surfaces.	Flute casts and large (up to 0.5 m) tree trunk fragments in the bed bases. Mud pebble lags, trough (up to 40 cm thick) and planar cross-bedded sets (up to 40 cm thick) (Fig. S11A–C), low-angle cross-bedding (Fig. S11D) and flaser bedding (Fig. S10). Abundant wavy bedding and double and single mud drapes towards the bed top. Herringbone cross-bedding and fluid escape structures (Fig. S11B, E). Climbing ripple cross-lamination, symmetrical and asymmetrical ripple cross-lamination both in the bottomsets and in the limits between cross-bedded sets. Planar and cross-lamination between cross-bedded sets.	W and SSW, and N.	Carbonaceous plant and tree trunk fragments. Bioturbation by *Skolithos*, *Psilonichnus* (Fig. S11F) and *Balanoglossites* (Fig. S11C).
FA2.8 Outer heterolithic tidal flats with ponds	Up to 15 m thick intervals of medium to very fine-grained ochre and white sandstones interbedded with black and grey siltstones, and subordinate ochre and grey marlstones and limestones, and ochre dolomite levels (Fig. S12A, D). Sandstones in metre-thick bodies with irregular bases and flat tops (Fig. S12D), internal centimetre to decimetre-thick lenticular and tabular beds. Siltstones in tabular and lenticular intervals up to 1.5 m thick. Marlstones in centimetre to decimetre-thick intervals. Limestones (mudstone and wackestone) in lenticular strata (0.5–4 m thick) internally divided into decimetre-thick beds.	Sandstones: mud clasts, flaser and wavy bedding, asymmetrical ripple cross-lamination, double mud drapes (Fig. S12E) and drapes of organic matter (Fig. S12F), and parallel lamination. Siltstones: parallel lamination and accumulations of carbonaceous plant fragments. Marlstones: parallel lamination. Limestones: cross-lamination and asymmetrical ripple cross-lamination to the bed tops.	Bipolarity N–S	Sandstone and siltstone: tree trunk and carbonaceous plant fragments, vertical burrows in bed tops. Marlstone: bivalves and ostracods. Limestone: ostracods with ornamentation, charophytes, bivalves, gastropods, fish teeth, oysters, organic matter, algae (*Dasycladales*), benthic foraminifera (Fig. S12C), serpulids, corals, Naticidae (Fig. S12B).
FA2.9 Outer estuary tidal sandbars	Medium to fine-grained white and yellowish sandstones arranged in fining-upward successions (Fig. 6B and Fig. S13A). Up to 13 m thick lenticular bodies with flat bases and very coarse-grained lags,	Groove and flute casts and tree trunk fragments in bed bases. Trough (10–70 cm thick) and planar (10–50 cm) cross-bedded sets, low angle cross-stratification, flaser and wavy bedding. Sigmoidal cross-bedding, mud	Strong bipolarity WNW and SE.	Coal fragments, organic matter, tree trunk fragments, bioturbation

Table 2. (continued)

Facies Association (FA)	Lithology and geometry	Sedimentary structures	Interpreted palaeoflow	Fossils and bioturbation
	including quartzite clasts, and convex tops. Internal large-scale surfaces defining lenticular beds and strata from 15 cm to 1.5 m in thickness.	drapes and drapes of organic matter, as well as tidal bundles defined by rhythmic grain-size variations on foreset lamination (Fig. S13B). Symmetrical and asymmetrical ripple cross-lamination and parallel lamination (Fig. S13C).		(*Taenidium*) and *Beaconites* to the bed top.
FA2.10 Flood-tidal delta (mouth of estuary)	Coarse to fine-grained white and ochre sandstones (Fig. S13D). Up to 4 m thick lenticular bodies, with flat bases (locally erosive) and convex tops, prograding to the NE and pinching out into central bay mudstones. Internal inclined concave–convex prograding surfaces define 0.2 to 0.8 m thick lenticular beds.	Mud clasts in the concave erosive bases, and trough and planar cross-bedded sets (0.2–0.4 m thick) (Fig. S13D). Low-angle stratification, mud drapes formed by carbonaceous fragments, asymmetrical and symmetrical ripple cross-lamination.	Main palaeoflow NE and E (progradation from cross-bedding), and subordinate S.	Tree trunk and coal fragments.
FA2.11 Washover fans (mouth of estuary)	Fine-grained, maroon, grey and ochre sandstones (Fig. 6C and Fig. S14A), locally, very coarse-grained sandstones with pebbles. Coarsening upward metre to decametre-thick successions internally arranged in tabular and lenticular layers up to 4.5 m thick, with erosive to flat bases and flat tops, and individual beds 10–80 cm thick. Sandstone wedges, as well as the whole FA, prograde towards the E, pinching out into central bay structureless mudstones (Fig. S14B).	Scour and groove marks, planar cross-bedding (Fig. S14F) and mud pebbles. Asymmetrical ripple cross-lamination, cross and parallel-lamination, and fluid-escape structures.	Main palaeocurrent ENE (from scour and groove marks) and N (from cross-bedding).	Bivalves, charophytes, and organic matter. Tree trunk fragments, vertical and horizontal burrows (Fig. S14C, D), and dinosaur tracks (Fig. S14E).
FA2.12 Tidal inlet (mouth of estuary)	Very coarse to very fine-grained grey and ochre sandstones. Lenticular bodies up to 13.5 m thick with concave bases and flat tops, internally divided by large-scale lateral accretion surfaces dipping towards the NNW (Fig. 6D–F and Figs S15 and S16). In detail, this FA shows different architectural elements (AE) from base to top: (i) AE1: erosive base with quartzite and mud pebbles lags (Fig. S16B, C). (ii) AE2: very coarse to coarse-grained sandstones divided by gently dipping concave and erosive lateral accretion surfaces that separate lenticular decimetre to metre-thick strata up to 2.6 m thick (Fig. S16E). (iii) AE3: coarse to medium-grained sandstones organized in tabular parallel beds. (iv) AE4: white very fine to fine-grained sandstones organized in lenticular to tabular beds.	AE2: trough and planar cross-bedded sets up to 1 m thick (Fig. S16D, F). Tidal bundles both on foreset and bottomset lamination (Fig. S16G). AE3: decimetre-thick sets of trough and planar cross-bedding, and asymmetrical and symmetrical ripple cross-lamination. AE4: trough and planar cross-bedded sets 15–30 cm thick (Fig. S16H), with scarce drapes of organic matter and vertical burrows.	Lateral accretion surfaces migrating towards the NW. AE2: palaeoflows S and SW, subsidiary E and NW. AE3: palaeoflows WNW, E to ESE, and SE. AE4: palaeoflow to the SE.	Carbonaceous plant fragments, organic matter, and tree trunk fragments
Open marine				
FA2.13 Shoreface	Very fine to fine-grained white and ochre sandstones in 20–40 cm thick tabular strata. Beds are bounded by irregular surfaces, locally showing mud layers (Figs S16B and S17).	Planar and low-angle cross-bedding, and thin mud layers. Wave ripple cross-lamination.	S.	NA

Table 3. Facies associations of the barrier island–lagoon system (Stage 3) of the Camarillas Formation in the Galve Sub-basin. See detailed explanation and interpretation in Appendix S1.

Facies Association (FA)	Lithology and geometry	Sedimentary structures	Interpreted palaeoflow	Fossils and bioturbation
Back barrier lagoon				
FA3.1 Tidal mud flat with tidal creeks and marshes	Purple and maroon mudstones organized in metre to decametre-thick tabular intervals, interbedded with metre-thick tabular levels of white coarse to fine-grained sandstones with concave and erosive bases. Tabular intervals of black siltstones and thin coal seams (Figs 7, 8A, 8D andFig. S18).	Mudstones: from structureless to laminated, with green mottling and slickensides. Sandstones: tool casts, planar, trough and herringbone cross-bedding, asymmetrical and symmetrical ripple cross-lamination, cross-lamination, mud drapes, and interference ripples. Siltstones: parallel lamination.	NE and bipolarity N and S.	Mudstones: bone fragments. Sandstone: bioturbation (*Planolites* and *Thalassinoides*). Siltstones: coal fragments, thin coal seams and palynomorphs.
FA3.2 Carbonate lagoon	Carbonate-dominated FA (Figs 7 and 8A and Fig. S16E, S18 and S20) with four main facies (Figs S19 and S20B): Facies 1: grey laminated marlstones in decimetre to metre-thick tabular intervals. Facies 2: grey mudstone/wackestone (locally packstone) limestones in decimetre to metre-thick lenticular and nodular intervals. Bed bases and tops irregular. Facies 3: grey wackestone/packstone (subordinate grainstone) limestones in lenticular and tabular metre-thick strata (up to 1.5 m thick and 13 km long). Facies 4: grey packstone limestones, with erosive bases, in centimetre-thick tabular intervals.	Facies 1: algal lamination, glauconite grains, ooids, intraclasts. Facies 2: black micritic matrix, floating quartz grains, marly and muddy intraclasts. Cross-lamination and parallel lamination, fluid-escape structures, ooids, serpulids, and levels of accumulated charophytes and dasyclads. Facies 3: peloids, black micritic matrix and floating quartz grains, parallel lamination, fluid-escape structures, asymmetrical ripple-cross lamination and Fe-rich surfaces. Locally, glauconite, irregular lamination and condensed intervals with fish teeth and Fe oxides. Facies 4: laminated, aligned bioclasts.	NA	Facies 1: ostracods, carbonaceous plant fragments, bivalves and vertical burrows. Facies 2 (Fig. S19A): gastropods, oysters, fish teeth, vertebrate fragments, organic matter, serpulids, charophytes and dasyclads, dinosaur tracks and bioturbations. Facies 3: bivalves, benthic foraminifera (Milliolids), ostracods, oysters, corals, bioturbation (*Spongeliomorpha*), serpulids, fish teeth and Fe crusts. Facies 4: bivalves, ostracods, Milliolids, dasyclads, black intraclasts (containing charophytes), fish teeth, oysters, and bone fragments.
FA3.3 Washover fan	Fine-grained maroon and ochre sandstones, occasionally coarse-grained and pebbles. Lenticular and tabular beds centimetre to metre-thick (up to 1.5 m thick) with flat to irregular and concave bases and flat bed tops.	Planar cross-bedding, asymmetrical ripple cross-lamination, mud clasts, cross and parallel lamination, and water-escape structures.	Bidirectionality NE and SE. Progradation to the E.	Tree trunk fragments, organic matter, locally oysters and charophytes. Bioturbation by *Arenicolites*, *Skolithos*, *Taenidium* and *Beaconites*, and dinosaur tracks.
FA3.4 Flood-tidal delta	Coarse to fine-grained ochre and white sandstones in metre to decametre-thick coarsening-upward bodies with flat bases and convex tops (Fig. 7A and Figs S18 and S20). Three architectural elements (AE), from base to top: (i) AE1 (prodelta): fine to very fine-grained sandstones with glauconite in tabular and lenticular	AE1: horizontal and vertical burrows, grain-size variations on foreset lamination, swaley cross-bedding, symmetrical and asymmetrical ripple cross-lamination (Fig. S16D–F). AE2: trough and planar cross-bedding (sets up to 80 cm thick), sigmoidal stratification, flaser and lenticular bedding, low-angle, cross and parallel	AE2: palaeoflow ENE, SE and W. AE3: palaeoflow to the ESE to SE, and NW to the top.	AE2: tree trunk and carbonaceous plant fragments, oysters, Bioturbation to the bed top.

Table 3. (continued)

Facies Association (FA)	Lithology and geometry	Sedimentary structures	Interpreted palaeoflow	Fossils and bioturbation
	strata with flat bases and irregular tops (Fig. S16C). Internal irregular surfaces defining levels up to 15 cm thick. (ii) AE2 (flood-tidal delta ramp): overlying AE1 or directly on back-barrier lagoon FAs, medium to fine-grained sandstones in coarsening-upward successions formed by stacked tabular and lenticular strata up to 4 m thick, with flat or slightly concave bases and flat tops. Internal inclined decimetre to metre-thick strata and layers bounded by planar and irregular surfaces dipping to the NW and SE. (iii) AE3 (channel of the flood-tidal delta): medium to fine-grained sandstones in up to 6 m thick bodies with erosive and concave bases and flat tops. Internal concave-convex reactivation surfaces define decimetre to metre-thick (15 to 150 cm) tabular and lenticular strata.	lamination, mud drapes. Slumps within individual beds. AE3: quartzite and mud pebbles lags, trough (sets 50–60 cm think) and planar drapes cross-bedding (15–50 cm thick), cross-lamination, parallel lamination among cross-bedded sets, locally mud and organic matter.		
Barrier-island				
FA3.5 Barrier island and tidal inlet	Very coarse-grained, with quartzite and mud pebble lags, to fine-grained ochre and white sandstones in metre-thick lenticular and tabular bodies with concave or flat bases, and internally divided by well-defined inclined lateral accretion surfaces with quartzite lags (Fig. 7B, 7C and Figs S18B, S21 and S22). Three architectural elements (AE) (Figs S23 and S24). (i) AE1 (tidal-inlet, channel): very coarse-grained (with pebbles) to fine-grained white and yellowish sandstones with fining-upward successions. Lenticular bodies up to 15 m thick, with planar to erosive (concave) bases. Internal lateral accretion surfaces dipping towards NE/ESE define lenticular bodies up to 3 m thick. Base of lateral accretion surfaces with quartzite and carbonate pebble lags up to 20 cm thick. (ii) AE2 (barrier-island spit): very coarse to fine-grained pinkish-white sandstones in fining-upward successions of metre to decametre-thick tabular to lenticular bodies with flat-sharp bases that pinch out to the N. Internal flat and irregular surfaces separate metre-thick tabular beds. (iii) AE3 (barrier-island spit to foreshore): Fine to very fine-grained maroon and yellowish-white sandstones with mud clasts layers in lenticular bodies up to 1 m thick.	AE1: lateral accretion surfaces bounding strata up to 3 m thick (Figs S21 and S22), with centimetre to metre-thick trough cross-bedded sets, metre-thick planar cross-bedded sets with grain-size variations on the bottomset lamination. Large-scale low-angle cross-stratification. Asymmetrical wave and symmetrical ripple cross-lamination. Quartzite and carbonate pebble (up to 5 cm in size) lags. AE2: centimetre to metre-thick planar cross-bedded sets with grain-size variations on the foreset and bottomset lamination. Flaser bedding, herringbone and low-angle cross-bedding. Occasionally, mud pebbles in bottomsets, parallel and cross-lamination in topsets, and mud drapes and drapes formed by organic matter in foresets and bottomsets. AE3: Trough and parallel cross-lamination, drapes with accumulation of organic matter and carbonaceous plant fragments.	AE1: internal accretion surfaces dip NE/ESE. Palaeoflows ENE, subordinate S, bipolarity E-W. AE2: bidirectionality ESE and NW.	AE1: tree trunk and bone fragments. Horizontal burrows at bed bases. AE2: carbonaceous plant fragments. AE3: *Skolithos* and root traces.

Table 3. (continued)

Facies Association (FA)	Lithology and geometry	Sedimentary structures	Interpreted palaeoflow	Fossils and bioturbation
Open marine platform				
FA3.6 Ebb-tidal delta	Medium to fine-grained ochre and white sandstones in coarsening-upward, locally fining-upward, successions. Lenticular metre-thick strata with flat bases and convex tops that pinch out towards N and S (Fig. 8D and Figs S25 and S26). Internal lenticular beds up to 50 cm thick with slightly erosive bases and top flat to slightly convex, with a thinning-upward succession. Inclined convex progradation surfaces in beds dip towards the S and E (Fig. S26B).	Quartzite and mud pebble lags, hummocky cross-stratification (HCS; Fig. S26E), sigmoidal stratification (Fig. S16G) and swaley cross-stratification (SCS). Low-angle cross-stratification, flaser bedding, locally mud drapes and drapes formed by organic matter on the parallel cross-bedding foresets. Wave ripple cross-bedding. Bed tops with wavy bedding, asymmetrical ripple and planar cross-lamination, cross-lamination, and mud drapes, (Fig. S26C, D).	Progradation S and E. Palaeoflows NNE and SSW.	Vertical and horizontal burrows.
FA3.7 Shoreface	Architectural Element 1 (AE1; upper shoreface): Coarse-grained, with quartzite and mud pebble lags, and medium to fine-grained yellowish-white sandstones. Lenticular bodies up to 5 m thick with flat bases and slightly convex tops. Internal convex reactivation surfaces separate 15–50 cm thick beds (Fig. S27A). AE2 (lower shoreface): Medium to fine-grained yellowish-white sandstones, with quartzite and mud pebble lags. Lenticular bodies with erosive–convex bases and irregular tops up to 1 m thick (Fig. S27C). Internal convex reactivation surfaces separate decimetre-thick beds.	AE1: Quartzite and mud pebble lags, decimetre-thick planar cross-bedded sets (Fig. S27A), swaley cross-stratification (Fig. S27B), mud layers, asymmetrical ripple cross-lamination, and cross and parallel-lamination. AE2: Quartzite and mud pebble lags. Hummocky cross-stratification (Fig. S27D), mud layers, asymmetrical ripple cross-lamination, and cross and parallel-lamination.	AE1: palaeocurrent ESE.	NA
FA3.8 Tidal bar	Architectural Element 1 (AE1): Very coarse-grained, with quartzite and mud clast pebbles, and medium-grained grey and white sandstones. Coarsening-upward tabular bodies up to 20 m thick, with flat bases and flat-convex tops that pinch out to the N. Internal irregular surfaces with quartzite pebble lags define tabular beds 15 cm to 1.5 m thick. AE2: Coarse (with pebbles), medium to fine-grained ochre and white sandstones with scattered fossils and intraclasts of carbonate and mud. Tabular bodies up to 4 m thick with sharp-flat bases, locally erosive, and wavy to flat tops that pinch out to the N and S. Internal S-dipping frontal accretion surfaces (locally concave and erosive) separate decimetre to metre-thick inclined beds (Fig. S28A, B).	AE1: quartzite pebble lags, trough (50–60 cm thick) and planar (15–50 cm thick) cross-bedded sets, asymmetrical and symmetrical ripple cross-lamination, erosional wavy surfaces, cross-lamination among cross-bedded sets, low-angle cross-lamination, grain-size variations on foreset lamination. AE2: trough cross-bedded sets. Planar cross-bedded sets (15–70 cm thick) to the bed tops, hummocky cross-bedding (Fig. S27C), grain size variations on foreset lamination, low-angle cross-stratification. Cross-lamination, locally planar lamination. Symmetrical ripple cross-lamination.	AE1: main palaeoflows NW and SW, subordinate ESE. AE2: frontal accretion surfaces towards the SSE, palaeocurrent NNW.	AE2: abundant oysters aligned in layers, fish teeth, and bone fragments.

tidal modulation of flows within these fluvial channels (Leckie & Rumple, 2003; Longhitano *et al.*, 2012). Floodplain mudstone deposits (FA1.3) (Appendix S1: Fig. S1D) show root traces, attesting to colonization of floodplain by plants after flood events (Li *et al.*, 2015).

These facies associations are inferred to have been deposited in tidal environments interbedded with deposits of muddy supratidal flats with marshes (FA1.4; Fig. 4A, Appendix S1: Fig. S2A and B), analogous to those described by Dalrymple *et al.* (1992) and Plink-Björklund (2005). These deposits show evidence of redox processes associated with variations of the groundwater level (Hurt & Carlisle, 2001; Jennings *et al.*, 2011), and frequent coal fragments due to reworking of coeval marshes (Johnson & Friedman, 1969; Bartholdy, 2012; Rodríguez-López *et al.*, 2021). The heterolithic facies of intertidal flats (FA1.5) (Fig. 4A, Appendix S1: Fig. S2A and B) contain crevasse splay deposits associated with periods of inundation by flood tides (Baeteman *et al.*, 1999; Capuzzo & Wetzel, 2004).

The intertidal to subtidal flat deposits (FA1.6) show palaeocurrent patterns and sedimentary structures associated with alternating ebb and flood tidal currents (Reineck & Wunderlich, 1968; Reineck & Singh, 1980). Abundant mud drapes and double mud drapes (Fig. 4B and D, Appendix S1: Figs S2C to F and S3A to D) are evidence of slack-water periods (Nio & Yang, 1991; Dalrymple, 1992; Hori *et al.*, 2001; Holz, 2003; Plink-Björklund, 2005) and successive high and low tides periods in the subtidal zone (Visser, 1980; Nio & Yang, 1991). Locally, ponds that facilitated carbonate production (FA1.7) (Appendix S1: Fig. S3D) developed in the tidal flats (Tucker & Wright, 1990; Flügel, 2010). They are characterized by a low-diversity faunal and ichnofacies assemblage suggesting restricted conditions and an environment affected by water salinity fluctuations (Mángano & Buatois, 2004; Schwarz *et al.*, 2011).

Tidal channel sandstone deposits (FA1.8) (Fig. 4B, C, E and F, Appendix S1: Figs S2C and D and S3A to C) contain inclined heterolithic stratification (IHS), resulting from sedimentation on point bars in meandering channels (Thomas *et al.*, 1987; Johnson & Dashtgard, 2014). Evidence of ebb and flood currents within these IHS deposits (Collison, 1996; Miall, 1996; Ghazi & Mountney, 2009) including bipolarity of cross-strata dip directions, mud drapes on the foresets and bottomsets of cross-strata, and flaser and wavy bedding, suggest variations in the flow associated with tidal currents (Ghosh *et al.*, 2005). Mud drapes are concentrated in the parts of the tidal channels characterized by high turbidity (Dalrymple *et al.*, 1990; Allen, 1991; Dalrymple, 1992; Plink-Björklund, 2005).

Subtidal sandbar sandstone deposits (FA1.9) contain rudists and fish teeth (Fig. 4D, Appendix S1: Figs S2E, F and S4) and developed in distal areas of macrotidal estuaries (Dalrymple & Zaitlin, 1989; Dalrymple *et al.*, 1990; Plink-Björklund, 2005).

Stage 2

Stage 2 is characterized by 13 facies associations (FA2.1 to FA2.13) that are interpreted to represent sedimentation in a wave-dominated, tide influenced estuary (mixed-energy estuary) that shows a clear inner-estuary, central-estuary and outer-estuary spatial organization (Table 2).

The inner zone of the estuary fill (FA2.1 to FA2.5) contains tidal bar deposits (FA2.1; Fig. 5A and C, Appendix S1: Figs S5 and S6) similar to those described by Plink-Björklund (2005). Bioturbation (*Rhizocorallium jenense*) at the base of sandy bar deposits indicates conditions of low salinity (mixed waters) in the inner estuary (Fürsich & Mayr, 1981; De, 2002; Goldring *et al.*, 2005), prior to transgression and preservation by transgressive inner tidal bars defining transgressive ravinement surfaces (Cattaneo & Steel, 2003). The sandy bayhead delta deposits (FA2.2) of the estuary (Fig. 5A, Appendix S1: Fig. S7) contain heterolithic facies (Holz, 2003; Plink-Björklund, 2005; Aschoff *et al.*, 2018) with mud drapes indicating slack water periods during tidal cycles where clay particles settled out from suspension (Nio & Yang, 1991; Vakarelov *et al.*, 2011). These features attest to the activity of semidiurnal tides in subtidal settings, in the more distal and marine-influenced areas of these transitional systems (Dalrymple & Choi, 2007; Steel *et al.*, 2012). The supratidal and intertidal mudflat deposits with crevasse splays and ponds (FA2.3; Fig. 5A to C, Appendix S1: Figs S6 and S8), similar to those described by Allen (1991) and Allen & Posamentier (1993), reflect redox processes associated with variations in the phreatic level (Leckie & Rumple, 2003; Kraus & Hasiotis, 2006). The low faunal diversity of both fossils and ichnofossils suggests carbonate production in restricted areas of the estuary affected by environmental stress due to salinity fluctuations

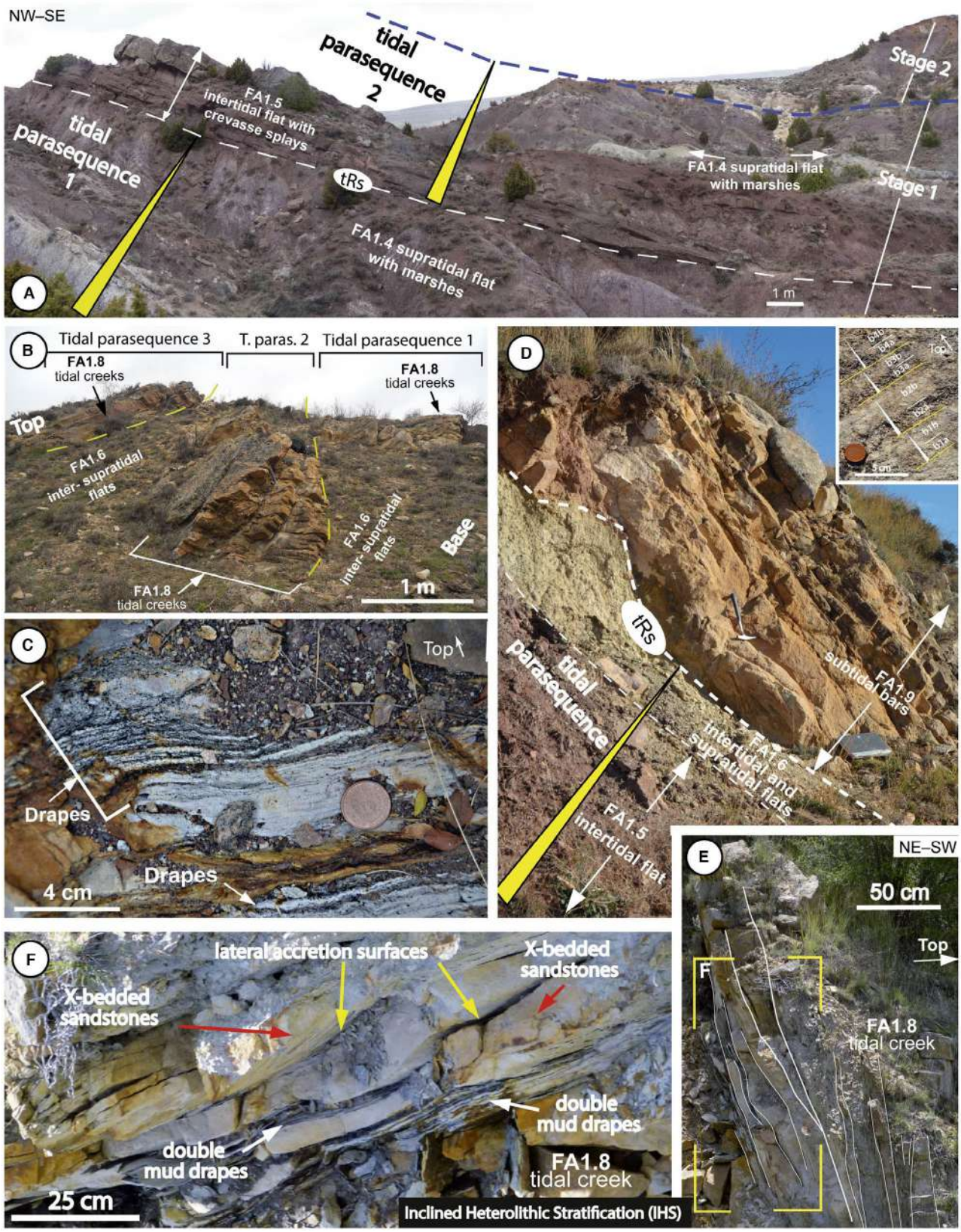

Fig. 4. Main facies associations (FAs) distinguished in the tide-dominated estuary of Stage 1 of the Camarillas Formation in the Galve Sub-basin. (A) A tidal ravinement surface (tRs) separates two tidal parasequences defined by a lower intertidal flat with crevasse splays (FA1.5) and an upper aggrading to prograding upper supratidal flat with marshes (FA1.4). The stratigraphic contact between Stage 1 and 2 is observed towards the top of the outcrop. (B) Vertical stacking of three tidal parasequences 1, 2 and 3, defined by lower tidal creeks (FA1.8) and upper intertidal and supratidal flats (FA1.6). Tidal creeks show evidence of subtidal deposition and thus the base of the channel defines tidal ravinement surfaces (tRs). (C) Neap–spring intervals showing double mud drapes formed in bottomsets of tidal bedforms. (D) Subtidal bars (FA1.9) showing rudists in the upper part of the sand bars. Retrograding subtidal bars define a tidal ravinement surface (tRs) eroding the underling intertidal and supratidal flats (FA1.6) of the top part of the underlying tidal parasequence. Detail shows tidal bundles (b1 to b4) developed in the large-scale cross-bedding foreset of a sandy tidal bedform of the subtidal bar (FA1.9); note the rhythmic repetition of discrete coarse-grained (a) and fine-grained (b) laminae in every tidal bundle. (E) Stratigraphic architecture of a tidal creek (FA1.8) encased in supratidal flat deposits (FA1.6). (F) Close-up view of (E) showing inclined heterolithic stratification (IHS) with lateral accretion surfaces, heterolithic intervals with double mud drapes, and cross-bedded sets.

(Mángano & Buatois, 2004; Reizopoulou & Nicolaidou, 2004; Schwarz *et al.*, 2011). The inner heterolithic intertidal flat deposits (FA2.4; Fig. 5A and D, Appendix S1: Figs S8E, S8F and S9A) contain double mud drapes suggesting semi-diurnal cyclicity in subtidal settings (De Boer *et al.*, 1989; Ainsworth & Walker, 1994; Johnson & Dashtgard, 2014) formed in the distal areas of these intertidal flats (Dalrymple & Choi, 2007). The inner estuary tidal channel deposits (FA2.5; Fig. 5A, B, D and E, Appendix S1: Figs S8E and S9) show evidence of tidal point-bars in meandering tidal creeks (Shanley *et al.*, 1992; Plink-Björklund, 2005). Ubiquitous double mud drapes attest to slack water sedimentation during periods of maximum turbidity (Dalrymple *et al.*, 1990; Allen, 1991; Plink-Björklund, 2005) in the subtidal zone of these tidal channels under a semi-diurnal tidal regime (Nio & Yang, 1991). The cyclic variability of grain sizes defines tidal bundles in the foresets of tidal bedforms (Shanley *et al.*, 1992; Dalrymple & Choi, 2007). Herringbone cross-stratification indicates ebb and flood current transport of sediments in the inner part of the estuary (Dalrymple & Choi, 2007), as well as the strong bipolarity of palaeocurrent directions (Willis *et al.*, 1999; Plink-Björklund, 2005; Carmona *et al.*, 2009; Bradley *et al.*, 2018).

The central part of the wave-dominated estuary is mainly represented by metres to tens of metres-thick aggrading successions of central bay mudstones (FA2.6; Fig. 6A and C, Appendix S1: Figs S8E, S10 and S14A) deposited under subtidal conditions (Allen, 1991; Dalrymple *et al.*, 1992; Allen & Posamentier, 1993; Bayet-Goll *et al.*, 2022).

The outer zone of the estuary contains tidal channel sandstone deposits (FA2.7; Fig. 6A, Appendix S1: Figs S10 and S11) with abundant double mud drapes formed under tidal currents (Shanmugam *et al.*, 2000; Steel *et al.*, 2012). Channel bases with lags constitute the deepest parts of the tidal channel in the subtidal zone (Steel *et al.*, 2012) and the lateral accretion surfaces define point-bars of the tidal channels (e.g. Johnson & Dashtgard, 2014). Deposits of the outer heterolithic tidal flats with ponds (FA2.8; Appendix S1: Fig. S12) formed on intertidal flats located among outer tidal bars of the estuary mouth (e.g. Jackson *et al.*, 2005). The outer estuary tidal sandbar deposits (FA2.9; Fig. 6B, Appendix S1: Fig. S13A to C), similar to those interpreted by other authors (Dalrymple *et al.*, 1992; Allen & Posamentier, 1993; Jackson *et al.*, 2005; Dalrymple & Choi, 2007), show flood tidal palaeocurrents (north-west) prevailing over the ebb flood currents (south-east). The interaction between these two tidal currents led to widespread tidal bundles and mud drapes on the tidal bedform (Dalrymple *et al.*, 1992; Plink-Björklund, 2005; Dalrymple & Choi, 2007). Ichnofossils *Taenidium* and *Beaconites* testify to the emergence of the upper part of the tidal bars in supratidal conditions (Melchor *et al.*, 2012). The flood-tidal delta deposits (FA2.10) record progradation into the central bay mudstones (Appendix S1: Fig. S13D); see analogues in Plink-Björklund (2005), FitzGerald *et al.* (2012) and Hayes & FitzGerald (2013), and coal clasts attest to active ravinement during retrogradation of the estuary mouth, eroding underlying back-barrier marshes and tidal flats (FitzGerald *et al.*, 2012; Austin *et al.*, 2018). The washover fan sandy deposits (FA2.11) developed as sands prograded into the back barrier central bay mudstones (Fig. 6C, Appendix S1: Fig. S14) of the

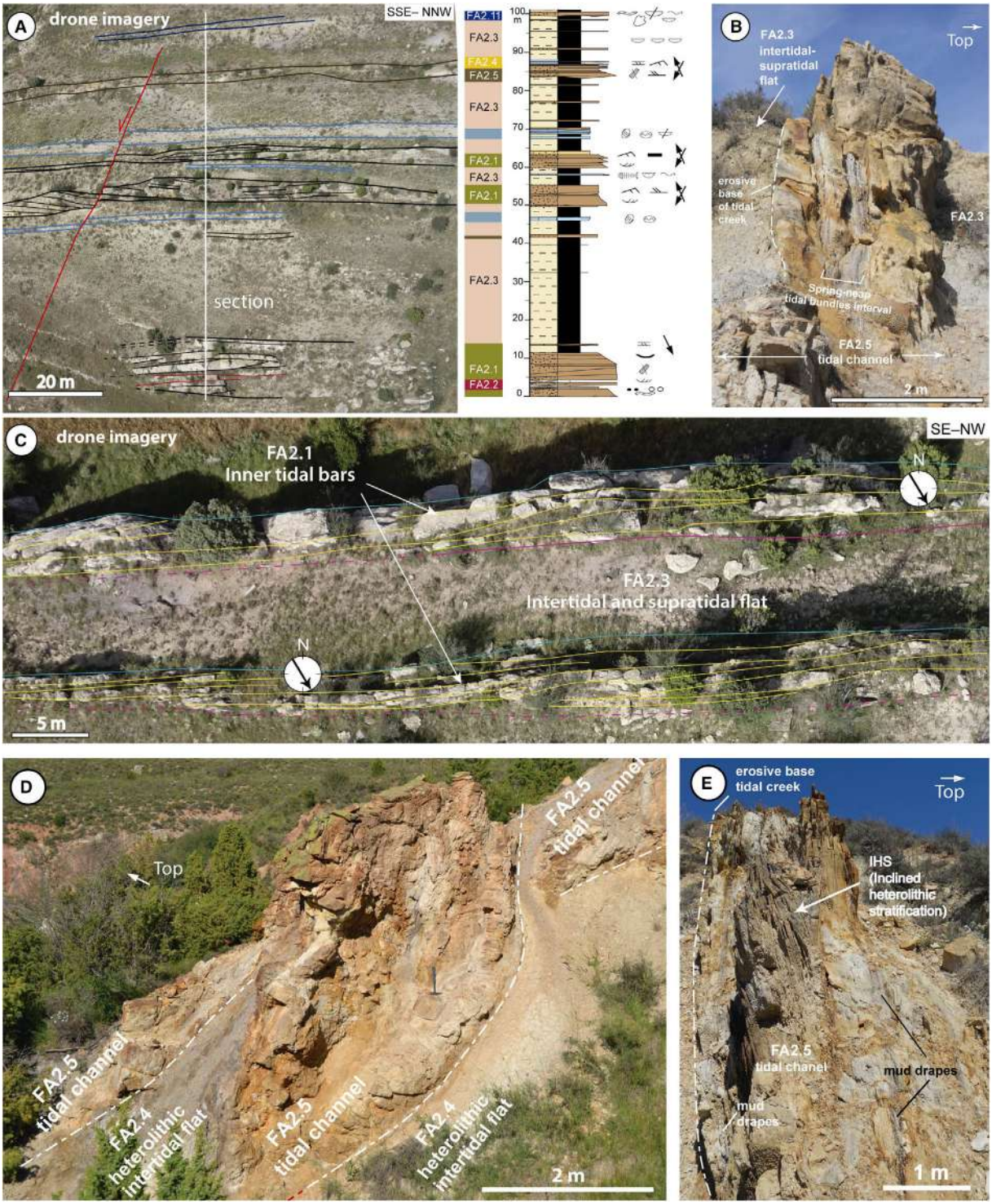

Fig. 5. Facies associations (FAs) distinguished in the inner part of the wave-tide (mixed)-dominated estuary of Stage 2 of the Camarillas Formation in the Galve Sub-basin. (A) Interpreted drone imagery and vertical distribution of FAs of Stage 2 in section 5. See Table 2 for FA codes. (B) Vertically oriented tidal channel sandstones eroding underlying intertidal–supratidal mud flat facies (FA2.3). Mud drape intervals are internally interbedded with trough cross-bedded sets representing neap bundles in the tidal channel sandstones. (C) Interpreted drone imagery of the stratigraphic architecture of inner tidal bars (FA2.1). (D) Tidal channels (FA2.5) showing erosive concave up bases eroding heterolithic facies (FA2.4). (E) Tidal channel showing a sharp erosive surface, inclined heterolithic stratification (IHS) and mud drapes.

estuary (Donselaar, 1996; Zonneveld *et al.*, 2001; Sedgwich & Davis, 2003; Hudock, 2013; May *et al.*, 2020). The tidal inlet facies associations (FA2.12) developed at the mouth of the estuary (Jackson *et al.*, 2005; Plink-Björklund, 2005). Altogether, the deposits record a succession of sandy architectural elements (AE) (Table 2, Fig. 6D to F, Appendix S1: Figs S15 and S16) from base to top: AE1, formed by microconglomerates with erosional base in the base of the tidal inlet; AE2, the thickest sandy interval representing lateral accretion due to the inlet migration, where ebb palaeocurrents dominated while reactivation surfaces formed due to southward tidal flood currents; AE3, horizontal strata with cross-bedded sets of the inlet platform split; and AE4, thinning-upward tabular sets of cross-bedding representing sedimentation in the spit of the barrier. This facies association correlates well with tidal inlets described in recent analogues at Fire Island in the USA (Kumar & Sanders, 1974; Donselaar, 1996). Ebb and flood tidal currents moved sediment in 2D and 3D megawaves forming tidal bundles, and slack-water periods led to the formation of mud drapes (Nio & Yang, 1989). The coeval open marine environment is characterized by trough cross-bedded shoreface sandstones (FA2.13; Appendix S1: Figs S16B and S17) developed by the action of waves in the open marine platform attached to the mouth of the estuary (Sha, 1990; Jackson *et al.*, 2005); the shoreface facies contains 'intrashoreface shales' formed in the upper shoreface (Haug Eide *et al.*, 2014). Despite good evidence of tidal currents, the stronger evidence of wave influence (inlets, barriers, bayhead deltas, central mud basin) warrants interpretation of Stage 2 as representing a wave-dominated, tide-influenced estuary succession.

Stage 3

Stage 3 is characterized by a barrier island–back barrier lagoon system in which eight facies associations (FA3.1 to FA3.8) have been identified, seven formed in a barrier island–back barrier lagoon system and one on a coeval open marine platform (Table 3).

The facies associations of the back-barrier lagoon (Fig. 7) include deposits of tidal mud flats with tidal creeks and marshes (FA3.1; Figs 7, 8A and 8D, Appendix S1: Fig. S18). Tidal creeks meandered in the muddy tidal flat under the influence of ebb and flood tidal currents (Willis *et al.*, 1999; Plink-Björklund, 2005; Carmona *et al.*, 2009).

The carbonate lagoon deposits (FA3.2) show a low diversity of both body and trace fossils (Figs 7 and 8A, Appendix S1: Figs S18, S19 and S20B), indicating stressed, restricted conditions in the lagoon (Mángano & Buatois, 2004; Reizopoulou & Nicolaidou, 2004; Schwarz *et al.*, 2011). Milliolids suggest low energy and restricted conditions associated with low concentration of oxygen and euryhaline environments (Schulze *et al.*, 2005; Tasli *et al.*, 2006; Rodríguez-López, 2008). Interbedded peloidal wackestone limestones indicate sedimentation in a low energy subtidal setting (Palma *et al.*, 2005), whereas bioclastic grainstones suggest sedimentation associated with high-energy conditions that could be driven by subtidal bottom currents in the sectors close to tidal inlets. Iron-(Fe-) rich hardgrounds are located in the northern and proximal sector of the lagoon (Moran, 1989; LaGesse & Read, 2006) and the widespread occurrence of glauconite grains, serpulids and accumulation of phosphates (fish teeth) reveal condensed intervals associated with periodic low sedimentation rates in the lagoon (Tucker & Wright, 1990; Chafetz & Reid, 2000; Gil *et al.*, 2006). The bioclastic limestones composed of broken bioclasts with erosive bases and aligned fossils are interpreted as tempestites (Aigner, 1985; Lee & Kim, 1992; Lee *et al.*, 2001).

The sandy washover fan deposits (FA3.3; Appendix S1), similar to others that have been described (Schwartz, 1975, 1982; Aigner, 1985; Lee & Kim, 1992; Zonneveld *et al.*, 2001; Sedgwich & Davis, 2003), contain *Arenicolites* suggesting endolithic organism colonization (Sedgwich & Davis, 2003).

The flood-tidal delta facies association (FA3.4; Fig. 7A, Appendix S1: Figs S18 and S20) is very similar to that described by Donselaar (1996). Architectural elements 1, 2 and 3 (AE1, AE2 and AE3 in Table 3) represent prodelta, ramp and channel facies, respectively, of the flood tidal delta. The complete succession is observed in the proximal sections close to the tidal inlets (to the west), while the distal sections show how the other architectural elements (flood ramp and channel of the flood tidal delta) interacted with the back-barrier FA. The prodelta facies shows swaley cross-bedding and tractive unidirectional bedforms associated with flood tidal currents (Cheel & Leckie, 1990). The flood ramp facies is formed by superimposed 2D and 3D megaripples with double mud drapes, tidal bundles showing evidence of flood and ebb tidal currents (Richards, 1994; Corcoran *et al.*, 1998; Holz, 2003). The occurrence of coal clasts in the

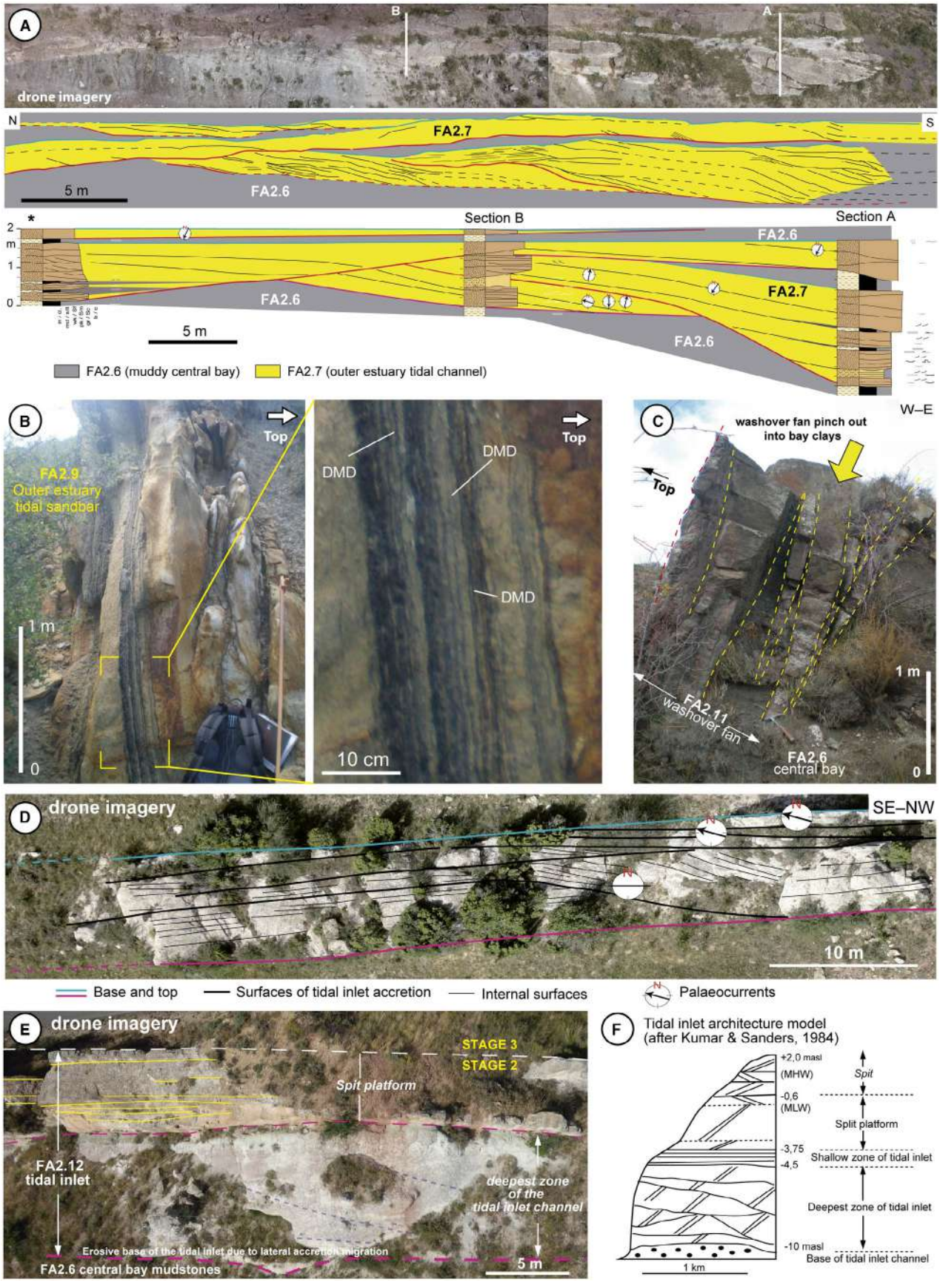

Fig. 6. Facies associations (FAs) distinguished in the central (bay) and outer part of the wave-tide (mixed)-dominated estuary of Stage 2 of the Camarillas Formation in the Galve Sub-basin. (A) Drone imagery and line drawing of an outer estuary tidal channel (FA2.7) encased in central bay mudstones (FA2.6), showing lateral accretion surfaces and bounding erosive surfaces. Below, stratigraphic correlation of sedimentological sections (see location in drone image) showing spatial variability of tidal currents with respect to the tidal channel architecture; shallower areas are dominated by NNW flood tidal currents, lower section shows bipolarity, and the thalweg of the tidal channel shows dominant ebb tidal palaeocurrents. Inclined heterolithic stratification (IHS) is observed in the point bar deposits to the south. (B) Outer estuary tidal sandbar deposits (FA2.9) with large-scale cross-bedding formed by superimposed cross-bedded sets of fine-grained sandstones and laterally continuous dark interbeds. Beds dip vertically, stratigraphic top to the right. Close-up view shows tidal rhythmites (DMD: double mud drapes). (C) Pinch out of washover fan sandstones (FA2.11) wedges into central way clays (FA2.6). (D) Interpreted drone imagery of a tidal inlet (FA2.12) showing lateral accretion surfaces left by the lateral migration of the inlet, and internal stratification. Palaeocurrents are oblique to the direction of lateral migration of the point bar as the ebb and flood tidal currents in the tidal inlet transport sediments. (E) Drone imagery of other tidal inlet deposit showing the internal architectural elements. (F) Tidal inlet architecture and vertical succession of subenvironments (after Kumar & Sanders, 1974). MHW, mean high water; MLW, mean low water; masl, metres above sea level.

bases of the flood tidal deltas is evidence of flooding and erosion of back-barrier marshes by the flood tidal delta channels (Van Wagoner *et al.*, 1990).

The barrier island and tidal inlet facies association (FA3.5) and its complex internal architectural elements (Figs 7B, 7C and 8, Appendix S1: Figs S18B, S21, S22, S23 and S24) represents sedimentation due to lateral migration of tidal inlets of clastic barrier islands (Kumar & Sanders, 1974; Donselaar, 1996). The vertical succession of the three architectural elements (AE) correlates with those described by Vilas *et al.* (2002) in active tidal inlets. AE1 with an erosive base and basal lag is a tidal inlet channel deposit covered by cross-bedded sandstones moved by ebb tidal currents (Vilas *et al.*, 2002). Large-scale lateral accretion surfaces formed as the tidal inlet migrated laterally due to the drift current parallel to the barrier island system (Donselaar, 1996). The migration of these tidal inlets is episodic and also depends on the sand storage capacity of the system (Tillmann & Wunderlich, 2013) and nearby continental platforms (Dias & Kjerfve, 2008). The flood tidal current palaeoflow is towards the south-east, and the east–west bipolarity measured in small-scale current structures indicates the activity of both ebb and flood tidal currents. AE2 overlies AE1 and represents the barrier-island platform of the spit that forms in the upper part of the barrier as the tidal inlet migrates laterally (Donselaar, 1996). This architectural element is rarely preserved because the dynamics of the tidal inlet lead to reworking and erosion of the spit. The occurrence of mud drapes and bipolarity of palaeocurrents is indicative of flood and ebb tidal currents in the tidal channels (Nio & Yang, 1989; Donselaar, 1996). The upper architectural element (AE3) records the spit to foreshore sedimentation of the barrier island showing *Skolithos* and well-sorted cross-bedded sandstones (Kumar & Sanders, 1974; Donselaar, 1996; Zonneveld *et al.*, 2001; Jackson *et al.*, 2005).

The open marine platform assemblage includes the facies associations of ebb-tidal delta (FA3.6), shoreface (FA3.7) and tidal sand bars (FA3.8). The stratigraphic architecture and facies associations of the ebb-tidal delta (FA3.6) (Fig. 8D, Appendix S1: Figs S25 and S26) are similar to both modern (Morales *et al.*, 2001) and ancient analogues (Cheel & Leckie, 1990). The good sorting of most of the sandy facies is attributed to wave activity (Sha, 1990) and the fine-grained fining-upward strata represent the distal facies of the ebb-tidal delta (Imperato *et al.*, 1988). The sandy beds bounded by accretion surfaces to the south-east that contain cross-bedding are interpreted as subtidal swash bars of the ebb-tidal delta (Morales *et al.*, 2001). The sandy facies with planar cross-bedding and palaeoflow to the north-east represents tidal bars developed in the shoreface close to the flood channel (Imperato *et al.*, 1988). The occurrence of hummocky cross-stratification (HCS) and swaley cross-stratification (SCS) are interpreted as storm-related deposits in the lower shoreface of the ebb-tidal delta (Cheel & Leckie, 1990; Ito *et al.*, 2001; Peropadre *et al.*, 2007). Tidal sand bars merge laterally to flood tidal channels with superimposed cross-bedding sets laterally to the

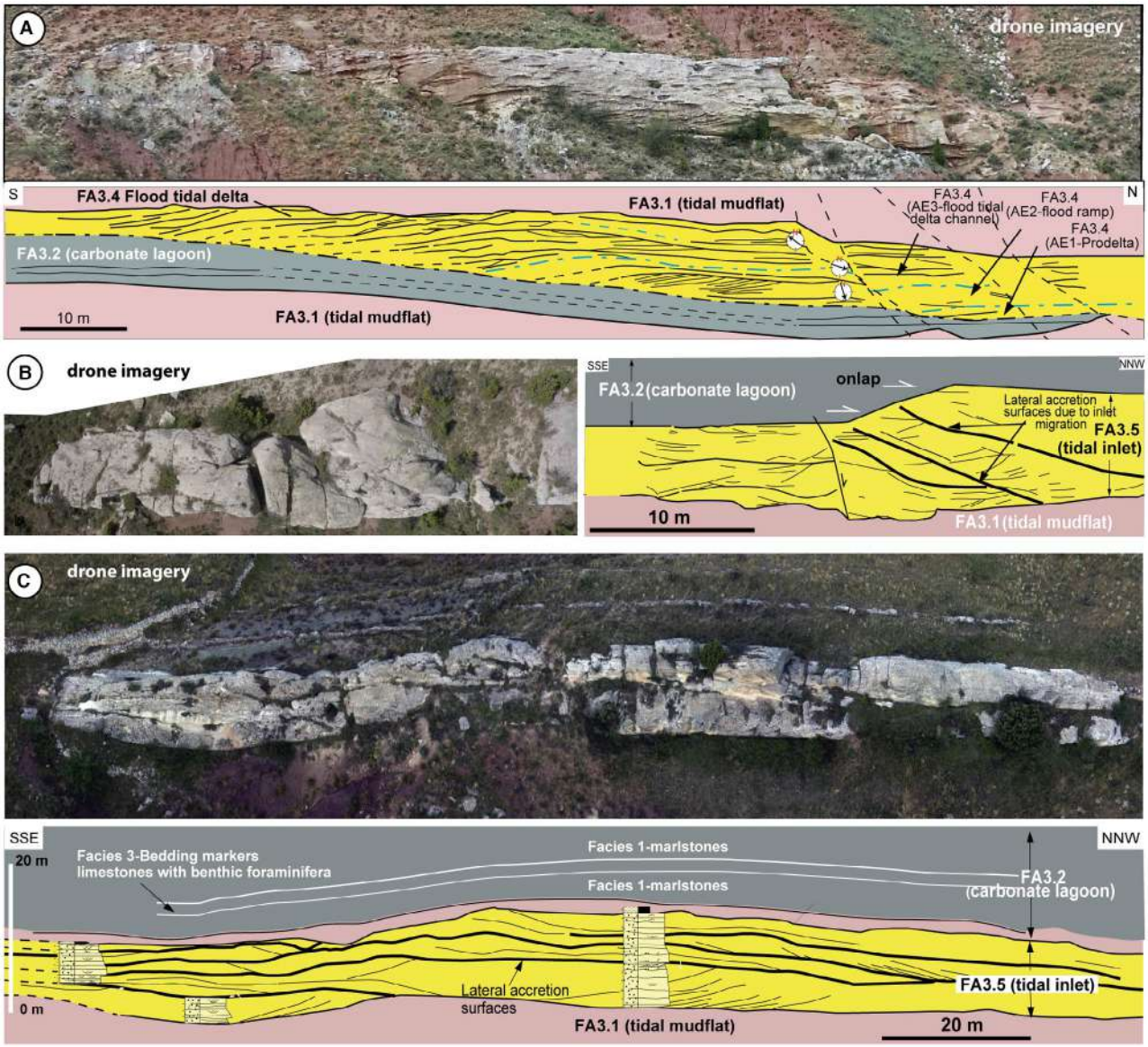

Fig. 7. Back-barrier lagoon facies associations (FAs) distinguished in the barrier island–lagoon system of Stage-3 of the Camarillas Formation in the Galve Sub-basin. (A) Drone imagery and line drawing with the stratigraphic architecture of the flood tidal delta (FA3.4) eroding underlying carbonate lagoonal facies (FA3.2) and tidal mudflat deposits (FA3.1) (see location in B). Flood tidal delta shows a sharp erosional base, and internally shows the vertical stacking pattern of architectural elements (AE), including the prodelta (AE-1) and flood ramp (AE-2) in the lower part, which are covered and eroded by the overlying flood tidal delta channel (AE-3). See detailed facies analysis in Fig. S20. (B) and (C) Drone images of tidal inlet sandstones deposits (FA3.5) and line drawings of stratigraphic architecture and FA distribution. Note that tidal inlet geobodies show: (i) sharp, erosive and generally flat (slightly irregular, locally) bases; (ii) general tabular geometry; (iii) a preserved positive apex in the stratification top leading to onlapping of overlying back-barrier lagoonal and tidal flat FA; and (iv) laterally continuous (>100 m) inclined lateral accretion surfaces due to tidal inlet migration.

main ebb-tidal delta. The occurrence of mud drapes and sigmoidal reactivation surfaces attests to tidal modulation in the channels and bars of the ebb-tidal delta (Richards, 1994; Corcoran *et al.*, 1998). The occurrence of low-angle cross-stratification and parallel lamination at the top of the facies association suggests reworking by waves in the intertidal levée of the margin of the ebb-tidal channel (Morales *et al.*, 2001) and/or in the platform of the spit of the associated

tidal inlet (Cheel & Leckie, 1990). Figure 8D shows a clear stratigraphic and genetic relationship between the ebb-tidal delta and the tidal inlet: the tidal inlet succession is covering and eroding the underlying ebb-tidal delta FA indicating that the lateral migration of the inlet led to the closure and cut off of the ebb-tidal delta disconnecting it from the back-barrier lagoon. This process is recorded twice in the figured outcrop.

The shoreface deposits (FA3.7) include upper shoreface sandstones (AE1) characterized by SCS, and the coarsening-upward trend in these sandstones (Appendix S1: Fig. S27) is associated with the increasing energy of the systems associated with waves (Kirschbaum & Hettinger, 2004; Clifton, 2006). The widespread occurrence of trough and planar cross-stratification indicates that alongshore-drift currents and waves transported sediments forming 2D and 3D megaripples between the fair-weather wave base (FWWB) and the lower wave base (LWB) (Coe, 2003). The occurrence of HCS is interpreted as related to storm currents above the SWB in the offshore transition zone (Duke *et al.*, 1991; Ito *et al.*, 2001). Intra-shoreface shales are commonly reported in similar shoreface successions in areas dominated by wave currents (Haug Eide *et al.*, 2014). The scarcity of bioturbation suggests a rapid migration rate of shoreface bedforms under high-energy conditions that prevented colonization of the upper shoreface (Plink-Björklund, 2005; Veiga *et al.*, 2005). AE2 is interpreted to represent the lower shoreface where HCS and wave ripples formed together with swaley cross-bedding, just above the FWWB.

The tidal bar deposits (FA3.8) show clear frontal accretion surfaces and a coarsening-upward trend (Appendix S1: Fig. S28), as the upper parts of the tidal bars are associated with higher-energy currents compared to the surrounding troughs (Dalrymple *et al.*, 2012; Olariu *et al.*, 2012). The erosive base is related to the migration of the tidal bar and the convex tops resulted from the migration of superimposed bedforms (Yang & Nio, 1989; Dalrymple & Rhodes, 1995; Longhitano, 2011; Olariu *et al.*, 2012). Both the frontal progradation direction towards the north-west and the palaeocurrent towards the south-west from superimposed forms indicate migration in the same direction as the parent tidal bedform (Dalrymple & Choi, 2007; Olariu *et al.*, 2012). The occurrence of HCS with bioclastic (oysters) sandstones is evidence of storm-related currents that affected the lower troughs of these tidal bars (Török, 1998). Bases of the barrier island sandstones constitute wave ravinement surfaces (wRs) (e.g. Cattaneo & Steel, 2003).

DISCUSSION

Depositional model and temporal evolution

Stage 1. Tide-dominated estuary

Stage 1 represents sedimentation in a tide-dominated estuary (13–249 m thick), with a depocentre located in the Camarillas Graben (Fig. 9). Stage 1 is spatially restricted to the Jorcas area showing a limited extent over the underlying El Castellar Formation. It is composed of 71% mudstone, 28% sandstone, and 2% carbonate and marlstone. The sandstone accumulation occurs in the hanging wall of the Miravete Fault (22–90% of total sandstone thickness) and in the Galve area, where the sandstone percentage reaches 42% of the total section. By contrast, the Camarillas and Jorcas areas show lower percentages of sandstone (9% and 15%, respectively). Stage 1 is comprised of two well-differentiated but coeval depositional systems, a fluvial system that transitions laterally and vertically to a tide-dominated system (Fig. 9B).

At the base of the northern and central sectors of the sub-basin, the fluvial system includes three subenvironments (Fig. 9A to C): fluvial channel (FA1.1), tide-influenced tidal channels (FA1.2) and floodplain (FA1.3). In the early part of Stage 1, a fluvial system was active with dominant palaeocurrents towards the south-east (Fig. 9B). Merging laterally and covering these fluvial channels, tide-influenced channels are observed with the first evidence of tidal mud drapes, tidal bundles and north-west and east bipolarity. These tide-influenced channels are located in the northern sections and the El Batán Fault sector (Fig. 9B).

The tidal system of Stage 1 is formed by seven stacked progradational parasequences (1 to 7 in Fig. 9B) that define a general aggradational–retrogradational pattern. This tidal system contains five FAs including muddy intertidal flats with crevasse splays (FA1.5), intertidal and subtidal flats (FA1.6), carbonate ponds (FA1.7), tidal channels (tidal creeks, FA1.8) and subtidal sandbars (FA1.9) (Fig. 9A). The spatial distribution of subenvironments is characterized by retrograding fluvial channels in section 5 merging laterally to the tidal system. Muddy intertidal flats (FA1.5)

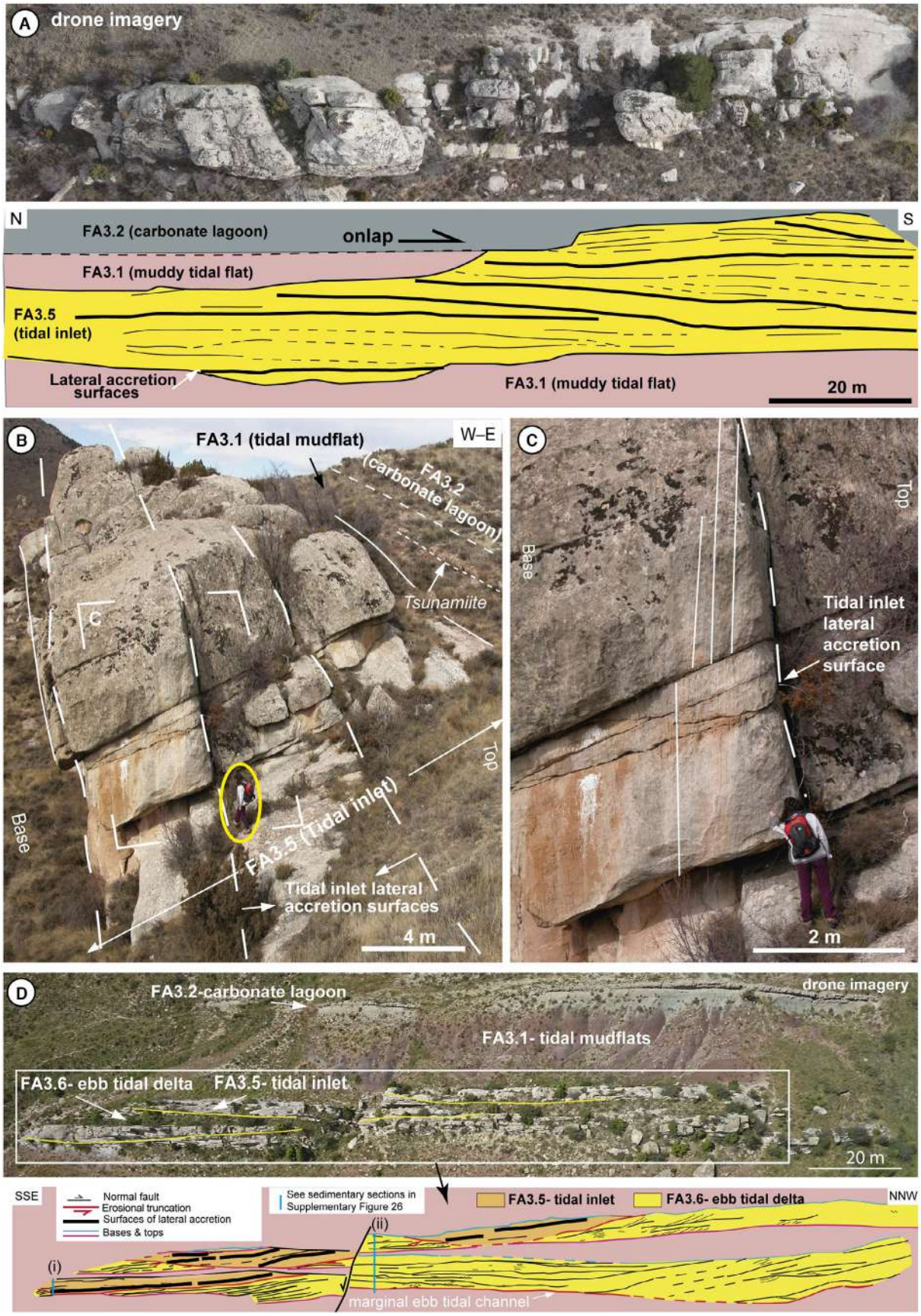

Fig. 8. Barrier island–tidal inlet and open marine facies associations (FAs) distinguished in the barrier island–lagoon system of Stage-3 of the Camarillas Formation in the Galve Sub-basin. (A) Drone imagery and line drawing of the stratigraphic architecture of a tidal inlet FA (FA3.5). Lateral accretion surfaces continue laterally for more than 80 m. The top of the tidal inlet deposit shows, again, a positive tip associated with the lateral migration of the tidal channel on which back-barrier tidal mudflats (FA3.1) and carbonate lagoon (FA3.2) deposits onlap. (B) Field photograph and (C) Close-up view of very large lateral accretion surfaces due to the tidal inlet migration (yellow ellipse encircles geologist for scale). (D) Drone imagery and line drawing of the stratigraphic architecture of ebb-tidal delta deposits (FA3.6) and related FAs showing two parasequences of ebb-tidal deltas sharply covered by eroding tidal inlet facies. Ebb-tidal deltas are prograding to the Tethys (south-east). Sedimentological sections (i) and (ii) can be seen in the Fig. S26.

occupied a widespread area (sections 6–16) and among subtidal sandbars in section 9. Intertidal flats are interbedded with carbonate ponds (FA1.7) and subtidal to intertidal mixed tidal flats (FA1.6) and with muddy supratidal flats with marshes (FA1.4). These tidal flats are interbedded with tidal channels (FA1.8) in the areas near the Miravete Fault, where these tidal creeks locally erode underlying subtidal sandbars (FA1.9) (Fig. 9B). Tidal channels show palaeocurrents towards north-east and WSW. The subtidal sandbars of FA1.9 in section 9 (Miravete area) represent the outermost area of tidal sedimentation (open marine). Tidal sandbars retrograde in the two upper parasequences reaching the northern profiles of the sub-basin (section 5, Fig. 9B) showing main palaeocurrents towards north-east and south-east, which represented flood and ebb tidal currents, respectively (Fig. 9C).

Stage 2. Mixed-energy, wave-dominated, tide-influenced estuary

Stage 2 represents sedimentation in a wave-dominated and tide-influenced estuary (Figs 10, 11 and 12). This stage is recognized across the entire Galve Sub-basin, and its development indicates an expansion of the depositional area. There are, however, significant variations of preserved total thickness. Similar to the previous stage, Stage 2 has maximum thicknesses in the Camarillas Graben (418 m thick) and thins towards the north (133 m thick) (Fig. 11). Deposits formed during this stage are made up of 79% mudstone, 20% sandstone, and 1% limestone and marlstone. Depocentres of sandy lithofacies are located in the northern and southern sectors of the basin (23–33%), whereas the central part of the basin contains lower percentage of sandstones (8–19%).

During Stage 2, a sandy bayhead delta, a muddy central section, and an outer sandy part accumulated (Figs 10 and 12). The proximal estuary area is located in the northern parts of the sub-basin (Figs 11 and 12) and shows five genetically related facies associations: inner tidal bars (FA2.1); bayhead delta (FA2.2); supratidal and intertidal mudflat with crevasse splays and ponds (FA2.3); inner heterolithic intertidal flat (FA2.4); and inner estuary tidal channels (FA2.5). Deposits in the central part of the sub-basin are central bay mudstones (FA2.6). Deposits in outer zone areas of the estuary, located towards the south, contain seven facies associations, including deposits of outer estuary tidal channels (FA2.7), outer heterolithic tidal flats with ponds (FA2.8), outer estuary tidal sandbars (FA2.9), flood-tidal delta in the mouth of the estuary (FA2.10), washover fans (FA2.11), tidal inlets (FA2.12) and the open marine shoreface (FA2.13).

Stage 2 is organized into 12 parasequences (1 to 12 in Fig. 11). This stage initially shows a regressive pattern (parasequences 1 to 3) towards the south of the Galve Sub-basin leading to the south-eastward progradation of the inner tidal bars of the estuary over intertidal flats surrounding the estuary margins in the central sector (section 7; Figs 11 and 12). At the north, sections 3 and 14 record several bayhead deltas, with south-east and east palaeocurrents, interbedded with supratidal and intertidal flats. The southernmost section 16 shows central bay mudstones interbedded with outer estuary tidal channels with palaeocurrents to the north-west and south-east indicating strong flood and ebb tidal currents.

This basal prograding interval of the estuary is overlain regionally by a complex retrograding estuarine interval (parasequence 4), by which the bayhead deltas are covered by retrograding intertidal flats interbedded with tidal channels and heterolithic tidal flat deposits. Abundant coal fragments and carbonaceous plant fragments are evidence of tidal salt marshes in the estuary. Palaeocurrents in the tidal creeks are variable, but they show a dominant SSW and north-west direction. The central bay of the

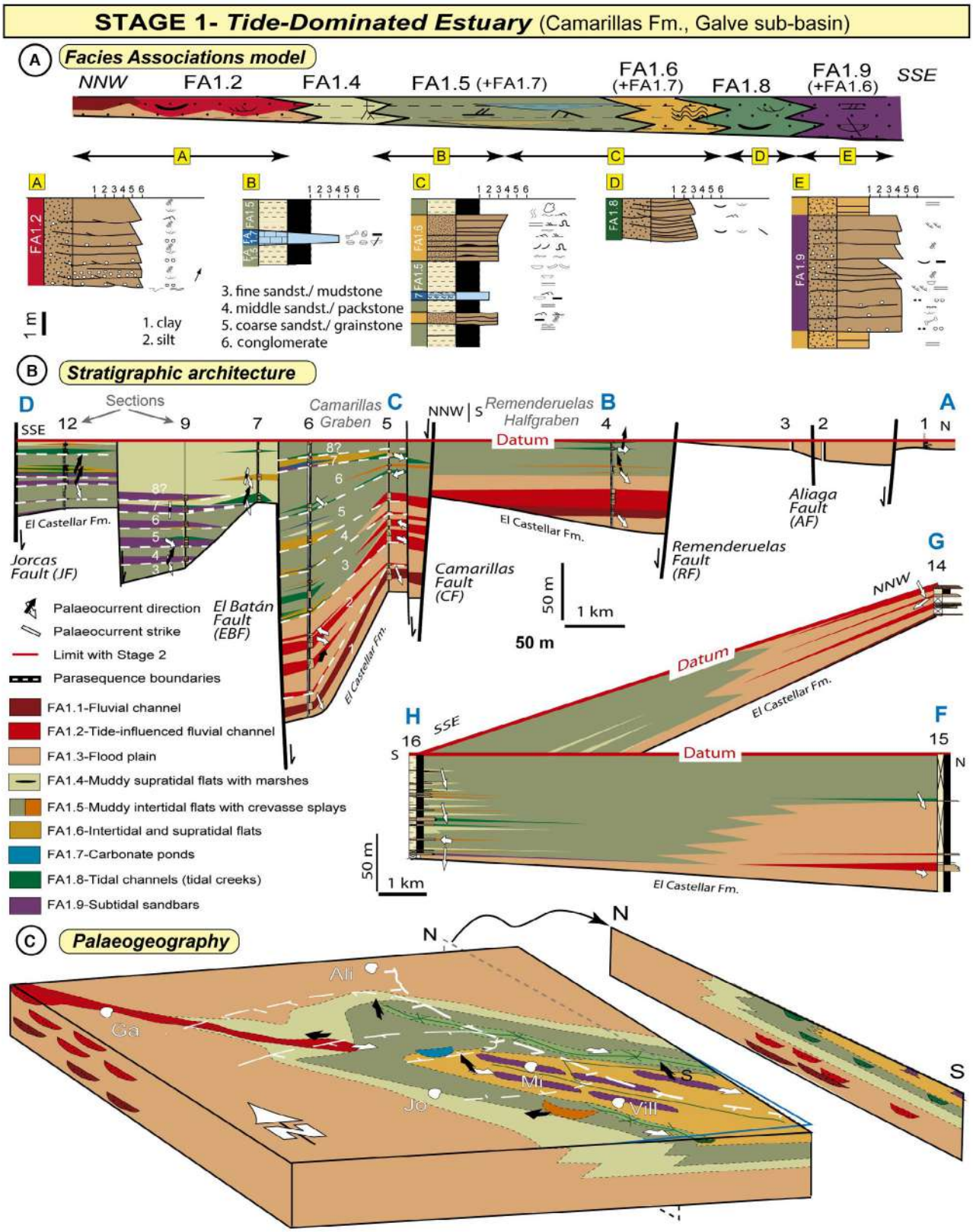

Fig. 9. Facies associations (FAs), stratigraphic architecture and palaeogeography of tide-dominated estuary of Stage 1. (A) Spatial distribution and common associations of FAs. See Table 1 for FA descriptions and interpretations and Fig. 3 for legend of sedimentological logs. (B) Stratigraphic–sedimentological architecture of FA showing the boundaries between parasequences (white discontinuous lines and white numbers) and the changes in thickness. See Fig. 2B for location of correlation panels and text for discussion. (C) Basin-scale genetic model showing the spatial distribution of the Barremian tide-dominated estuary. Tethys Sea is towards the south-east and the Iberian Massif to the north-west. Main synsedimentary extensional faults are indicated. Letters refer to geographical references (villages): Ali, Aliaga; Jo, Jorcas; Ga, Galve; Mi, Miravete; Vi, Villarroya de los Pinares.

estuary shows thick muddy facies interbedded with outer tidal channel and outer hetherolitic tidal flat deposits (section 15) with dominant flood tidal currents towards the north and showing marine bioturbation (Figs 11 and 12). In the outer area of the estuary for this same interval, central bay mudstones are interbedded with tidal inlet sandstones and washover fans that pinch out to the north, indicating that the barrier island of the mouth of the estuary was located to the south.

Next, the estuary system shifted towards the south concurrent with a significant period of vertical aggradation (parasequences 5 to 10), for which every parasequence is regressive. The long-term evolution of the system led to deposition of central bay mudstones interbedded with flood tidal deltas (section 16) and prograding towards the north, and outer estuary tidal bars that show bidirectionality (south-east and north-west) and reach central sections (section 6) in the estuary. The uppermost two parasequences (11 and 12; Fig. 11) define a marked retrogradational pattern. The outer sector of the mixed estuary was characterized by complex transitions between coeval FAs, including intertidal and subtidal flats, carbonate ponds and washover fans (retrograding to the north-east and east). Similar coexistence of estuarine systems and barrier-islands as those of the Camarillas Formation have also been described previously from depositional systems in the Upper Cretaceous Sego Sandstone Member, in Colorado USA (Painter *et al.*, 2013), and similar outer estuarine sandbars have been also described by Steel *et al.* (2012) in the tide-dominated estuarine system of the Campanian Chimney Rock Sandstone (Plink-Björklund, 2008) and by Allen & Johnson (2010, 2011) and Johnson *et al.* (2017) in the Late Cretaceous John Henry Member in Utah.

Stage 3. Barrier island systems

Two sub-stages (3a and 3b) are recognized (Fig. 13). Sub-stage 3a deposits are 62% sandstone, 30% mudstone and 9% carbonate and marlstone. Sub-stage 3a deposits vary in thickness from 19 to 149 m, with a depocentre in the Camarillas Graben (Fig. 14). Thickness variations are due to the synsedimentary activity of the extensional faults associated with the basin, especially the Remenderuelas, El Batán, Camarillas and Jorcas faults (Navarrete *et al.*, 2013a; Navarrete, 2015). The Miravete Fault was characterized by less activity relative to stages 1 and 2.

Sub-stage 3a deposits are interpreted to be from a mixed-siliciclastic–carbonate barrier island–back barrier lagoon system (Navarrete *et al.*, 2013b) comprised of eight facies associations, organized within six parasequences (Fig. 13). Facies associations include those associated with the back-barrier lagoon (tidal mudflats with tidal creeks and marshes, FA3.1; carbonate back-barrier lagoon, FA3.2), the interaction among the back-barrier lagoon and the barrier island system (washover fans, FA3.3; flood-tidal delta, FA3.4), those properly related to the barrier island dynamics (tidal inlet/barrier island, FA3.5) or resulting from the interaction of the barrier island and the open marine system (ebb-tidal deltas, FA3.6), and coeval open marine environments (shoreface, FA3.7; and tidal bars, FA3.8) (Figs 14 and 15). A similar spatial distribution of coeval depositional systems is observed from the Holocene to Recent Rømø barrier island in the Danish Wadden Sea (Johannessen *et al.*, 2008) and the occurrence of barrier islands retrograding over back-barrier marshes has been reported from Chesapeake Bay deposits (Cooper, 2013; Cooper *et al.*, 2018).

Although sub-stage 3a deposits record higher-order cycles of progradation and retrogradation (parasequences 1 to 7 in Fig. 14), the system shows a general retrograding pattern to the north and east of the sub-basin. In this way, the barrier island system of stage 3a retrogrades over the underlying mixed-estuary system, so that the first shoreface associated with the barrier island is

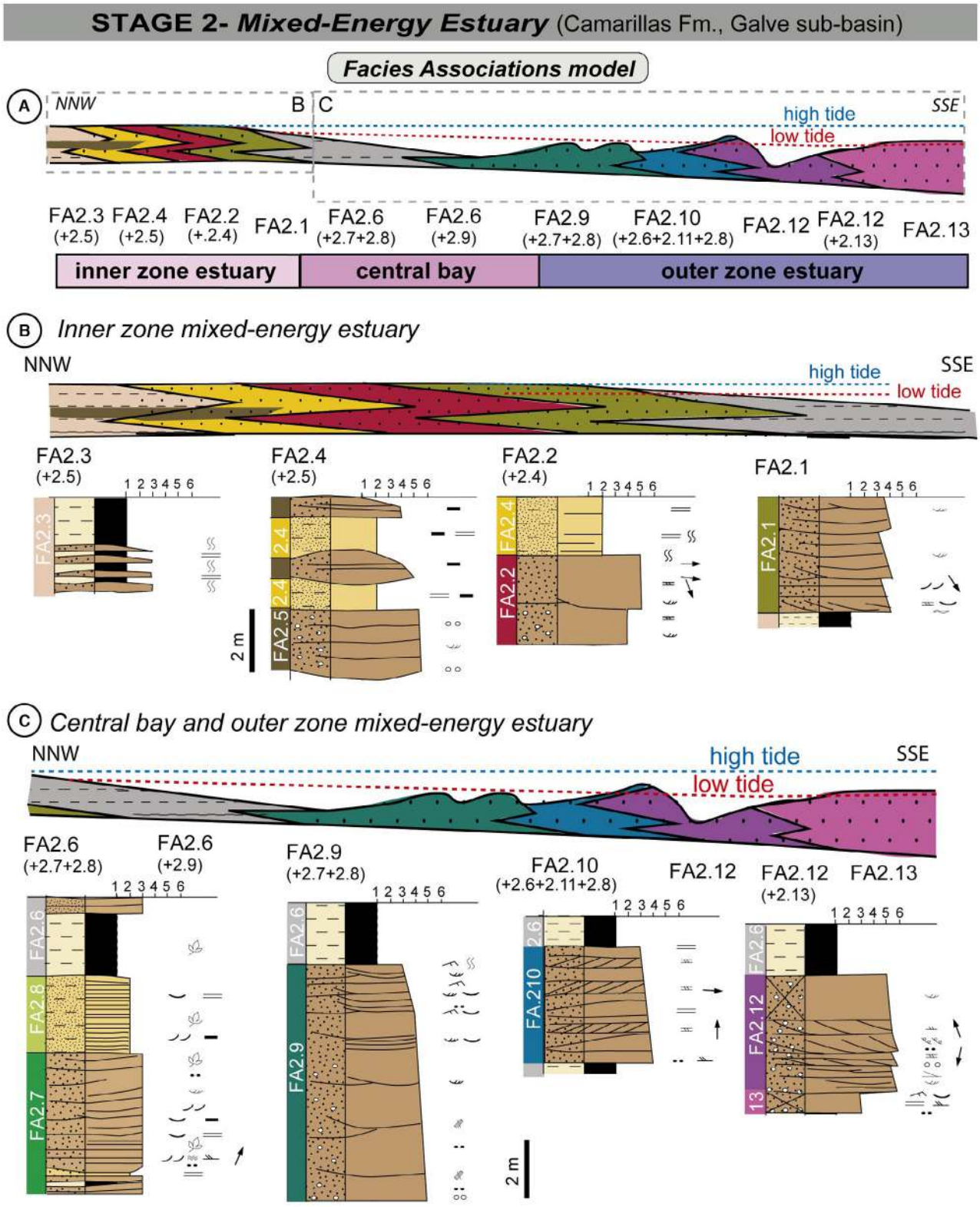

Fig. 10. Facies associations (FAs) of the mixed-energy estuary of Stage 2. (A) Spatial distribution and common associations of FAs. See Table 2 for descriptions and interpretations of FA. (B) Associations of FA in the inner estuary. (C) Associations of FA in the central bay and outer estuary. See legend of sedimentological logs in Fig. 3.

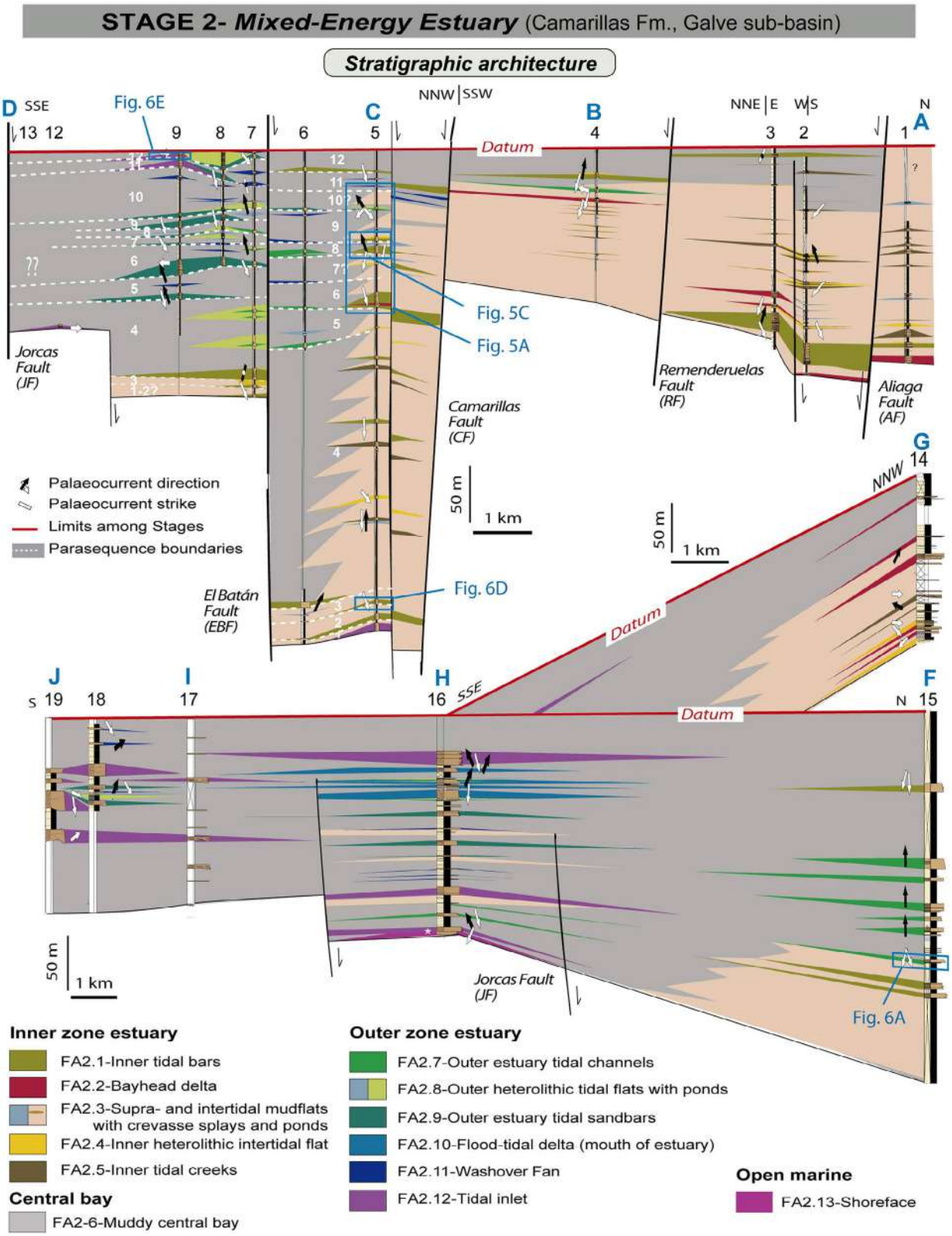

Fig. 11. Stratigraphic–sedimentological architecture correlation of facies associations (FA) of mixed-energy estuary of Stage 2. See Table 2 for descriptions and interpretations of FA, and Fig. 2B for location of correlation panels. Parasequence boundaries are marked by discontinuous black lines and numbers. Central and outer sector of the estuary to the south, and inner zone to the north.

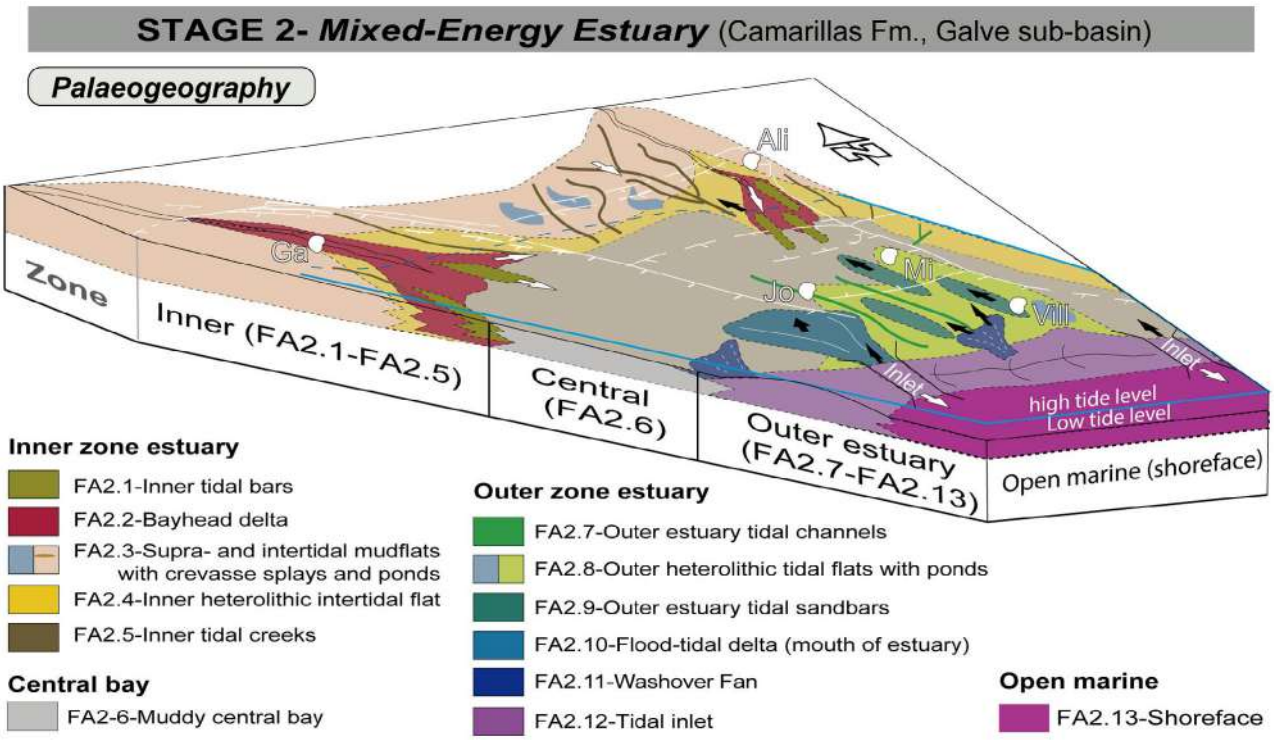

Fig. 12. Basin-scale genetic model showing the spatial distribution of the Barremian mixed-energy estuary of Stage 2. Tethys Sea is towards the south-east and the Iberian Massif to the north-west. Letters refer to geographical references (villages): Ali, Aliaga; Jo, Jorcas; Ga, Galve; Mi, Miravete; Vi, Villarroya de los Pinares. Main synsedimentary extensional faults are indicated. The spatial distribution of facies associations (FAs) and zones of the estuary are indicated. See Table 2 for descriptions and interpretations of FAs.

recorded for the first time in section 5 (parasequence 3). After this initial retrogradation, the barrier island depositional system and associated subenvironments prograded towards the south and west of the basin (sections 12 and 13) creating an extensive back-barrier lagoon to the north and east of the sub-basin (parasequences 4 and 6). This lagoon was characterized by an extensive back-barrier muddy tidal flat (FA3.1) with interbedded coal seams due to the presence of back-barrier marshes and tidal creeks. Lagoonal carbonates appear in four successive intervals and are characterized by a low diversity of biota, including bivalves, charophytes, ostracods and gastropods. The first carbonate interval is the most extensive (parasequence 4), being recorded in the whole basin from sections 3 to 12 (in the north and south), and from section 11 to 14 (east and west) where it is eroded by flood-tidal delta deposits (FA3.4) (Fig. 14); the successive three back-barrier lagoonal intervals show more restricted areas (sections 13 and 15 to the north and east, respectively). Lagoonal marlstones appear between tidal flats and carbonate lagoons in areas towards the north, with a major input of siliciclastic sediments. These back-barrier carbonates contain tempestite intervals and washover fan deposits (FA3.3) that pinch out into the back-barrier system to the north, north-east and south-east, corroborating the existence of a siliciclastic barrier island to the south and west of the basin (Figs 14 and 15). The upper back-barrier system (parasequence 6) contains a thin, basin-wide tsunamite (Navarrete *et al.*, 2014).

The sandy barrier island generated by the lateral migration of tidal inlets formed the outer zone of the barrier system (Figs 13 and 14). It passes laterally to the back-barrier lagoon to the north and to open marine waters of the Tethys to the south (Fig. 15). Flood tidal currents moved siliciclastic sediments of the barrier island into the back-barrier lagoon with a dispersion of palaeocurrents from north-west to south-east, suggesting again the location of the barrier islands to the west and south of the basin. The recurrent retrogradations of the barrier islands and associated flood-tidal and ebb-tidal deltas (for example, parasequences 3 and 6; Fig. 14)

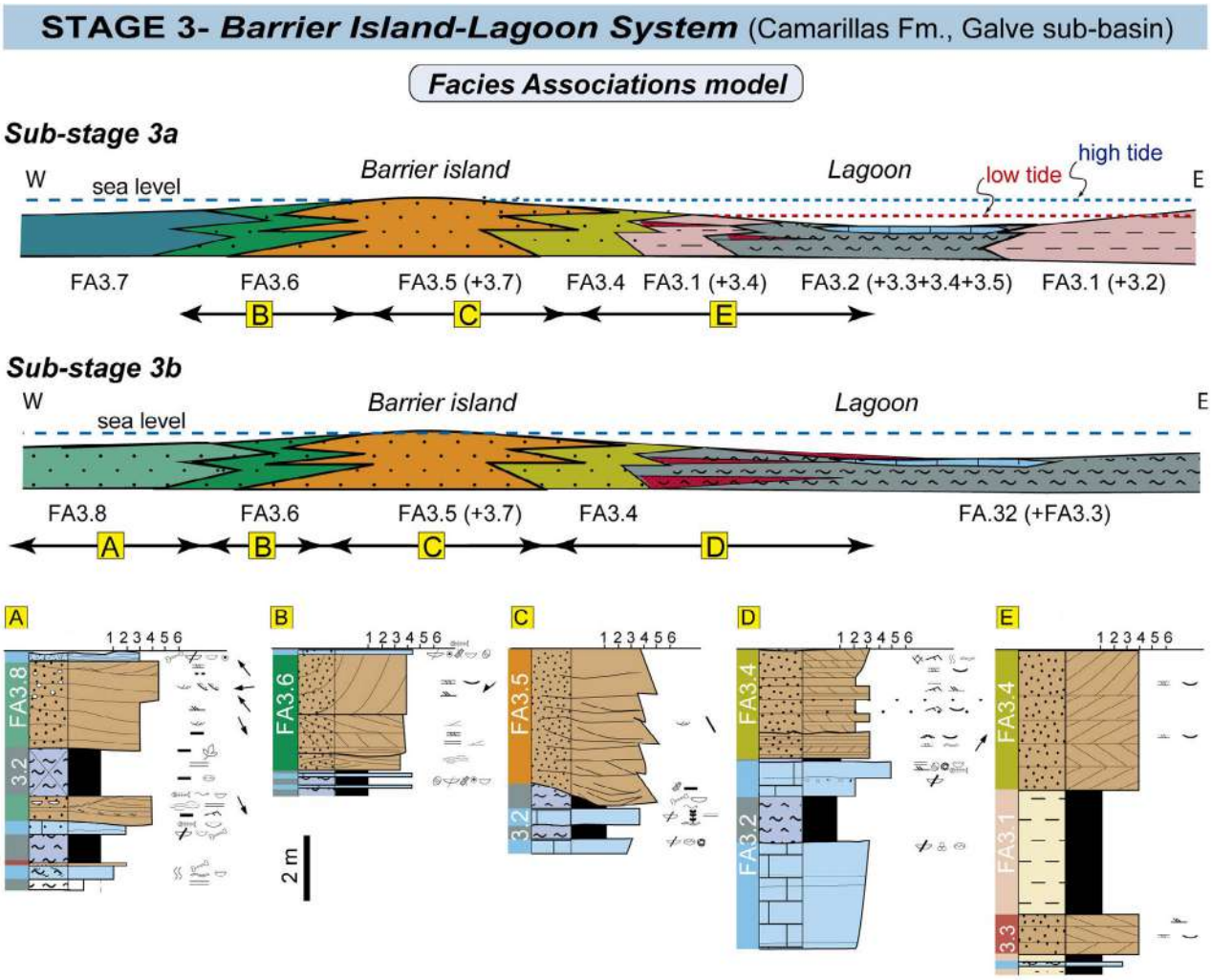

Fig. 13. Spatial distribution of facies associations (FAs) showing the common associations of FA of the barrier island–tidal inlet system of Stage 3, separating sub-stages 3a and 3b. See Table 3 for descriptions and interpretations of FAs.

led to the development of tidal ravinement surfaces that eroded underlying back-barrier deposits. Tidal inlets migrated to the south-east and north-east. The net aggrading stacking pattern of sub-stage 3a causes the barrier island successions to be sharply covered by aggrading back-barrier depositional systems, contrary to the frequent ravinement of barrier islands by shoreface deposits in stacked parasequences in these depositional systems (e.g. Allen & Johnson, 2011; Mulhern *et al.*, 2019).

Sub-stage 3b deposits are thinner than 3a deposits (4–26 m) and represent a regional transgression leading to an increase in carbonate deposition within the basin (reaching 68% versus 20% sandstone and 12% mudstones; Figs 13, 14 and 15). The thickness of this interval is remarkably consistent compared with earlier stage deposits (Fig. 14), suggesting a decrease in extension rates associated with synsedimentary faulting. Although sub-stage 3b depositional environments were similar to those of the barrier island system that accumulated during sub-stage 3a, more restricted back-barrier lagoon deposits suggest that there were a smaller number of tidal inlets.

Sub-stage 3b begins with a barrier island system, oriented north–south, following the strike of the NNW–SSE Cañada Vellida and WSW–ENE Jorcas faults (Fig. 15). This barrier island was located in sections 13, 15 and 16 in Galve–Camarillas–Jorcas and lateral facies change to back-barrier carbonates (FA3.2) to the north-east

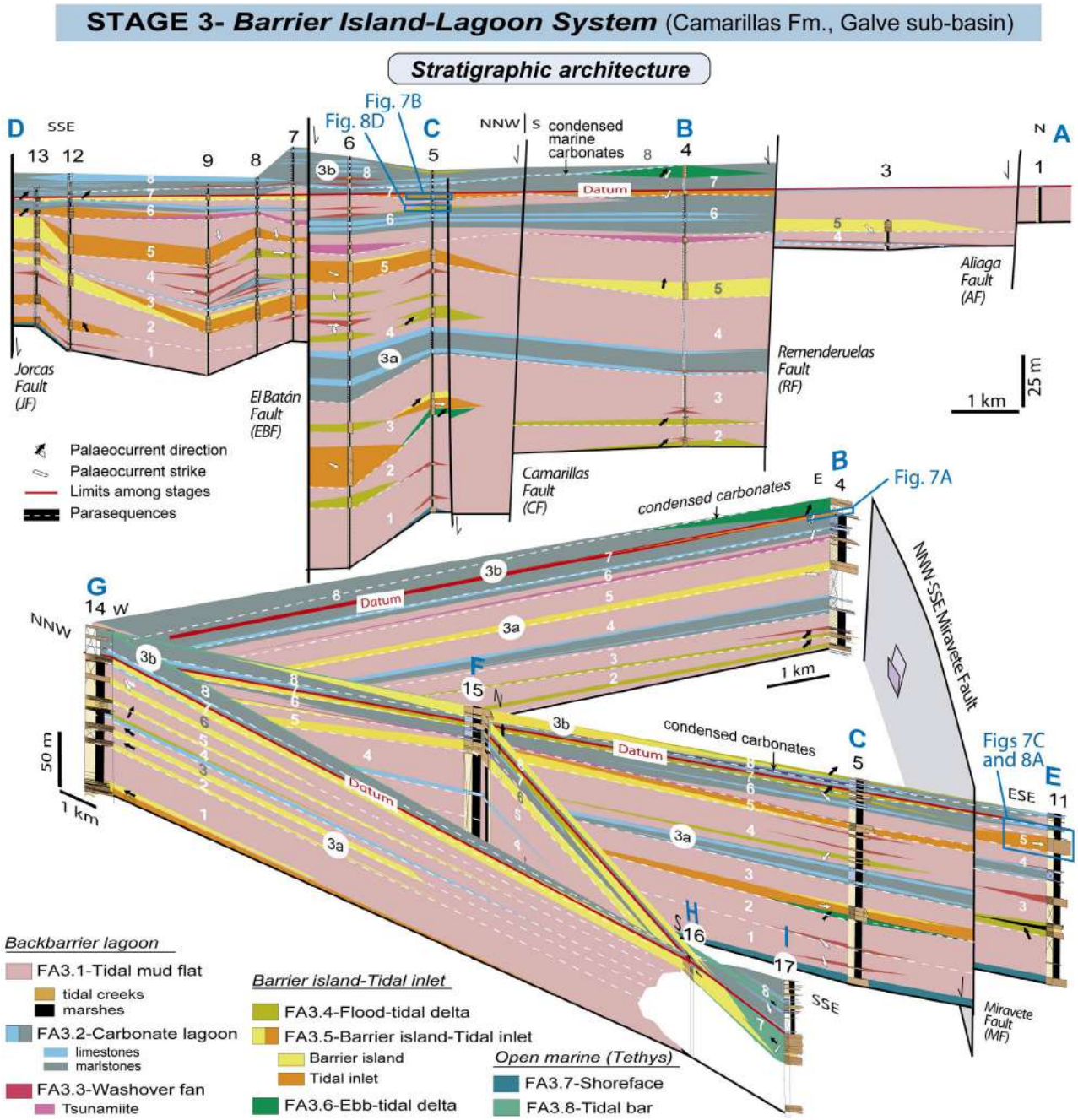

Fig. 14. Stratigraphic–sedimentological architecture of facies associations (FAs) of barrier island–lagoon system of Stage 3 (sub-stages 3a and 3b). See Table 3 for descriptions and interpretations of FAs and Fig. 2B for correlation panels location. Parasequence boundaries are marked by discontinuous black lines and numbers.

and to open marine tidal bars (FA3.8) to the south (Figs 14 and 15). During this sub-stage, tidal inlets migrated to the south-east/ESE with a subsidiary component to the east/west. Open marine tidal bars moved to the south-east with bipolarity to the north. During this interval the back-barrier lagoon (FA3.2) and its associated washover fans (FA3.3), flood-tidal deltas (FA3.4) and ebb-tidal deltas (FA.3.6) prograded. The system experienced abrupt retrogradations whereby open marine deposits (condensed carbonates in parasequence 8; Fig. 14) abruptly covered both flood tidal delta deposits and back-barrier lagoonal deposits, defining transgressive

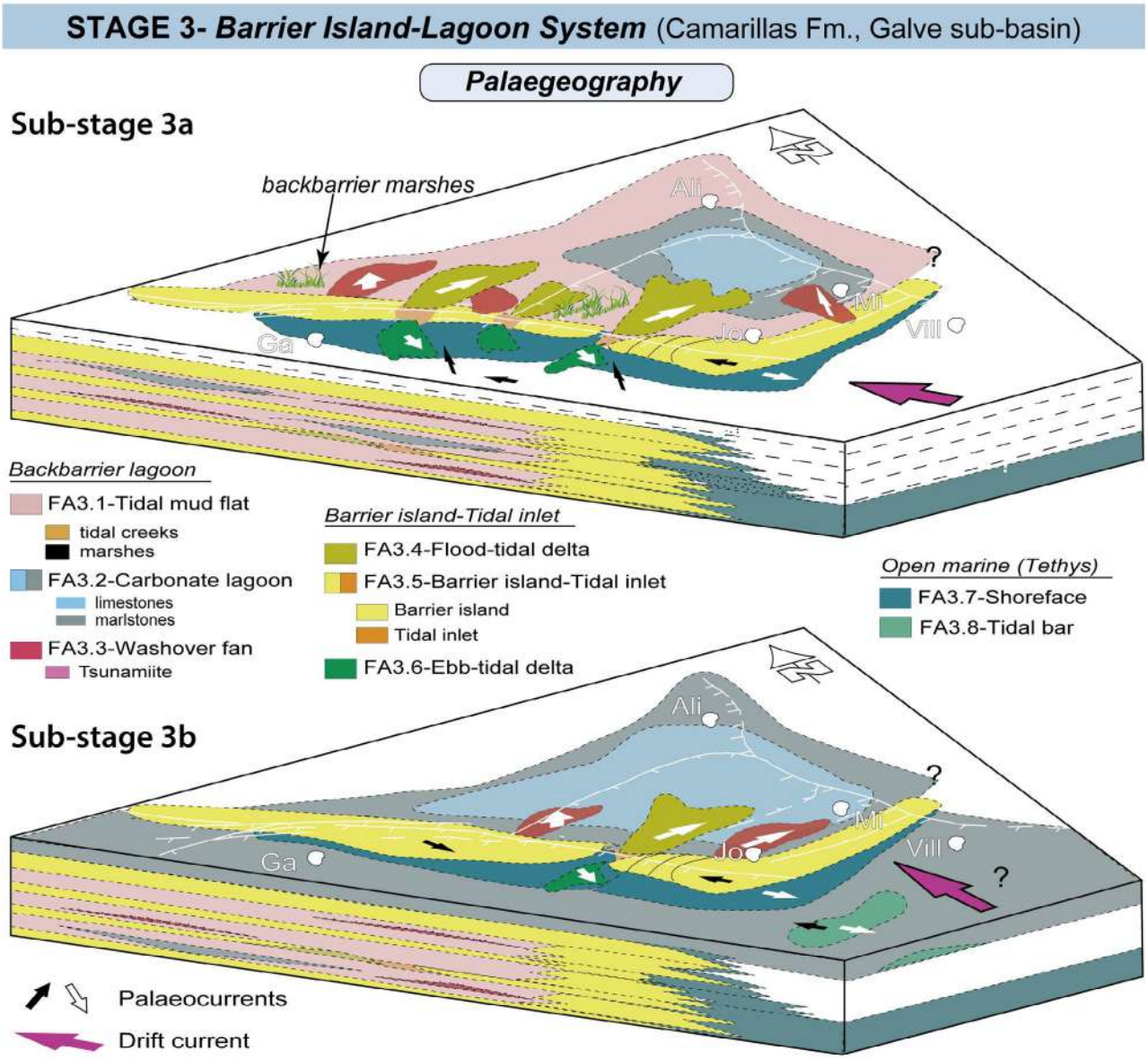

Fig. 15. Basin-scale genetic model showing the spatial distribution of the Barremian barrier island–tidal inlet Stage 3 (sub-stages 3a and 3b). Tethys Sea is towards the south-east and the Iberian Massif to the north-west. Letters refer to geographical references (villages): Ali, Aliaga; Jo, Jorcas; Ga, Galve; Mi, Miravete; Vi, Villarroya de los Pinares. Main synsedimentary extensional faults are indicated. The spatial distribution of facies associations (FAs) and zones of the estuary are indicated. See Table 3 for descriptions and interpretations of FAs.

surfaces containing glauconite, serpulid and phosphate accumulations (Amorosi, 1995; Dreyer *et al.*, 1999; Navarrete *et al.*, 2013b). Following these brief retrograding events, back-barrier lagoon progradation is restored along with flood tidal deltas, which is evidence for the restoration of active back-barrier systems after regional transgressive events. Recurrent retrogradations of tidal inlets/barrier island-derived flood-tidal deltas led to reworking of back-barrier marshes that formed extensive lags of carbonaceous plant fragments at the base of flood tidal deltas. The flood tidal delta located in section 5 with palaeocurrents to the east and north-east corroborates the location of a system of barrier islands to the south. Sand wave deposits can be correlated with these flood tidal delta systems.

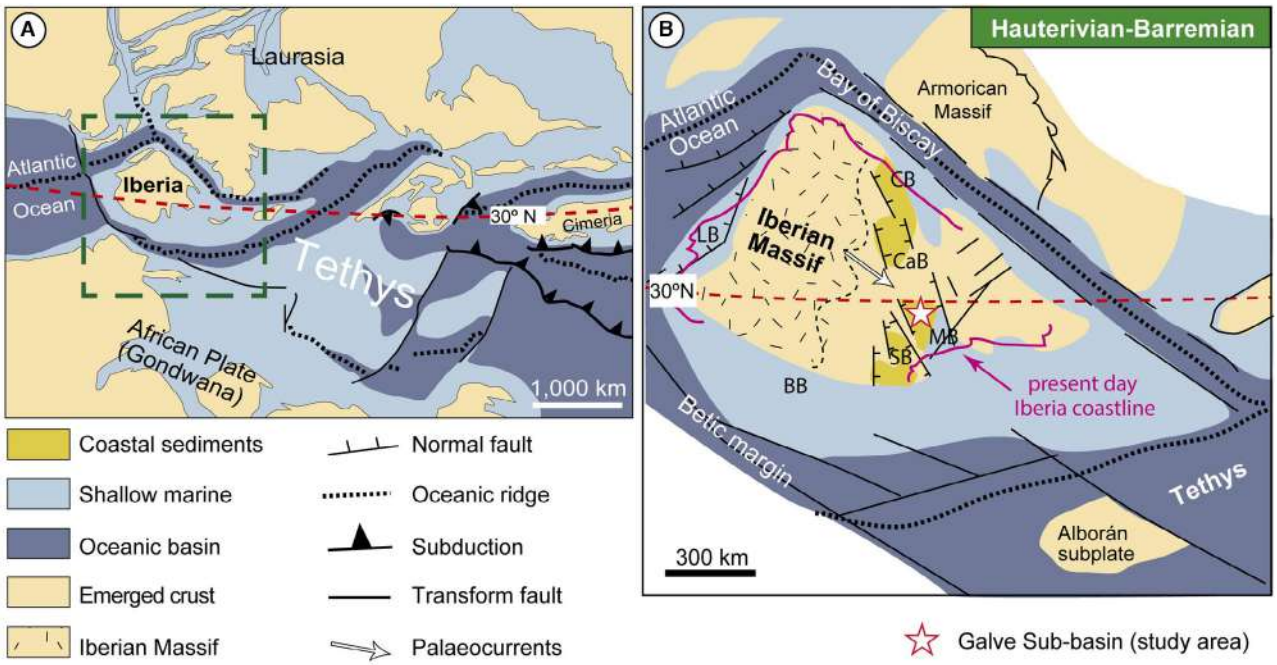

Fig. 16. (A) Western Tethys palaeogeography showing the location of Iberia (modified after Blakey, 2014). (B) Detailed Hauterivian–Barremian palaeogeography showing the location (red star) of the studied area (Galve Sub-basin) (modified after Salas *et al.*, 2001). BB, Betic Basins; CaB, Cameros Basin; CB, Cantabrian Basin; LB, Lusitanian Basin; MB, Maestrazgo Basin; SB, South Iberian Basin.

Overall evolution

The vertical evolution of the three siliciclastic depositional stages described in the Lower–Upper Barremian Camarillas Formation of the Galve Sub-basin is retrogradational. This general transgressive trend supports a significant eustatic sea-level rise during the Early Barremian, which has been interpreted to reach 160 to 170 m above present sea level (Haq, 2014). During this period, Haq (2014) also inferred short-order cycles of eustatic variations in sea level that correlated with the development of major sequence boundaries and sea-level events. The three distinct stages in the present study may be related to these sea-level events, but additional analyses need to be done to provide age constraints for the sediments in order to correlate them.

A thick muddy coastal succession in a rift basin

The Camarillas Formation includes an unusually thick accumulation (300 to 1000 m) of paralic deposits. Muddy deposits account for up to 70% of the total thickness of estuarine stages 1 and 2, decreasing to 30% during the barrier island Stage 3. The great thickness of the unit and its thickness changes are attributed to high subsidence and sedimentation rate associated with extensional faulting in a rift basin setting (Figs 9B, 11 and 14). Navarrete *et al.* (2013a) and Navarrete (2015) relate the structural controls on sedimentation to two sets of normal faults trending NNW–SSE and ENE–WSW (Fig. 2B). Based on cyclostratigraphy analysis, Navarrete (2015) infers a time span of 0.7, 0.5 and 0.7 Ma for stages 1, 2 and 3, respectively, and a mean sedimentation rate >200 m/Ma for the entire unit (based on cyclostratigraphic analysis and total compacted thickness; Navarrete, 2015). In the thickest section (profile 5; Figs 9, 11 and 14), sedimentation rates reached 184, 830 and 224 m/Ma for stages 1, 2 and 3, respectively. This paralic system had three main sources of sediments: (i) fine-grained fluvial sediments derived from distant source areas to the west that accumulated in the central bay and associated lateral tidal marshes and mud flats; (ii) sand-dominated sediments derived from coastal drift currents reworked by the combined action of waves and tides; and (iii) windblown dust that may have been a primary contributor to the fine-grained fraction of these

coastal sedimentary environments (e.g. Brookfield, 2004), considering the long-term arid climate setting that governed Barremian sedimentation on the Iberian plate (e.g. Rodríguez-López *et al.*, 2006; Navarrete, 2015; Dinis *et al.*, 2020).

The preferential accumulation of sandy facies was governed by the synsedimentary activity of normal faults that controlled the location of sandy barrier islands in uplifted footwall fault blocks characterized by high-energy sedimentary environments (Navarrete *et al.*, 2013b). This ultimately formed a preferential trap for back barrier fine-grained sediments, which accumulated within central bays in areas of high subsidence and low energy leading to thick synrift mudstone intervals. Similarly thick syntectonic bay-estuary mudstones accumulated in the Sanriku-oki forearc basin, north-east, Japan, where muddy facies are up to 110 m thick (Takano & Tsuji, 2017).

The long-term aggradational to retrogradational trend of the Barremian paralic succession in the Galve Sub-basin was punctuated by regressive parasequences, the bases of thick sandy barrier island parasequences constituting wave ravinement surfaces (wRs), and the bases of tidal flat parasequences and tidal inlets representing tidal ravinement surfaces (tRs) (*sensu* Cattaneo & Steel, 2003). The vertical stacking pattern of tidal and barrier-island parasequences in Stages 2 and 3 (Figs 11 and 14) attests to rapid and recurrent transgressive–regressive cycles (Navarrete *et al.*, 2013b). Although the long-term aggrading nature and the exceptional preserved thickness of the succession confirm an active role of tectonic subsidence, the parasequence stacking patterns point to a superimposed high-order allogenic control on the paralic succession. Cretaceous glacioeustasy cannot be ruled out as an allogenic control (Peropadre *et al.*, 2013), because recent work demonstrates an active early Cretaceous cryosphere during the supposed archetypal Cretaceous super greenhouse (Rodríguez-López *et al.*, 2022).

Siliciclastic sediments and source area: Barremian Iberia microplate, palaeoclimate forcing and palaeoceanic response

A peculiar feature of the Galve Sub-basin is the intercalation of siliciclastic units, the most important being the Barremian Camarillas Formation, in the dominantly carbonate basin fill that characterized the latest Jurassic–Early Cretaceous synrift transitional to shallow marine sequence. Palaeogeographical reconstructions for the Barremian (Dercourt *et al.*, 1986, 2000; Favre & Stampfli, 1992; Stampli & Borel, 2002; Blakey, 2008, 2014) show emerged continental areas (Iberian Massif) in the central and western sector of the Iberian microplate (Fig. 16). During the Barremian, Iberia was bounded by extensional margins: the Betic margin to the south-east, the Central Atlantic to the north-west, and the Bay of Biscay to the north-east. Several authors have suggested that this palaeogeography could lead to significant flexural uplift of the Iberian crust during the Early Cretaceous (Rodríguez-López *et al.*, 2010; Peropadre, 2012). This uplift could have been particularly significant on the north-western margin (Lusitanian Basin) due to extension rates (2 cm/yr) associated with the Central Atlantic rift that triggered a first phase of counter-clockwise rotation of the Iberian microplate (Olivet *et al.*, 1984; Ziegler, 1988; Favre & Stampfli, 1992; Vissers & Meijer, 2012; Frasca *et al.*, 2020).

Lithospheric thinning coupled with thermal uplift of the rifted (shoulder) margin in western Iberia (e.g. Winterer *et al.*, 1988) likely created a major uplifted source area for both the peripheral Cretaceous basins in Iberia (Lusitanian, Cantabrian and Betic basins) and intraplate basins (Cameros, Maestrazgo and South Iberian) (e.g. Mas *et al.*, 1993; Vilas *et al.*, 2002; Dinis *et al.*, 2008; Liesa *et al.*, 2019). This uplifted Iberian Massif hosted the headwaters to a drainage network feeding depositional systems of the Tethys Sea. The Palaeozoic plutonic and metamorphic rocks of the massif (Fig. 1A), located 300 km west of the study area, acted as the main sediment source for the Barremian siliciclastic coastal depositional systems of the Camarillas Formation, as suggested by provenance analysis (Caja, 2004; Caja *et al.*, 2005) and the distribution of palaeocurrents (Soria, 1997; Navarrete, 2015).

The large volume of clastic sediments recorded in the Camarillas Formation of the Galve Sub-basin, and nearby sub-basins of the Maestrazgo Basin (Liesa *et al.*, 2019), suggests increased denudation rates of the Iberian Massif, as described by Winterer *et al.* (1988). These high rates of erosion could have been facilitated both by tectonic uplift of the terrane and by favourable climatic conditions. Tectonically induced uplift was probably an important factor because, during the Barremian, most of the basins in Iberia (Maestrazgo, South Iberian, Cameros) recorded the phase of greatest

subsidence (>200 m/Ma) of the syn-extensional stage of the Latest Jurassic–Early Cretaceous (Salas & Casas, 1993; Salas *et al.*, 2001; Liesa *et al.*, 2006, 2019; Omodeo Salè *et al.*, 2014). The authors interpret that extensional tectonism controlled basin subsidence at different scales, as well as differential uplift of basin margins and sediment source areas, as suggested by extensive rotation of blocks and differential erosion associated with recognized faults in the peripheral zones of such basins (Capote *et al.*, 2002; Liesa *et al.*, 2019, and references therein).

The high erosion rates of the Iberian Massif during the Barremian would imply scarce vegetation (e.g. Dalrymple *et al.*, 1992; Zaitlin *et al.*, 1994), with a predominance of xerophyte species such as *Classopollis* (Jarzen & Nichols, 1996). *Classopollis* has been recorded in the coastal systems studied here, with abundance in the range of 60 to 90% in the upper levels of Stage 2 (Navarrete, 2015), which clearly suggests arid palaeoclimate conditions (Vakhrameev, 1991). Although the Barremian climatic interpretation of Iberia at a subtropical latitude (e.g. Scotese *et al.*, 2021) is still under discussion, this and other evidence points to a dry and warm climate. A dry and warm climate is suggested by fossil records (Médus, 1970), mudstone compositions (Dinis *et al.*, 2020) and palaeosols (Bárdossy, 1982; Wright *et al.*, 2000; Godet *et al.*, 2008; Föllmi, 2012), and is supported by palaeoclimate models (LAM; Haywood *et al.*, 2004) that predict relatively high surface temperatures and low precipitation rates for the Early Cretaceous.

The palaeogeographical location of the basin in tropical latitudes under a prevailing arid climate would have implied torrential rains concentrated during the rainy years, causing the discharge of large sediment volumes into the basin, irregularly distributed across sequential years. The elevated massif under a prevailing arid climate with strong seasonality would have been affected by a mountain climate regime receiving significant precipitation, as occurs in the Atlas Ranges in Morocco (Cecil, 1990).

The scarcity of carbonate deposits in the studied succession could be related to the calcification global crisis that occurred during the Early Cretaceous, as suggested by carbon isotope anomalies in both pelagic environments and carbonate platforms of northern Tethys (e.g. Föllmi *et al.*, 1994, 2006; Weissert & Erba, 2004). The scarcity of carbonates in the Barremian Iberian Basin could also be related to palaeoceanic conditions after the Faraoni Event (Oceanic Anoxic Event, OAE) in the late Hauterivian (*ca* 131 Ma), close to the Hauterivian–Barremian boundary (*ca* 130.6 Ma) (e.g. Bodin *et al.*, 2006; Baudin & Riquier, 2014). The occurrence of minor carbonate ponds in the inner estuaries could be related to the upwelling of phreatic waters in coastal areas. After the Faraoni event, Tethys also experienced a significance influx of nutrients (Bodin *et al.*, 2006). During this period, the palaeoceanic record of $\delta^{13}C$ remained stable based on the compensation produced by the increment of dissolved inorganic carbon to the ocean basin (Godet *et al.*, 2006). At the early Barremian–late Barremian boundary, there was an increase in positive values of the $\delta^{13}C$ related to the widespread carbonate factory, leading to thick Urgonian carbonate platforms in France and Switzerland as well as in Iberia, where the clastic estuarine and barrier island systems of the Camarillas Formation are covered by the Urgonian platforms (Godet *et al.*, 2006).

CONCLUSIONS

The global scarcity of well-preserved successions of (i) barrier island systems and (ii) continental and paralic Barremian records make the Camarillas Formation a key target for Lower Cretaceous palaeoclimate studies and for improving the understanding of the sedimentology and stratigraphic architecture of paralic depositional systems. The Barremian Camarillas Formation records synrift sedimentation in a coastal setting that produced a highly aggradational pattern of repeated progradational–transgressive depositional systems leading to exceptional preservation of tidal environments.

Based on combined field and drone surveys, this study identifies key stratigraphic markers that allowed for correlation of depositional systems at the basin scale. Three main evolutionary stages have been interpreted for the Camarillas Formation. During the first stage, an estuary dominated by tides was established in the Galve Subbasin, with a north-west/south-east general orientation. Proximal fluvial channels were coeval with tidal estuarine deposits leading to a stacking of seven parasequences bounded by tidal ravinement surfaces. A mixed-energy, wave-dominated, tide influenced estuary system characterized Stage 2, with a well-defined barrier island in its mouth that interacted with a back barrier lagoon

to form washover fan deltas penetrating the lagoon, as well as flood-tidal deltas entering the back-barrier system. Tidal inlets connected the open waters of the Tethys with the restricted sectors of the back-barrier lagoons. Ebb tidal currents and reworking by waves formed ebb-tidal deltas that retrograded over the underlying back-barrier lagoonal facies. In Stage 3, a barrier island system was coeval with a carbonate back-barrier lagoon. The Camarillas Formation constitutes an excellent field analogue for the study of compartmentalization processes in coastal and paralic reservoirs of interest for subsurface reservoirs in these depositional systems.

The depositional systems of the Camarillas Formation show a general transgressive trend that corresponds to global eustatic sea-level rise that occurred during the Barremian. The large volume of clastic sediments delivered to the basin is attributed to two main factors: (i) tectonic uplift of the Iberian Massif associated with extensional tectonism that affected Iberian plate margins; and (ii) arid climatic conditions that favoured the erosion of basement granitic rocks that composed the highlands.

ACKNOWLEDGEMENTS

We thank Chief Editor Dr Piret Plink-Björklund, and Associate Editor Dr Theresa Schwartz for their comments and suggestions. We also thank Prof. Cari Johnson, Prof. Ron Steel and Dr Brian Willis for their encouraging and constructive reviews that helped us to improve the manuscript. We thank Dr José Carlos García-Ramos for the ichnofacies characterization. Authors would like to acknowledge the use of *Servicio General de Apoyo a la Investigación-SAI, Universidad de Zaragoza*. This research was supported by the *Agencia Estatal de Investigación* (AEI/10.13039/501100011033) of the Spanish Government (grant number PID2019-108705-GB-I00) and the Aragon Regional Government (grant number E32_20R: Geotransfer research group). This work is also funded by the "Convocatoria de Ayudas para la recualificación del sistema universitario Español 2021–2023, Financiado por la Unión Europea-Next Generation EU", Vicerrectorado de Investigación, Universidad del País VascoUPV/EHU to J.P.R.L. This work is a contribution to the Research Group of the Basque Government IT-1602-22 (Grupo Consolidado del Gobierno Vasco IT-1602-22).

CONFLICT OF INTEREST

We declare that we do not have any commercial or associative purpose that could represent a conflict of interest or that could have influenced the work submitted.

DATA AVAILABILITY STATEMENT

The data that support the findings of this study are available from the corresponding author upon reasonable request.

REFERENCES

Aigner, T. (1985) Storm depositional systems. Dynamic stratigraphy in modern and ancient shallow-marine sequences. *Lecture Notes in Earth Science*, **3**, 174.

Ainsworth, R.B. and **Walker, R.G.** (1994) Control of estuarine valley-fill deposition by fluctuationof relative sea-level, cretaceous Bearpaw-horseshoe canyon transition, Drumheller, Alberta, Canada. In: *Incised-Valley Systems: Origin and Sedimentary Sequences* (Eds Dalrymple, R.G., Boyd, R. and Zaitlin, B.A.), *SEPM Spec. Pub*, **51**, 159–174.

Allen, J.R.L. (1991) Sedimentary processes and Facies in the Gironde estuary; a recent model for macrotidal estuarine systems. In: *Clastic Tidal Sedimentology* (Eds Smith, D.G., Reinson, G.E., Zaitlin, B.A. and Rahmani, R.A.), *Memoir Canadian Society of Petroleum Geologists*, **16**, 29–39.

Allen, J.L. and **Johnson, C.L.** (2010) Sedimentary facies, paleoenvironments, and relative sea level changes in the John Henry member, cretaceous straight cliffs formation, southern Utah. In: *Geology of South-Central Utah* (Eds Carney, S., Tabet, D. and Johnson, C.), *UGA Guidebook*, **39**, 225–247.

Allen, J.L. and **Johnson, C.L.** (2011) Architecture and formation of transgressive-regressive cycles in marginal marine strata of the John Henry member, straight cliffs formation, upper cretaceous of southern Utah, USA. *Sedimentology*, **58**, 1486–1513.

Allen, G.P. and **Posamentier, H.W.** (1993) Sequence stratigraphy and Facies model of an Incised Valley fill: the Gironde estuary, France. *J. Sediment. Res.*, **63**, 378–391.

Amorosi, A. (1995) Glaucony and sequence stratigraphy: a conceptual framework of distribution in siliciclastic sequences. *J. Sediment. Res.*, **65**, 419–425.

Antolín-Tomas, B., **Liesa, C.L.**, **Casas, A.M.** and **Gil-Peña, I.** (2007) Geometry of fracturing linked to extensión and basin formation in the Maestrazgo Basin (eastern Iberian chain, Spain). *Rev. Soc. Geol. Esp.*, **20**, 351–365.

Aschoff, J.L., **Olariu, C.** and **Steel, R.J.** (2018) Recognition and significance of bayhead delta deposits in the rock record: A comparison of modern and ancient systems. *Sedimentology*, **65**, 62–95.

Aurell, M., **Bádenas, B.**, **Gasca, J.M.**, **Canudo, J.I.**, **Liesa, C.**, **Soria, A.R.**, **Moreno-Azanza, M.** and **Najes, L.** (2016) Stratigraphy and evolution of the Galve sub-basin (Spain) in the middle Tithonian-early Barremian: implications for the setting and age of some dinosaur fossil sites. *Cretaceous Res.*, **65**, 138–162.

Aurell, M., **Fregenal-Martínez, M.**, **Bádenas, B.**, **Muñoz-García, M.B.**, **Élez, J.**, **Meléndez, N.** and **de Santisteban, C.** (2019) Middle Jurassic–early cretaceous tectono-sedimentary evolution of the southwestern Iberian Basin (Central Spain): major palaeogeographical changes in the tectonic framework of the Western Tethys. *Earth Sci. Rev.*, **199**, 983.

Austin, P.T., **Vila-Concejo, A.**, **Short, D.A.** and **Ranasinghe, R.** (2018) A multi-scale conceptual model of flood-tide delta morphodynamics in micro-tidal estuaries. *Geosciences*, **8**, 324.

Baeteman, C., **Beets, D.J.** and **Strydonck, M.V.** (1999) Tidal crevasse splays as the cause of rapid changes in the rate of aggradation in the Holocene tidal deposits of the Belgian coastal plain. *Quat. Int.*, **56**, 3–13.

Bárdossy, G. (1982) Karst bauxites. Bauxite deposits on carbonate rocks. *Develop. Econ. Geol.*, **14**, 441.

Bartholdy, J. (2012) Salt marsh sedimentation. In: *Principles of Tidal Sedimentology* (Eds Davis, R.A. and Dalrymple, R.W.), pp. 151–186. Springer, Dordrecht.

Baudin, F. and **Riquier, L.** (2014) The late Hauterivian Faraoni "oceanic anoxic event": an update. *Bull. Soc. Géol. France*, **185**, 359–377.

Bayet-Goll, A., **Sharafi, M.**, **Jazimagh, N.** and **Brandano, M.** (2022) Understanding along-strike variability in controlling mechanisms of paleoenvironmental conditions and stratigraphic architecture: Ordovician successions in the Alborz Mountains of Iran at the northern Gondwana margin. *Mar. Petrol. Geol.*, **140**, 654.

Benallack, K., **Green, A.N.**, **Humphries, M.S.**, **Cooper, J.A.G.**, **Dladla, N.N.** and **Finch, J.M.** (2016) The stratigraphic evolution of a large back-barrier lagoon system with a non-migrating barrier. *Mar. Geol.*, **379**, 64–77.

Blakey, R. (2008) Gondwana paleogeography from assembly to breakup – a 500 million year odyssey. In: *Resolving the Late Paleozoic Ice Age in Time and Space* (Eds Fielding, C.R., Frank, T.D. and Isbell, J.L.), *Geological Society of America*, *Special Paper*, **441**, 1–28.

Blakey, R. (2014) Available at: http://cpgeosystems.com/125_Cret_EurMap_sm.jpg.

Bodin, S., **Vermeulen, J.**, **Godet, A.** and **Föllmi, K.B.** (2006) New data on the age of the installation of Urgonian-type carbonates along the northern Tethyan margin: biostratigraphy of the Chopf member (Helvetic Alps, eastern Switzerland). *C.R. Geosci.*, **338**, 727–733.

Bover-Arnal, T. (2010) *The Aptian Evolution of the Galve Sub-Basin (Maestrat Basin, E Iberia).* PhD Thesis, University of Bayreuth, Bayreuth, 222 pp.

Bradley, G.M., **Redfern, J.**, **Hodgetts, D.**, **George, A.D.** and **Wach, G.D.** (2018) The applicability of modern tidal analogues to pre-vegetation paralic depositional models. *Sedimentology*, **65**, 2171–2201.

Brookfield, M.E. (2004) The enigma of fine-grained alluvial basin fills: the Permo-Triassic (Cumbrian coastal and Sherwood groups) of the Solway Basin, NW England and SW Scotland. *Int. J. Earth Sci.*, **93**, 282–296.

Caja, M.A. (2004) *Procedencia y diagénesis de los sedimentos del Jurásico superior-Cretácico inferior (facies Weald) en las subcuencas occidentales de la Cuenca del Maestrazgo, Cordillera Ibérica Oriental.* PhD Thesis, University Complutense of Madrid, Madrid, 293 pp.

Caja, M.A., **Salas, R.**, **Marfil, R.** and **Lago, M.** (2005) Heavy mineral composition and geochemistry of the weald facies from the Maestrat Basin (Spain): provenance implications for La Jurassic-early cretaceous rifting stage. *Geogaceta*, **38**, 11–14.

Canerot, J., **Cugny, P.**, **Pardo, G.**, **Salas, R.** and **Villena, J.** (1982) Ibérica Central y Maestrazgo. In: *El Cretácico de España*, pp. 273–344. Univ. Complutense de Madrid, Madrid.

Capote, R., **Muñoz, J.A.**, **Simón, J.L.**, **Liesa, C.L.** and **Arlegui, L.E.** (2002) Alpine tectonics I: the alpine system north of the Betic cordillera. In: *The Geology of Spain* (Eds Gibbons, W. and Moreno, T.), pp. 367–400. The Geological Society, London.

Capuzzo, N. and **Wetzel, A.** (2004) Facies and basin architecture of the late carboniferous Salvan-Dorénaz continental basin (Western Alps, Switzerland/France). *Sedimentology*, **51**, 675–697.

Carmona, N.B., **Buatois, L.A.**, **Ponce, J.J.** and **Gabriela, M.** (2009) Ichnology and sedimentology of a tide-influenced delta, lower Miocene Chenque formation, Patagonia, Argentina: trace-fossil distribution and response to environmental stresses. *Palaeogeogr., Palaeoclimatol., Palaeoecol.*, **273**, 75–86.

Cattaneo, A. and **Steel, R.J.** (2003) Transgressive deposits: a review of their variability. *Earth-Sci. Rev.*, **62**, 187–228.

Cecil, C.B. (1990) Palaeoclimate controls on stratigraphic repetition of chemical and siliciclastic rocks. *Geology*, **18**, 533–536.

Chafetz, H.S. and **Reid, A.** (2000) Syndepositional, shallow water precipitation of glauconitic minerals. *Sediment. Geol.*, **136**, 29–42.

Cheel, R.J. and **Leckie, D.A.** (1990) A tidal-inlet complex in the cretaceous epeiric sea of North America: Virgelle member. Milk River formation, souther Alberta, Canada. *Sedimentology*, **37**, 67–81.

Chentnik, B., **Johnson, C.L.**, **Mulhern, J.** and **Stright, L.** (2015) Valleys, estuaries, and lagoons: Paleoenvironments and regressive-transgressive architecture of the upper cretaceous straight cliffs formation. *J. Sed. Res.*, **85**, 1166–1196.

Clifton, H.E. (2006) A re-examination of facies models for clastic shorefaces. In: *Facies Models Revisited* (Eds Posamentier, H.W. and Walker, R.G.), *SEPM Spec. Publ*, **84**, 293–337.

Coe, A.L. (2003) *The Sedimentary Record of Sea-Level Change.* Cambridge and Open University Press, Cambridge, 287 pp.

Collison, J.D. (1996) Alluvial sediments. In: *Sedimentary Environments and Facies* (Ed. Reading, H.G.), pp. 37–82. Blackwell Publishing, Oxford.

Cooper, J.A.G. (2013) Mesoscale geomorphic change on low-energy barrier islands in Chesapeake Bay, USA. *Geomorphology*, **199**, 82–94.

Cooper, J.A.G., **Green, A.N.** and **Loureiro, C.** (2018) Geological constraints on mesoscale coastal barrier behaviour. *Glob. Planet. Change*, **168**, 15–34.

Corcoran, P.L., **Mueller, W.U.** and **Chown, E.H.** (1998) Climatic and tectonic influences on fan deltas and wave to tide controlled shoreface deposits: evidence from the Archaean Keskarrah formation, Slave Province, Canada. *Sediment. Geol.*, **120**, 125–152.

Dalrymple, R.W. (1992) Tidal depositional systems. In: *Facies Models: Response to Sea Level Changes* (Eds Walker, R.G. and James, N.P.), pp. 195–218. Geology Association Canada, Newfoundland.

Dalrymple, R.W. and **Choi, K.** (2007) Morphologic and facies trends through the fluvial-marine transition in tide-

dominated depositional systems: a schematic framework for environmental and sequence-stratigraphic interpretation. *Earth-Sci. Rev.*, **81**, 135–174.

Dalrymple, R.W. and **Rhodes, R.N.** (1995) Estuarine dunes and barforms. In: *Geomorphology and Sedimentology of Estuaries* (Ed. Perillo, G.M.), *Developments in Sedimentology*, **53**, 359–422.

Dalrymple, R.W. and **Zaitlin, B.A.** (1989) Tidal sedimentation in the macrotidal Cobequid Bay – Salmon River estuary, bay of Fundy. In: *Field Guide, 2nd. International Symposium Clastic Tidal Deposits*. Canadian Society of Petroleum Geologists, Calgary, 84 pp.

Dalrymple, R.W., **Knight, R.J.**, **Zaitlin, B.A.** and **Middleton, G.V.** (1990) Dynamics and Facies model of a macrotidal sand-bar complex, Cobequid Bay-Salmon River estuary. *Sedimentology*, **37**, 577–612.

Dalrymple, R.W., **Zaitlin, B.A.** and **Boyd, R.** (1992) Perspective: estuarine Facies models: conceptual basis and stratigraphic implications. *J. Sediment. Res.*, **62**, 1130–1146.

Dalrymple, R.W., **Mackay, D.**, **Ichaso, A.A.** and **Choi, K.S.** (2012) Processes, Morphodinamics, and Facies of tide-dominated estuaries. In: *Principles of Tidal Sedimentology* (Eds Davis, R.A. and Dalrymple, R.W.), pp. 79–108. Springer, Dordrecht.

De, C. (2002) Continental mayfly burrows within relict-ground in inter-tidal beach profile of bay of Bengal coast: a new ichnological evidence of Holocene marine transgression. *Current Sci.*, **83**, 64–67.

De Boer, P.L., **Oost, A.P.** and **Visser, M.J.** (1989) The diurnal inequality of the tide as a parameter for recognizing tidal influences. *J. Sediment. Petrol.*, **59**, 912–921.

Dercourt, J., **Zonenshain, L.P.**, **Ricou, L.E.**, **Kazmin, V.G.**, **Le Pichon, X.**, **Knipper, A.L.**, **Grandjacquet, C.**, **Sborshchikov, I.M.**, **Geyssant, J.**, **Lepvrier, C.**, **Pechersky, D.H.**, **Boulin, J.**, **Sibuet, J.C.**, **Savostin, L.A.**, **Sorokhtin, O.**, **Westphal, M.**, **Bazhenov, M.L.**, **Lauer, J.P.** and **Biju-Duval, B.** (1986) Geological evolution of the Tethys Belt from the Atlantic to the Pamirs since the Lias. *Tectonophysics*, **123**, 241–315.

Dercourt, J., Gaetani, M., Vrielynck, B., Barrier, E., Biju-Duval, B., Brunet, M.F., Caoet, J.P., Crasquin, S. and Sandulescu, M. (Eds) (2000) *Atlas Peri-Tethys, Palaeogeographical Maps*. CCGM/CGMW, Paris, 269 pp.

Dias, G.T.M. and **Kjerfve, B.** (2008) Barrier and beach ridge Systems of Rio de Janeiro coast. In: *Geology and Geomorphology of Holocene Coastal Barriers of Brazil* (Eds Dillenburg, S. and Hesp, P.), pp. 225–252. Springer, Berlín.

Díaz Molina, M. and **Yébenes, A.** (1987) La sedimentación litoral y continental durante el Cretácico inferior. Sinclinal de Galve, Teruel. *Estudios Geológicos*, Volumen extraordinario Galve-Tremp: 3–21.

Dinis, J., **Rey, J.**, **Cunha, P.P.**, **Callapez, P.** and **Reis, R.P.** (2008) Stratigraphy and allogenic controls of the western Portugal cretaceous: an updated synthesis. *Cretac. Res.*, **29**, 772–780.

Dinis, P.A., **Carvalho, J.**, **Callapez, P.M.**, **Mendes, M.M.**, **Santos, V.F.** and **Fernandes, P.** (2020) Composition of lower cretaceous mudstones of the Algarve Basin and implications for Iberian paleoclimates. *Cretaceous Res*, **110**, 404.

Donselaar, M.E. (1996) *Barrier Island Coasts and Relative Sea Level Rise: Preservation Potential, Facies Architecture and Sequence Analysis*. PhD Thesis, Utrecht University, Utrecht, 223 pp.

Dreyer, T., **Corregidor, J.**, **Arbues, P.** and **Puigdefàbregas, C.** (1999) Architecture of the tectonically influenced Sobrarbe deltaic complex in the Ainsa Basin, northern Spain. *Sediment. Geol.*, **127**, 127–169.

Duke, W.L., **Arnott, R.W.C.** and **Cheel, R.J.** (1991) Shelf sandstones and hummocky cross- stratification: new insights on a stormy debate. *Geology*, **19**, 625–628.

Dunham, R.J. (1962) Classification of carbonate rocks according to depositional texture. In: *Classification of carbonate rocks* (Ed. Ham, W.E.), *Am. Ass. Pet. Geol. Memoir*, **1**, 108–121.

Embry, A.F. and **Klovan, J.S.** (1971) A late Devonian reef tract on northeastern Banks Island, N.W.T. *Bull. Canad. Petrol. Geol.*, **4**, 730–781.

Favre, P. and **Stampfli, G.M.** (1992) From rifting to passive margin: the example of the Red Sea, Central Atlantic and alpine Tethys. *Tectonophysics*, **215**, 69–97.

FitzGerald, D., **Buynevich, I.** and **Hein, C.** (2012) Morphodynamics and facies architecture of tidal inlets and tidal deltas. In: *Principles of Tidal Sedimentology* (Eds Davis, R.A. and Dalrymple, R.W.), pp. 301–333. Springer, Dordrecht.

Flügel, E. (2010) *Microfacies of Carbonate Rocks: Analysis, Interpretation and Application*, 2nd edn. Springer, Heidelberg, 984 pp.

Föllmi, K.B. (2012) Early cretaceous life, climate and anoxia. *Cretaceous Res.*, **35**, 230–257.

Föllmi, K.B., **Weissert, H.**, **Bisping, M.** and **Funk, H.** (1994) Phosphogenesis, carbon-isotope stratigraphy, and carbonate-platform evolution along the lower cretaceous northern Tethyan margin. *Geol. Soc. Am. Bull.*, **106**, 729–746.

Föllmi, K.B., **Godet, A.**, **Bodin, S.** and **Linder, P.** (2006) Interactions between environmental change and shallow-water carbonate build-up along the northern Tethyan margin and their impact on the early cretaceous carbon-isotope record. *Paleoceanography*, **21**, 4211–4216.

Frasca, G., **Manatschal, G.**, **Cadenas, P.**, **Miró, J.** and **Lescoutre, R.** (2020) A kinematic rconstruction of Iberia using intracontinental strike-slip corridors. *Terra Nova*, **33**, 573–581.

Fürsich, F.T. and **Mayr, H.** (1981) Non-marine Rhizocorallium (trace fossil) from the upper freshwater Molasse (upper Miocene) of southern Germany. *Neues Jahrbuch für Geologie und Palaöntologie, Monatshefte*, **6**, 321–333.

Gallin, W., **Johnson, C.L.** and **Allen, J.** (2010) Fluvial and marginal marine architecture of the John Henry Member, Straight Cliffs Formation, Kelly Grade of the Kaiparowits Plateau, south central Utah. In: *Geology of South-Central Utah* (Eds Carney, S., Tabet, D. and Johnson, C.), *UGA Guidebook*, **39**, 248–275.

Ghazi, S. and **Mountney, N.P.** (2009) Facies and architectural element analysis of a meandering fluvial succession: the Permian Warchha sandstone, salt Range, Pakistan. *Sediment. Geol.*, **221**, 99–126.

Ghosh, S.K., **Chakraborty, C.** and **Chakraborty, T.** (2005) Influence of fluvial-tidal interactions on the nature of cross-stratified packages in a deltaic setting: examples from the Barakar coal measure (Permian), Satpura Gondwana Basin, Central India. *Geol. J.*, **40**, 65–81.

Gil, J., **García-Hidalgo, J.F.**, **Segura, M.**, **García, A.** and **Carenas, B.** (2006) Stratigraphic architecture, palaeogeography and sea-level changes of a third order depositional sequence: the late Turonian–early Coniacian

in the northern Iberian ranges and central system (Spain). *Sediment. Geol.*, **191**, 191–225.

Gjelberg, J. and **Steel, R.** (2012) Depositional model for the lower cretaceous Helvetiafjellet formation on Svalbard – diachronous vs. layer-cake models. *Nor. J. Geol.*, **92**, 41–54.

Godet, A., **Bodin, S.**, **Föllmi, K.B.**, **Vermeulen, J.**, **Gardin, S.**, **Fiet, N.**, **Adatte, T.**, **Berner, Z.**, **Stüben, D.** and **van de Schootbrugge, B.** (2006) Evolution of the marine stable carbone isotope record during the early cretaceous: a focus on the late Hauterivian and Barremian in the Tethyan realm. *Earth Planet. Sci. Lett.*, **242**, 254–271.

Godet, A., **Bodin, S.**, **Adatte, T.** and **Föllmi, K.B.** (2008) Platform induced clay-mineral fractionation along a northern Tethyan basin-platform transect: implications for the interpretation of early cretaceous climate change (late Hauterivian-early Aptian). *Cretaceous Res*, **29**, 830–847.

Goldring, R., **Pollard, J.E.** and **Radley, J.D.** (2005) Trace fossils and pseudofossils from the Wealden strata (non-marine Lower Cretaceous) of southern England. *Cretaceous Res*, **26**, 665–685.

Green, A.N., **Pillay, T.**, **Cooper, J.A.G.** and **Guisado-Pintado, E.** (2019) Overwash-dominated stratigraphy of barriers with intermittent inlets. *Earth Surf. Process. Landforms*, **44**, 2097–2111.

Haq, B.U. (2014) Cretaceous eustasy revisited. *Glob. Planet. Change*, **113**, 44–58.

Haug Eide, C., **Howel, J.** and **Buckley, S.** (2014) Distribution of discontinuous mudstone beds within wave-dominated shallow-marine deposits: star point sandstone and Blackhawk formation, eastern Utah. *Am. Ass. Pet. Geol. Bull.*, **98**, 1401–1429.

Hayes, M.O. and **FitzGerald, D.M.** (2013) Origin, evolution, and classification of tidal inlets. *J. Coast. Res.*, **69**, 14–33.

Haywood, A.M., **Valdes, P.J.** and **Markwick, P.J.** (2004) Cretaceous (Wealden) climates: a modelling perspective. *Cretac. Res.*, **25**, 303–311.

Holz, M. (2003) Sequence stratigraphy of a lagoonal estuarine system-an example from the lower Permian Rio Bonito formation, Paraná Basin, Brazil. *Sediment. Geol.*, **162**, 305–331.

Hori, K., **Saito, Y.**, **Zhao, Q.**, **Cheng, X.**, **Wang, P.**, **Sato, Y.** and **Li, C.** (2001) Sedimentary facies of the tide-dominated paleo-Changjiang (Yangtze) estuary during the last transgression. *Mar. Geol.*, **177**, 331–351.

Hudock, J.W. (2013) *Barrier Island Associated Washover Fan and Flood Tidal Delta Systems: A Geomorphologic Analysis and Proposed Classification Scheme for Modern Washover Fans and Examination of a Flood Tidal Delta Complex in the Cretaceous Upper McMurray Formation, Alberta, Canada.* MSc Thesis, University of Texas at Austin, Austin, TX, 118 pp.

Hurt, G.W. and **Carlisle, V.W.** (2001) Delineating hydric soils. In: *Wetland Soils: Their Genesis, Morphology, Hydrology, Landscapes and Classification* (Eds Richardson, J.L. and Vepraskas, M.J.), pp. 183–206. Lewis Publishers, Boca Raton, FL.

Imperato, D.P., **Sexton, W.J.** and **Hayes, M.O.** (1988) Stratigraphy and sediment characteristics of a mesotidal ebb-tidal delta, north Edisto inlet, South Carolina. *J. Sediment. Petrol.*, **58**, 950–958.

Ito, M., **Ishigaki, A.**, **Nishikawa, T.** and **Saito, T.** (2001) Temporal variation in the wavelength of hummocky cross-stratification: implications for storm intensity through Mesozoic and Cenozoic. *Geology*, **29**, 87–89.

Jackson, C.A.L., **Gawthorpe, R.L.**, **Carr, I.D.** and **Sharp, I.R.** (2005) Style and sequence of deformation during extensional fault-propagation folding: examples from the Hammam Faraun and El-Qaa fault blocks, Suez rift, Egypt. *Sedimentology*, **52**, 313–338.

Jarzen, D.M. and **Nichols, D.J.** (1996) Pollen. In: *Palynology: Principles and Applications* (Eds Jansonius, J. and McGregor, D.C.), *Am. Assoc. Stratigr. Palynol. Found*, **1**, 261–291.

Jennings, D., **Lovelace, D.** and **Driese, S.G.** (2011) Differentiating paleowetland subenvironments using a multi-disciplinary approach: an example from the Morrison formation, south Central Wyoming, USA. *Sediment. Geol.*, **238**, 23–47.

Johannessen, P.N., **Nielsen, L.H.**, **Nielsen, L.**, **Møller, I.**, **Pejrup, M.**, **Andersen, T.J.**, **Korshøj, J.**, **Larsen, B.** and **Piasecki, S.** (2008) Sedimentary facies and architecture of the Holocene to recent Rømø barrier Island in the Danish Wadden Sea. *Geol. Surv. Den. Green. Bull.*, **15**, 49–52.

Johannessen, P.N., **Nielsen, L.H.**, **Nielsen, L.**, **Møller, I.**, **Pejrup, M.** and **Andersen, T.J.** (2010) Architecture of an upper Jurassic barrier Island sandstone reservoir, Danish central Graben: implications of a Holocene–recent analogue from the Wadden Sea. In: *Petroleum Geology: From Mature Basins to New Frontiers* (Eds Vining, B.A. and Pickering, S.C.), *Proceedings of the 7th Petroleum Geology Conference*, **7**, 145–155.

Johnson, S.M. and **Dashtgard, S.E.** (2014) Inclined heterolithic stratification in a mixed tidal fluvial channel: differentiating tidal versus fluvial controls on sedimentation. *Sediment. Geol.*, **301**, 41–53.

Johnson, K.G. and **Friedman, G.M.** (1969) The truly clastic correlatives (upper Devonian) of New York state: a model for recognition of alluvial, dune, tidal nearshore (bar and lagoon), and offshore sedimentary environments in a tectonic delta complex. *J. Sediment. Petrol.*, **39**, 451–485.

Johnson, C.L., **Stright, L.**, **Purcell, R.** and **Durkin, P.** (2017) Stratigraphic evolution of an estuarine fill succession, and reservoir characterization of inclined heterolithic strata, cretaceous of southern Utah, USA. In: *Sedimentology of Paralic Reservoirs: Recent Advances*, *Geol. Soc. London Spec*, **444**, 251–286.

Kirschbaum, M.A. and **Hettinger, R.D.** (2004) Facies analysis and sequence stratigraphic framework of Upper Campanian Strata (Neslen and Mount Garfield Formations, Bluecastle Tongue of the Castlegate Sandstone, and Mancos Shale), Eastern book Cliffs, Colorado and Utah. *Geological Survey Digital Data Series*, DDs-69-G, 46 pp.

Kraus, M.J. and **Hasiotis, S.T.** (2006) Significance of different modes of rhizolith preservation to interpreting paleoenvironmental and paleohydrologic settings: examples from Paleogene paleosols, Bighorn basin, Wyoming, U.S.A. *J. Sediment. Res.*, **76**, 633–646.

Kumar, N. and **Sanders, J.E.** (1974) Inlet sequence: a vertical succession of sedimentary structures and textures created by the lateral migration of tidal inlets. *Sedimentology*, **21**, 491–532.

LaGesse, J. and **Read, J.F.** (2006) Updip sequence development on a wave- and current- dominated, mixed carbonate-siliciclastic continental shelf: Paleogene, North Carolina, eastern U.S.A. *Sediment. Geol.*, **184**, 155–182.

Leckie, D.A. and **Rumple, T.** (2003) Tide-influenced sedimentation in a rift basin-cretaceous Qishn formation, Masila block, Yemen: a billion barrel oil field. *Am. Ass. Pet. Geol. Bull.*, **87**, 987–1013.

Lee, Y.I. and **Kim, J.C.** (1992) Storm influenced siliciclastic and carbonate ramp deposit, the lower Ordovician Dumugol formation, South Korea. *Sedimentology*, **39**, 951–969.

Lee, Y.I., **Hyeong, K.** and **Yoo, C.M.** (2001) Cyclic sedimentation across a middle Ordovician carbonate ramp (Duwibong formation), Korea. *Facies*, **44**, 61–74.

Li, Y., **Zhang, Q.** and **Yao, J.** (2015) Investigation of residence and travel times in a large floodplain Lake with complex lake–river interactions: Poyang lake (China). *Water*, **7**, 1991–2012.

Liesa, C.L., **Soria, A.R.** and **Meléndez, A.** (2000) Lacustrine evolution in a basin controlled by extensional faults: the Galve subbasin, Teruel, Spain. In: *Lake Basins through Space and Time* (Eds Gierlowski-Kordesch, E.H. and Kelts, K.R.), *American Association of Petroleum Geologists, Studies in Geology*, **46**, 295–302.

Liesa, C.L., **Casas, A.M.**, **Soria, A.R.**, **Simón, J.L.** and **Meléndez, A.** (2004) Estructura extensional cretácica e inversión terciaria en la región Aliaga-Montalbán. In: *Itinerarios Geológicos por Aragón* (Eds Colombo, F., Liesa, C.L., Meléndez, G., Pocoví, A., Sancho, C. and Soria, A.R.), pp. 151–180. Sociedad Geológica de España, Zaragoza.

Liesa, C.L., **Soria, A.R.**, **Meléndez, N.** and **Meléndez, A.** (2006) Extensional fault control on the sedimentation patterns in a continental rift basin: El Castellar formation, Galve sub-basin, Spain. *Geol. Soc. London*, **163**, 487–498.

Liesa, C.L., **Soria, A.R.**, **Casas, A.**, **Aurell, M.**, **Meléndez, N.**, **Bádenas, B.**, **Fregenal-Martínez, M.**, **Navarrete, R.**, **Peropadre, C.** and **Rodríguez-López, J.P.** (2019) The south-Iberian, central Iberian and Maestrazgo basins (chapter 5, late Jurassic-early cretaceous rifting). In: *The Geology of Iberia: A Geodynamic Approach, Vol. 3 (the Alpine Cycle)* (Eds Oliveira, J.T. and Quesada, C.), pp. 214–228. Springer, Cham. Regional Geology Reviews.

Liesa, C.L., **Casas-Sainz, A.M.**, **Aurell, M.**, **Simón, J.L.** and **Soria, A.R.** (2023) Salt tectonics vs inversion tectonics: the anticlines of the western Maestrazgo revisited (eastern Iberian chain, Spain). *Basin Res.*, **35**, 295–335.

Longhitano, S.G. (2011) The record of tidal cycles in mixed silici–bioclastic deposits: examples from small Plio-Pleistocene peripheral basins of the microtidal Central Mediterranean Sea. *Sedimentology*, **58**, 691–719.

Longhitano, S.G., **Chiarella, D.**, **Di Stefano, A.**, **Messina, C.**, **Sabato, L.** and **Tropeano, M.** (2012) Tidal signatures in Neogene to quaternary mixed deposits of southern Italy straits and bays. *Sediment. Geol.*, **279**, 74–96.

Mángano, M.C. and **Buatois, L.A.** (2004) Ichnology of carboniferous tide-influenced environments and tidal flat variability in the north American midcontinent. In: *The Application of Ichnology to Palaeoenvironmental and Stratigraphic Analysis* (Ed. McIlroy, D.), *Geol. Soc., London, Spec. Publ*, **228**, 157–178.

Martín-Closas, C. (1989) *Els caròfits del Cretaci inferior de les conques perifèriques del Bloc de l'Ebre*. PhD Thesis, Univ. de Barcelona, Barcelona, 581 pp.

Mas, R., **Alonso, A.** and **Guimerà, J.** (1993) Evolución tectonosedimentaria de una cuenca extensional intraplaca: La Cuenca finijurásica-eocretácica de los Cameros (La Rioja-Soria). *Rev. Soc. Geol. Esp.*, **6**, 129–144.

May, S.M., **Callow, J.N.**, **Brill, D.**, **Hoffmeister, D.** and **May, J.H.** (2020) Revealing sediment transport pathways and geomorphic change in washover fans by combining drone-derived digital elevation models and single grain luminescence data. *J. Geophys. Res. Earth Surf.*, **125**, e2020JF005792.

Médus, J. (1970) A palynological method for stratigraphical correlations. An study of the Barremian, Aptian and Albian complex of north-eastern Spain and of Roussillon in France. *Grana*, **10**, 149–158.

Melchor, R.N., **Genise, J.F.**, **Buatois, L.A.** and **Umazano, A.M.** (2012) Fluvial environments. In: *Trace Fossils as Indicators of Sedimentary Environments* (Eds Knaust, D. and Bromley, R.G.), *Developments in Sedimentology*, **64**, 329–378.

Meléndez, N., **Liesa, C.L.**, **Soria, A.R.** and **Meléndez, A.** (2009) Lacustrine system evolution during early rifting: El Castellar formation (Galve sub-basin, central Iberian chain). *Sediment. Geol.*, **222**, 64–77.

Miall, A.D. (1996) *The Geology of Fluvial Deposits; Sedimentary Facies, Basin Analysis, and Petroleum Geology*. Springer-Verlag, New York, NY, 582 pp.

Morales, J.A., **Borrego, J.**, **Jiménez, I.**, **Monterde, J.** and **Gil, N.** (2001) Morphostratigraphy of an ebb-tidal delta system associated with a large spit in the Piedras estuary mouth (Huelva coast, southwestern Spain). *Mar. Geol.*, **172**, 225–241.

Moran, L.K. (1989) *Petrography of Unconformable Surfaces and Associated Stratigraphic Units of the Eocene Castle Hayne Formation, Southeastern North Carolina Coastal Plain*. PhD Thesis, Univ. East Carolina, Greenville, 337 pp.

Mulhern, J. and **Johnson, C.L.** (2017) Time–space variability of paralic strata deposited in a high accommodation, high sediment supply setting: example from the cretaceous of Utah. *Sedimentol. Paralic. Reser.*, **444**, 349–392.

Mulhern, J.S., **Johnson, C.L.** and **Martin, J.M.** (2019) Modern to ancient Barrier Island dimensional comparisons: implications for analog selection and Paleomorphodynamics. *Front. Earth Sci.*, **7**, 109.

Mulhern, J.S., **Johnson, C.L.** and **Green, A.N.** (2021) When is a barrier Island not an Island? When it is preserved in the rock record. *Front. Earth Sci.*, **8**, 437.

Navarrete, R. (2015) *Controles alocíclicos de la sedimentación barremiense en la Subcuenca de Galve (Fm. Camarillas, margen occidental de la Cuenca del Maestrazgo)*. PhD Thesis, Universidad de Zaragoza, Zaragoza, 444 pp.

Navarrete, R., **Liesa, C.L.**, **Soria, A.R.** and **Rodríguez-López, J.P.** (2013a) Actividad de fallas durante el depósito de la Formacion Camarillas (Barremiense) en la Subcuenca de Galve (E de España). *Geogaceta*, **53**, 61–64.

Navarrete, R., **Rodríguez-López, J.P.**, **Liesa, C.L.**, **Soria, A.R.** and **Veloso, F.M.L.** (2013b) Changing physiography of rift basins as a control on the evolution of mixed siliciclastic–carbonate back-barrier systems (Barremian Iberian Basin, Spain). *Sediment. Geol.*, **289**, 40–61.

Navarrete, R., **Liesa, C.L.**, **Castanera, D.**, **Soria, A.R.**, **Rodríguez-López, J.P.** and **Canudo, J.I.** (2014) A thick Tethyan multi-bed tsunami deposit preserving a dinosaur megatracksite within a coastal lagoon (Barremian, eastern Spain). *Sediment. Geol.*, **313**, 105–127.

Navarrete, R., **Soria, A.R.**, **Liesa, C.L.** and **Rodríguez-López, J.P.** (2016) Reinterpretación paleoambiental de la Formación Camarillas en la subcuenca de Galve (Barremiense, Cordillera Ibérica). *Geo-Temas*, **16**, 233–236.

Nio, S.D. and **Yang, C.S.** (1989) *Recognition of Tidally-Influenced Facies and Environments. Short Course Note Series 1*. InterGeos B.V., Leiderdorp, 230 pp.

Nio, S.D. and **Yang, C.S.** (1991) Diagnostic attributes of clastic tidal deposits: a review. In: *Clastic Tidal*

Sedimentology (Eds Smith, D.G., Reinson, G.E., Zaitlin, B.A. and Rahmani, R.A.), *Canadian Society of Petroleum Geologist*, **16**, 3–28.

Olariu, C., **Steel, R.J.**, **Dalrymple, R.W.** and **Gingras, M.K.** (2012) Tidal dunes versus tidal bars: the sedimentological and architectural characteristics of compound dunes in a tidal seaway, the lower Baronia sandstone (lower Eocene), Ager Basin, Spain. *Sediment. Geol.*, **279**, 134–155.

Olivet, J.L., **Bonnin, J.**, **Beuzart, P.** and **Auzende, J.M.** (1984) *Cinématique de l'Atlantique Nord et Central*. Rapports scientifiques et techniques du Centre National pour l'Exploitation des Oceans, Paris, 108 pp.

Omodeo Salè, S., **Guimerà, J.**, **Mas, R.** and **Arribas, J.** (2014) Tectono-stratigraphic evolution of an inverted extensional basin: the Cameros Basin (north of Spain). *Int. J. Earth Sci.*, **103**, 1597–1620.

Painter, C.S., **York-Sowecke, C.C.** and **Carrapa, B.** (2013) Sequence stratigraphy of the upper cretaceous sego sandstone member reveals spatio-temporal changes in depositional processes, Northwest Colorado, U.S.A. *J. Sediment. Res.*, **83**, 323–338.

Palma, R.M., **Lo Forte, G.L.**, **Medhli, M.** and **Piethé, R.D.** (2005) High frequency subtidal-peritidal cycles of the Callovian Calabozo formation (Neuquén Basin, Western Argentina): preliminary approach. *Geol. Acta*, **3**, 119–132.

Peropadre, C. (2012) *El Aptiense del Margen Occidental de la Cuenca del Maestrazgo: Controles Tectónico, Eustático y Climático en la Sedimentación*. PhD Thesis, Universidad Complutense de Madrid, Madrid, 649 pp.

Peropadre, C., **Meléndez, N.** and **Liesa, C.L.** (2007) Heterogeneous subsidence and paleogeographic elements in an extensional setting revealed through the correlation of a storm deposit unit (Aptian, E Spain). *J. Iberian Geol.*, **33**, 79–91.

Peropadre, C., **Liesa, C.L.** and **Meléndez, N.** (2013) High-frequency, moderate to high-amplitude sea-level oscilations during the late early Aptian: insights into the mid-Aptian event (Galve sub-basin, Spain). *Sed. Geol.*, **294**, 233–250.

Pettijohn, F.P., **Potter, P.E.** and **Siever, R.** (1973) *Sand and Sandstones*. Springer-Verlag, New York-Heidelberg-Berlin, 618 pp.

Plink-Björklund, P. (2005) Stacked fluvial and tide-dominated estuarine deposits in highfrequency (fourth-order) sequences of the Eocene Central Basin, Spitsbergen. *Sedimentology*, **52**, 391–428.

Plink-Björklund, P. (2008) Wave-to-tide facies change in a Campanian shoreline complex, chimney rock tongue, Wyoming-Utah, U.S.A. recent advances in models of siliciclastic shallow-marine stratigraphy. *SEPM Spec. Publ.*, **90**, 265–291.

Reineck, H.E. and **Singh, I.B.** (1980) *Depositional Sedimentary Environments*, 2nd edn. Springer-Verlag, New York, NY, 549 pp.

Reineck, H.E. and **Wunderlich, F.** (1968) Classification and origin of flaser and lenticular bedding. *Sedimentology*, **11**, 99–104.

Reizopoulou, S. and **Nicolaidou, A.** (2004) Benthic diversity of coastal brackish-water lagoons in western Greece. *Aquatic Conserv.*, **14**, 93–102.

Richards, M.T. (1994) Transgression of an estuarine cannel and tidal flat complex. The lower Triassic of Barleg, Alpes de haute Provence, France. *Sedimentology*, **41**, 55–82.

Roberts, E.M. (2007) Facies architecture and depositional environments of the upper cretaceous Kaiparowits formation, southern Utah. *Sediment. Geol.*, **197**, 207–233.

Rodríguez-López, J.P. (2008) *Sedimentología y Evolución del Sistema Desértico Arenoso (erg) Desarrollado en el Márgen Occidental del Tethys Durante el Cretácico Medio. Cordillera Ibérica. Provincias de Teruel y Zaragoza*. Unpublished PhD Thesis, Universidad Complutense de Madrid-Consejo Superior de Investigaciones Científicas, Madrid, 500 pp.

Rodríguez-López, J.P., **de Boer, P.L.**, **Meléndez, N.**, **Soria, A.R.** and **Pardo, G.** (2006) Windblown desert sands in coeval shallow marine deposits: a key for the recognition of coastal ergs in the mid-cretaceous Iberian Basin, Spain. *Terra Nova*, **18**, 314–320.

Rodríguez-López, J.P., **Meléndez, N.**, **de Boer, P.L.** and **Soria, A.R.** (2010) The action of wind and water in a mid-cretaceous subtropical erg-margin system close to the Variscan Iberian massif, Spain. *Sedimentology*, **57**, 1315–1356.

Rodríguez-López, J.P., **Soria, A.R.** and **Liesa, C.L.** (2021) Extreme-flood-related peat blocks: an anthropocene analogue to ancient coalforming environments. *J. Sediment. Res.*, **91**, 243–261.

Rodríguez-López, J.P., **Wu, C.**, **Vishnivetskaya, T.A.**, **Murton, J.B.**, **Tang, W.** and **Ma, C.** (2022) Permafrost in the Cretaceous supergreenhouse. *Nat. Commun.*, **13**, 7946.

Salas, R. (1987) *El Malm i el Cretaci Inferior entre el Massís de Garraf i la Serra d'Espadà*. PhD Thesis, Universidad de Barcelona, Barcelona, 345 pp.

Salas, R. and **Casas, A.** (1993) Mesozoic extensional tectonics, stratigraphy and crustal evolution during the alpine cycle of the eastern Iberian basin. *Tectonophysics*, **228**, 33–55.

Salas, R., **Guimerà, J.**, **Mas, R.**, **Martín-Closas, C.**, **Meléndez, A.** and **Alonso, A.** (2001) Evolution of the Mesozoic central Iberian rift system and its Cenozoic inversión (Iberian chain). In: *Peri-Tethys Memoir 6: Peri-Tethyan Rift/Wrench Basins and Passive Margins* (Eds Ziegler, P.A., Cavazza, W., Robertson, A.H.F. and Crasquin-Soleau, S.), *Mémoires du Muséum National d'Histoire Naturelle*, **186**, 145–185.

Schudack, U. and **Schudack, M.** (2009) Ostracod biostratigraphy in the lower cretaceous of the Iberian chain (eastern Spain). *J. Iberian Geol.*, **35**, 141–168.

Schulze, F., **Kuss, J.** and **Marzouk, A.** (2005) Platform configuration, microfacies, and cyclicities of the upper Albian to Turonian of west-Central Jordan. *Facies*, **50**, 505–527.

Schwartz, R.K. (1975) *Nature and Genesis of Some Storm Washover Deposits*. U.S. Army Corps of Engineers Technical Memorandum, New York, No. 61. 69 p.

Schwartz, R.K. (1982) Bedform and stratification characteristics of some modern small-scale washover sand bodies. *Sedimentology*, **29**, 835–849.

Schwarz, E., **Veiga, G.D.**, **Spalletti, L.A.** and **Massaferro, J.L.** (2011) The transgressive infill of an inherited-valley system: the Springhill formation (lower cretaceous) in southern Austral Basin, Argentina. *Mar. Petrol. Geol.*, **28**, 1218–1241.

Scotese, C., **Song, H.**, **Mills, B.J.W.** and **Van der Meer, D.G.** (2021) Phanerozoic paleotemperatures: the earth's changing climate during the last 540 million years. *Earth-Sci. Rev.*, **215**, 503.

Sedgwich, P.E. and **Davis, R.A.** (2003) Stratigraphy of washover deposits in Florida: implications for recognition in the stratigraphic record. *Mar. Geol.*, **200**, 31–48.

Sha, L.P. (1990) *Sedimentological Studies of the Ebb-Tidal Deltas along the West-Frisian Islands, The Netherlands*. PhD Thesis, Utrecht Universiteit, Utrecht, 159 pp.

Shanley, K.W., **McCabe, P.J.** and **Hettinger, R.D.** (1992) Tidal influence in cretaceous fluvial strata from Utah, USA: a key to sequence stratigraphic interpretation. *Sedimentology*, **39**, 905–930.

Shanmugam, G., **Poffenberger, M.** and **Toro Álava, J.** (2000) Tide-dominated estuarine Facies in the Hollin and Napo ("T" and "U") formations (cretaceous), Sacha Field, Oriente Basin, Ecuador. *Am. Ass. Pet. Geol. Bul.*, **84**, 652–682.

Sharma, M., **Sharma, S.**, **Shukla, K.U.** and **Singh, B.I.** (2002) Sandstone body architecture and stratigraphic trend in the middle Siwalik succession of the Jammu area, India. *J. Asian Earth Sci.*, **20**, 817–828.

Sixsmith, P.J., **Hampson, G.J.**, **Gupta, S.**, **Johnson, H.D.** and **Fofana, J.F.** (2008) Facies architecture of a net transgressive sandstone reservoir analog: the cretaceous Hosta tongue, New Mexico. *Am. Ass. Pet. Geol. Bull.*, **92**, 513–547.

Soria, A.R. (1997) *La sedimentación en las cuencas marginales del surco ibérico durante el Cretácico inferior y su control estructural*. PhD Thesis, Univ. of Zaragoza, Servicio de Publicaciones de la Universidad de Zaragoza, Zaragoza, 363 pp.

Stampli, G.M. and **Borel, G.D.** (2002) A plate tectonic model for the Paleozoic and Mesozoic constrained by dynamic plate boundaries and restored synthetic oceanic isochrons. *Earth Planet. Sci. Lett.*, **196**, 17–33.

Steel, R.J., **Plink-Bjorklund, P.** and **Aschoff, J.** (2012) Tidal deposits of the Campanian Western interior seaway, Wyoming, Utah and Colorado, USA. In: *Principles of Tidal Sedimentology* (Eds Davis, R.A. and Dalrymple, R.W.), pp. 437–472. Springer, Dordrecht.

Takano, O. and **Tsuji, Y.** (2017) Fluvial to bay sequence stratigraphy and seismic facies of the cretaceous to Paleogene successions in the MITI Sanriku-oki well and the vicinities, the Sanriku-oki forearc basin, Northeast Japan. *Isl. Arc*, **26**, e12184.

Tasli, K., **Özer, E.** and **Koç, H.** (2006) Benthic foraminiferal assemblages of the cretaceous platform carbonate succession in the Yavca área (Bolkar Mountains, S. Turkey): biostratigraphy and paleoenvironment. *Geobios*, **39**, 521–533.

Thomas, R.G., **Smith, D.G.**, **Wood, J.M.**, **Visser, J.**, **Calverley-Range, E.A.** and **Koster, E.H.** (1987) Inclined heterolithic stratification–terminology, description, interpretation and significance. *Sediment. Geol.*, **53**, 123–179.

Tillmann, T. and **Wunderlich, J.** (2013) Barrier rollover and spit accretion due to the combined action of storm surge induced washover events and progradation: insights from ground-penetrating radar surveys and sedimentological data. In: *Proceedings 12th International Coastal Symposium (Plymouth, England)* (Eds Conley, D.C., Masselink, G., Russel, P.E. and O'Hare, T.J.), *Journal of Coastal Research, Special Issue*, **65**, 600–605.

Török, Á. (1998) Controls on development of mid-Triassic ramps: examples from southern Hungary. In: *Carbonate Ramps* (Eds Wright, V.P. and Burchette, T.P.), *Geol. Soc., London, Spec. Publ*, **149**, 339–367.

Tucker, M.E. and **Wright, V.P.** (1990) *Carbonate Sedimentology*. Blackwell, Oxford, 482 pp.

Vakarelov, B.K., **Ainsworth, R.B.** and **MacEachern, J.A.** (2011) Recognition of wave, tide-influenced shoreline systems in the rock record: variations from a microtidal shoreline model. *Sediment. Geol.*, **279**, 23–41.

Vakhrameev, V.A. (1991) *Jurassic and Cretaceous Floras and Climates of the Earth*. Cambridge University Press, Cambridge, 318 pp.

Van Wagoner, J.C., **Posamentier, H.W.**, **Mitchum, R.M.**, **Vail, P.R.**, **Sarg, J.F.**, **Loutit, T.S.** and **Hardenbol, J.** (1990) An overview of the fundamentals of sequence stratigraphy and key definitions. In: *Sea-Level Changes—An Integrated Approach* (Eds Wilgus, C.K., Hastings, B.S., Kendall, G.S.C., Posamentier, H.W., Ross, C.A. and Van Wagoner, J.C.), *Society of Economy Paleontologist and Mineralogist, Special Publication*, **42**, 39–45.

Veiga, G.D., **Howell, J.A.** and **Strömbäck, A.** (2005) Anatomy of a mixed marine/non-marine lowstand wedge in a ramp setting. The record of a Barremian/Aptian complex relative sea level fall in Central Neuquén Basin, Argentina. In: *The Neuquén Basin: A Case Study in Sequence Stratigraphy and Basin Dynamics* (Eds Veiga, G.D., Spalletti, L.A., Howell, J.A. and Schwarz, E.), *Geological Society of London Special Publication*, **252**, 139–162.

Vilas, L., **Arias, C.**, **García-Hernández, M.**, **Ruiz-Ortiz, P.A.** and **Castro, J.M.** (2002) Lower cretaceous of the Prebetic. In: *The Geology of Spain* (Eds Gibbons, W. and Moreno, T.), pp. 257–259. The Geological Society, London.

Villanueva-Amadoz, U. (2009) *Nuevas aportaciones palinoestratigráficas para el intervalo Albiense-Cenomaniense en el Sector NE de la Península Ibérica. Implicaciones paleogeográficas y paleoclimáticas*. PhD Thesis, Univ. de Zaragoza, Zaragoza, 632 pp.

Villanueva-Amadoz, U., **Sender, L.M.**, **Royo-Torres, R.**, **Verdú, F.J.**, **Pons, D.**, **Alcalá, L.** and **Díez, J.B.** (2015) Palaeobotanical remains associated with dinosaur fossils from the camarillas formation (Barremian) of Galve (Teruel, Spain). *An Int. J. Paleobiol.*, **27**, 374–388.

Visser, M.J. (1980) Neap–spring cycles reflected in Holocene subtidal largescale bedform deposits: a preliminary note. *Geology*, **8**, 543–546.

Vissers, R.L.M. and **Meijer, P.T.** (2012) Mesozoic rotation of Iberia; subduction in the Pyrenees? *Earth-Sci. Rev.*, **110**, 93–110.

Weissert, H. and **Erba, E.** (2004) Volcanism, CO_2 and palaeoclimate: a late Jurassic-early cretaceous carbon and oxygen isotope record. *J. Geol. Soc. London*, **161**, 1–8.

Willis, B.J., **Bhattacharya, J.P.**, **Gabel, S.K.** and **White, C.D.** (1999) Architecture or a tide influenced river delta in the frontier formation of Central Wyoming, USA. *Sedimentology*, **46**, 667–688.

Winterer, E.L., **Gee, J.S.** and **Van Waasbergen, R.J.** (1988) The source area for lower cretaceous clastic sediments of the Galicia margin: geologic and tectonic and erosional history. In: *Proceedings of the Ocean Drilling Program, Scientific Results* (Eds Boillot, G., Winterer, E.L., et al.), Vol. **103**, pp. 697–732. Ocean Drilling Program, College Station, TX.

Wright, V.P., **Taylor, K.G.** and **Beck, V.H.** (2000) The paleohydrology of lower cretaceous seasonal wetlands, Isle of Wight, southern England. *J. Sediment. Res.*, **70**, 619–632.

Yang, C. and **Nio, S.** (1989) An ebb-tide delta depositional model; a comparison between the modern eastern Scheldt tidal basin (Southwest Netherlands) and the lower Eocene Roda sandstone in the southern Pyrenees (Spain). *Sediment. Geol.*, **64**, 175–196.

Zaitlin, B.A., **Dalrymple, W.** and **Boyd, R.** (1994) The stratigraphic organization of incised-valley systems associated with relative sea-level changes. In: *Incised-Valley Systems: Origin and Sedimentary Sequences* (Eds Dalrymple, R.W., Boyd, R. and Zaitlin, B.A.), *SEPM Special Publication*, **51**, 41–50.

Ziegler, A.M. (1988) Evolution of the Arctic-North Atlantic and the Western Tethys. *Am. Ass. Pet. Geol. Mem.*, **43**, 198.

Zonneveld, J.P., **Gingras, M.K.** and **Pemberton, S.G.** (2001) Trace fossil assemblages in a middle Triassic mixed siliciclastic-carbonate marginal marine depositional system, British Columbia. *Palaeogeogr., Palaeoclimat., Palaeoecol.*, **166**, 249–276.

Manuscript received 13 September 2022; revision accepted 2 March 2023

Supporting Information

Additional information may be found in the online version of this article:

Appendix S1. Facies Associations of the Camarillas Formation (Galve Sub-basin) by Stages: Descriptions, Interpretations and Palaeocurrents.